12-31-2008

Investigation of the performance of flexible pavement systems under moving loads using finite element analyses

Dona Jacqueline Johnson
Rowan University

INVESTIGATION OF THE PERFORMANCE OF FLEXIBLE PAVEMENT SYSTEMS UNDER MOVING LOADS USING FINITE ELEMENT ANALYSES

by

Dona Jacqueline Johnson

A Thesis Submitted to the

Graduate Faculty in Partial Fulfillment of the

Requirements for the Degree of

MASTER OF SCIENCE

Department: Civil and Environmental Engineering

Major: Engineering (Mechanical Engineering)

Approved:

Members of the Committee

_____
In Charge of Major Work

_____

_____
For the Major Department

_____

_____
For the College

Rowan University
Glassboro, New Jersey
2008

ABSTRACT

Dona Johnson
INVESTIGATION OF THE PERFORMANCE OF FLEXIBLE PAVEMENT SYSTEMS UNDER MOVING LOADS USING FINITE ELEMENT ANALYSES
2008
Dr. Beena Sukumaran
Masters of Science in Engineering (Mechanical Engineering)

The introduction of larger and heavier aircraft with more complex wheel configurations is making the current design methods inadequate for airfield pavements. In addition, airport pavements experience significant wander. However, the effect of wander on airport pavement performance has not been evaluated. In previous studies, the stress interactions between each tire of a triple-dual-tandem (TDT) axle used on B-777 and A380 aircraft cannot be captured using a two-dimensional model. In addition, many of these studies have assumed a linear-elastic material behavior of the pavement layers.

The purpose of this study is to conduct a three-dimensional finite element analysis to quantify and evaluate the effects of wander and aircraft wheel configurations on the mechanical response of the pavement layers. The flexible pavement system that is modeled in this study is comprised of a medium and low strength subgrade. The stress-strain response of the base, subbase, and subgrade layers are simulated using an elasto-plastic model and the asphalt layer is modeled separately as a viscoelastic and elasto-plastic material. The entire pavement system is also modeled as layered linear elastic. The data collected from this study will show how flexible airport pavements are affected when wander is considered. Correlations between deformations from a single wheel and 4- and 6- wheel configurations are also studied.

ACKNOWLEDGEMENTS

I would like to thank my advisor, Beena Sukumaran for the opportunity to work on this project. Her confidence in me and unwavering support was the driving force that helped me in completing my project. It was her encouragement that caused me to push myself harder and to better myself in the process. I would like to thank Dr. Mehta and Dr. Von Lockette for taking time out of their busy schedules to be a part of my committee, their help and guidance has provided me with the necessary tools that have led me to become a better engineer.

I would like to thank my family and friends who have supported me throughout this project. It was their encouragement and reassuring words that gave me confidence to take on this challenge. I would like to thank all those that have helped and assisted me with this project.

I would also like to thank the Federal Aviation Administration for the research grant that made this work possible. In addition, I would like to thank Drs. Gordon Hayhoe and David Brill of the FAA for their assistance with the project.

TABLE OF CONTENTS

LIST OF FIGURES

LIST OF TABLES

LIST OF ABREVIATIONS

1. AASHTO = American Association of State Highway and Transportation Officials
2. ACN = Aircraft Classification Number
3. APSDS = Airport Pavement Structural Design System
4. CBR = California Bearing Ratio
5. CDF = Cumulative Damage Factor
6. ESWL = Equivalent Single Wheel Load
7. FAA = Federal Aviation Administration
8. FE = Finite Element
9. FEM = Finite Element Method
10. ICAO = International Civil Aviation Organization
11. LCN = Load Classification Number
12. LCPC = Laboratoire Central des Ponts et Chaussées
13. LED = Layered Elastic Design
14. LFC = Low Strength Subgrade Flexible Pavement with Conventional Base
15. MFC = Medium Strength Subgrade Flexible Pavement with Conventional Base
16. MWHGLT = Multiple Wheel Heavy Gear Load Tests
17. NAPTF = National Airport Pavement Test Facility
18. P/C = Pass to Coverage ratio
19. PCN = Pavement Classification Number
20. STBA = Service Technique des Bases Aériennes
21. TDT = Triple Dual Tandem
22. WES = Waterways Experimental Station

CHAPTER 1: INTRODUCTION

1.1 Problem Statement

The introduction of larger and heavier aircraft with more complex wheel configurations is making the current design methods inadequate for airfield pavements. In addition, airport pavements experience significant wander. However, the effect of wander on airport pavement performance has not been evaluated. In addition, the stress interactions between each tire of a triple-dual-tandem (TDT) axle used on B-777 and A380 aircraft is a three dimensional problem and cannot be captured using the two-dimensional model that most design methods are based upon. Some design methods use a single "equivalent" wheel load to estimate the effects of larger wheel group. Through empirical testing these effects are then scaled to match the deflection caused by a larger wheel group. These scaling factors do not take into account the wheel spacing, pavement type, or weight on the wheels. Also previous studies have assumed a linear-elastic material behavior of the pavement layers. Linear elastic does not estimate the amount of permanent deformation imparted on the pavement structure or the amount of upheaval; both of these mechanical responses are crucial to determine when a pavement has failed.

This research will counteract these problems with current computational design models by using a three-dimensional environment to perform mechanical testing. With three dimensional testing there will be no need for equivalent wheel loading, instead full loading on a whole gearing will be used. This study will also test and compare using other material properties besides linear elastic such as viscoelasticity and plasticity models.

1.2 Hypothesis

1. The use of the whole gear configuration instead of a single wheel demonstrates more accurately the mechanical effects on flexible pavement (current design methods estimate pavement thickness and deflection predictions by use of one or two wheels instead of the whole gear).
2. Use of a single wheel, instead of multiple wheels, helps to isolate the effects of trafficking after 8 runs with wander.
3. Viscoelastic properties depict the mechanical response of flexible pavement more realistically than plasticity models and linear elastic models.

1.3 Significance of Research

The industry of airport pavement design will benefit from the results of this study. Design and analysis tools for flexible pavement analysis will be developed that are calibrated to loads from new heavier aircraft. These tools will use three dimensional analysis environments to study the load interaction between wheels in a set of landing gear which cannot be realistically modeled as two dimensions. The true nature of pavement response will be evaluated and better understood through the use of a more accurate modeling environment with more realistic material properties, loading cases, and pavement geometry. Current designs use extrapolations of full scale test data beyond the limits of the experiment. This flaw in design causes the new pavements to be thicker than necessary and is less economical to produce. This study is the first critical step in quantifying the damage due to wheel configuration and wander. This will provide an invaluable tool in future design of airfield pavements.

1.4 Study Objectives

The study will focus on using a more simplified finite element model to assess the effect of single wheel loads on the pavement system. In addition, more complicated gear configurations will be used to understand the differences in strains that develop in the pavement systems. The feasibility of using a more complicated moving wheel load analysis will be investigated. Below are the overall objectives of the research:

- The Drucker Prager model, a material model that describes clayey and granular material, is refined. In a previous study performed at Rowan University, the base and subbase layers, which used this plasticity model, had a dilation component that was suppressed, which affected the accuracy of the results. The suppression of dilation angle causes the pavement, after loading, to not produce upheaval which is used as a failure indicator. In this study, this aspect is revisited and the material models used will be further validated using available laboratory test data.
- Both viscoelastic and Drucker Prager properties for the asphalt layer are investigated and validated by comparing against material data supplied by NAPTF.
- An investigation into the effect of a single wheel load with wander on pavement performance is performed. The results of this study will yield a clearer picture of how wander affects a pavement without the added complexity of the influence of wheel configurations.
- Further exploration of the effect of complex gear loading configurations on the pavement systems and the feasibility of using moving wheel load analysis in designing the pavement structure will also be examined.

1.5 Research Approach

1.5.1 Literature Review

Airport pavement design encompassing purely empirical to the most recently developed mechanistic-empirical methods will be reviewed within the literature review. Finite element analysis techniques in both two- and three-dimensional analysis with both elastic and elasto-plastic material properties will be conducted to enhance the knowledge of modeling and pavement analysis. In addition, background information on material properties, multi-wheel, multi-gear configuration and wander effects will also be reviewed. The goals of the literature review are to:

1. Understand current and in development airport design methodology for flexible pavements.
2. Understand the effects of wander on pavement performance.
3. Understand the effects of gear configuration on pavement performance.

1.5.2 Data Acquisition

Data for each layer of the flexible pavement will be collected to determine appropriate material properties and suitable plasticity models. This task will determine the constitutive properties of the subgrade and flexible pavements based on test data that is available from the FAA and literature review.

1.5.3 Finite Element Model Design and Validation

1.5.3.1 Design

The information from the literature review and data acquisition will provide the necessary background to develop a finite element model using the finite element package ABAQUS (HKS, 2006). For each available pavement structure, a finite element model will be developed that will enable the testing of the proposed hypothesis.

1.5.3.2 Validation

The model will be compared against test data available from the FAA. Load-deformation test data under wheel loading on the flexible pavement is used for comparison with the flexible pavement model to verify material properties. The trends in the main study will expand the knowledge into the effects of wander and wheel configuration.

1.5.4 Results Analysis

The results of these studies are analyzed qualitatively, since full scale testing was not available at the time. Predictions from finite element analysis will be compared to see the effect of complex wheel load configuration on the_performance of the pavement systems. Predictions from finite element analysis will be analyzed to see the effect of wander and wheel configuration on the performance of various types of pavement systems.

1.6 Thesis Structure

This thesis contains an extensive literature review and background section in Chapter 2. The purpose of this section is to help future finite element researchers gain sufficient background knowledge to understand this research study. It begins with the flexible pavement design methods used in airports which were adapted from methods used in highway pavement industry. In addition, it also describes finite element modeling of flexible pavement, multi-wheel multi-gear interaction, and the effects of wander. The last topic covered in the literature review section will be that of the material properties used in the models such as plasticity models, viscoelastic properties, and the Prony series. The literature review section allows for those not familiar with specific aspects of this project to refresh themselves and bring themselves up to speed with the research that has been conducted in the area of pavement design and analysis.

Following the literature review section are the verification studies in Chapter 3 used to ensure that the results being obtained from the various models are realistic and the material properties used are valid for the various layers of the pavement structure. Chapter 4 discusses the results of the various finite element studies conducted on several pavement structures. Chapter 4 is the critical chapter showing the results of the various analyses. Chapter 5 discusses the conclusions, and recommendations of this study. The last section in Chapter 5 outlines additional studies that have to be done and arise as a result of this study.

CHAPTER 2: LITERATURE REVIEW

2.1 Full Scale Test

2.1.1 The Waterways Experiment Station (WES) Tests

2.1.1.1 Background

US Army Corps of Engineers has performed full scale pavement trafficking for over 60 years, which form the empirical basis for the world's airport pavement design systems. The raw data for these tests have been reported in great detail so that future designers and researchers are able to re-interpret the test results using more powerful analytical tools as they become available. Researchers typically use the WES tests to calibrate their models which provide empirical evidence for their theoretical analyses.

In the late 60s and early 70s, series of tests were conducted at the Waterways Experiment station in Vicksburg, Mississippi called the Multiple Wheel Heavy Gear Load Tests (MWHGLT). The pavements ranged from thicknesses of 380mm to 1040mm and consisted of unbound granular material surfaced with a 75mm asphalt layer. These pavements were trafficked to failure with a single and multi-wheel configuration with loadings that mimic full aircraft weight. The California Bearing Ratio (CBR) pavement design method from full scale test data is described in Instruction Report S-77-1 by Ahlvin et al. (1971) and describes the design methodology that was developed as a result of the WES tests utilizing the CBR test as an input for design. The failure criterion used in these tests were 25mm of rutting or 25 mm of upheaval outside the trafficked area, or cracking which would allow for water to permeate.

2.1.1.2 Shortfalls of WES testing

Fundamental limitations of the test data are discussed in detail by Barker and Gonzalez (1994). Design of major pavements now commonly entails substantial extrapolations beyond the data base with respect to (Rodway 1995):

- Load repetitions. The median level of test traffic to failure was 3000 coverages with one test to 7000 coverages. Major pavements are now commonly designed for several hundred thousand coverages.
- Pavement thicknesses. The median thickness of pavements in the WES test was 400 mm with one pavement at 1.25 m. Thicknesses exceeding 2 m are now common.
- Pavement structures. Only unbound granular pavements were tested. It is more common now to incorporate thick bound layers into structures and some authorities require it.
- Subgrade strength. Majority of test data were for low strength subgrades with CBR around 4 (median 7).
- Wheel Configurations. No elongated wheel configurations were tested and interaction between landing gears was not investigated.

There is no way at present to quantify the effects of these extrapolations. As a result of these limitations and difficulty in extrapolating the design data to larger and heavier aircrafts, the National Airport Pavement Test Facility (NAPTF) was built to conduct more full scale tests. This will be discussed in more detail in the following section.

2.1.2 National Airport Pavement Test Facility (NAPTF)

The NAPTF is located at the Federal Aviation Administration (FAA) William J. Hughes Technical Center, Atlantic City International Airport, New Jersey. A 1.2 million-lb pavement testing machine spans two sets of railway tracks that are 76 feet apart. The vehicle is equipped with six adjustable dual-wheel loading modules. A hydraulic system applies the load to the wheels on the modules. The major specifications for the test track are as follows (Hayhoe 2004):

- Test pavement 900 feet long by 60 feet wide.
- Nine independent test items (six flexible and three rigid) along the length of the track and includes low, medium and high strength subgrades.
- Twelve test wheels capable of being configured to represent two complete landing gear trucks having from two to six wheels per truck and adjustable up to 20 feet forwards and sideways.
- Wheel loads adjustable to a maximum of 75 kips per wheel.

The main purpose of the NAPTF is to prove whether the empirical methods are valid and whether layered elastic system solutions can be calibrated to reflect real world full strength pavement behavior under aircraft loads (Gervais et al 2003). The next sections describe some of the design modification factors used to account for larger and heavier aircrafts with more complex gear configurations.

2.1.3 Airbus Tests

The A380 Pavement Experimental Program was started by the Airbus Industrie, the Service Technique des Bases Aériennes (STBA), and the Laboratoire Central des Ponts et Chaussées (LCPC). The main purpose of this program is to provide full-scale

data which is compared against theoretical simulations using multi-layered elastic models by the STBA and LCPC.

The pavement test facility built in Toulouse was representative of the four internationally recognized subgrade categories A, B, C and D for flexible structures. The pavement structures consist of three layers above the subgrade: subbase, base courses and asphalt surfacing. Only the subbase had a variable thickness depending on the subgrade category and for comparison purposes. Each layer of pavement structures was instrumented with sensors, especially to measure deflections and elongation (Airbus 2001).

The simulation vehicle was able to represent full-scale Main Landing Gear configurations of various wide bodies: A380, A340, B747, and B777. Up to 22 wheels could be individually loaded up to 32 tons. The vehicle features variable dimensions for landing gear position, wheels and axle spacing.

The program focused in 1998 and early 1999 on quasi-static comparisons of Landing Gear configurations. These tests provided data on effects of interference when wheels or leg spacing changed, comparisons between various A380, A340, A320 L/G configurations and with their main competitors (Airbus 2001).

Full scale testing results are used as the basis for pavement design methods. These results are used to calibrate design standards. Each of these design methods will be explained in the next section.

2.2 Flexible Pavement Design

2.2.1 California Bearing Ratio Test (CBR)

2.2.1.1 Background

The California Bearing Ratio (CBR) test is a simple strength test that compares the bearing capacity of a material with that of a well-graded crushed stone. It is primarily intended for, but not limited to, evaluating the strength of cohesive materials having maximum particle sizes less than 0.75 in. (AASHTO, 2000). It was developed by the California Division of Highways around 1930 and was subsequently adopted by numerous states, counties, U.S. federal agencies and internationally. As a result, most agency and commercial geotechnical laboratories in the U.S. are equipped to perform CBR tests.

The basic CBR test involves applying a load to a small penetration piston at a rate of 0.05 in per minute and recording the total load at penetrations ranging from 0.025 in up to 0.300 in. Figure 2.1 is a sketch of a typical CBR sample.

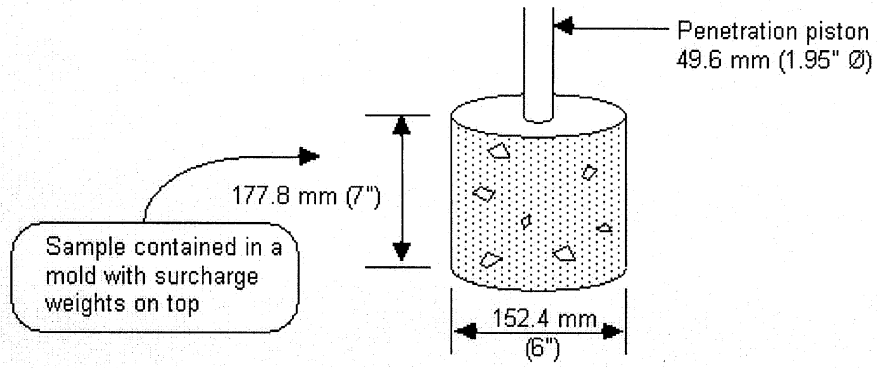

Figure 2.1: CBR Sample

Values obtained are inserted into the following equation to obtain a CBR value:

$$CBR\ (\%) = 100\left(\frac{x}{y}\right) \qquad (2.1)$$

where: x = material resistance on the piston (pressure) for .1 or .2 in of penetration

y = standard unit load (pressure) for well graded crushed stone

= 1000 psi for 0.1 in penetration

= 1500 psi for 0.2 in penetration

Table 2.1 shows some typical CBR ranges.

Table 2-1: Typical CBR Ranges (University of Washington 2004)

General Soil Type	USC Soil Type	CBR Range
Coarse-grained Soils	GW	40-80
	GP	30-60
	GM	20-60
	GC	20-40
	SW	20-40
	SP	10-40
	SM	10-40
	SC	5-20
Fine-grained Soils	ML	15 or less
	CL LL<50%	15 or less
	OL	5 or less
	MH	10 or less
	CH LL >50%	15 or less
	OH	5 or less

Figure 2.2 provides a description of the various soil group types seen in Table 2.1.

Group Symbol	Typical Names
GW	Well-graded gravels and gravel-sand mixtures, little or no fines
GP	Poorly graded gravels and gravel-sand mixtures, little or no fines
GM	Silty gravels, gravel-sand-silt mixtures
GC	Clayey gravels, gravel-sand-clay mixtures
SW	Well-graded sands and gravelly sands, little or no fines
SP	Poorly graded sands and gravelly sands, little or no fines
SM	Silty sands, sand-silt mixtures
SC	Clayey sands, sand-clay mixtures
ML	Inorganic silts, very fine sands, rock four, silty or clayey fine sands
CL	Inorganic clays of low to medium plasticity, gravelly/sandy/silty/lean clays
OL	Organic silts and organic silty clays of low plasticity
MH	Inorganic silts, micaceous or diatomaceous fine sands or silts, elastic silts
CH	Inorganic clays or high plasticity, fat clays
OH	Organic clays of medium to high plasticity
PT	Peat, muck, and other highly organic soils

Prefix: G = Gravel, S = Sand, M = Silt, C = Clay, O = Organic
Suffix: W = Well Graded, P = Poorly Graded, M = Silty, L = Clay, LL < 50%, H = Clay, LL > 50%

Figure 2.2: Unified Soil Classification System from ASTM D 2487 (1993)

The empirical CBR highways method was adapted in 1942 to design flexible aircraft pavements. Boussinesq's single layer elastic theory allowed the CBR method to be extrapolated for higher single wheel aircraft loads. The solutions to this method were limited to stress, strain and deflection directly under the loading.

2.2.1.2 CBR Failure Mode

The way in which failure is assumed to occur with this method is by overstressing the subgrade which causes surface rutting. The end of the pavement life is when the surface ruts to where it is too rough for traffic, or fails to shed water, which leads to loss of friction.

2.2.1.3 CBR Shortfalls

Pavement failure due to fatigue cracking of the asphalt layer or of other bound layers is not considered in this method. The CBR design procedure protects the subgrade by adding more pavement thickness and thereby increasing the pavement life, but not by improving the pavement materials.

The CBR curve was constructed from full-scale trafficking tests to failure conducted by the US Army Corps of Engineers and will be explained in more detail in the following section. The pavement these tests were performed on were unbound granular materials, which means the basic CBR method contained no way of taking into account the benefits of bound layers. However, now in practice equivalency factors are used to take this into account. These factors are based on layered elastic analysis, limited field measurements of stress, strain and deflection, and limited full-scale testing.

The CBR method is only appropriate when the design pavement thickness is comparable to the test pavements. It becomes less applicable when loads become higher and at greater repetitions. The way to improve pavement performance in these cases is to improve quality of top layers rather than increasing pavement thickness (Rodway 1995).

Below is an example of the CBR design curve for the Boeing 787 with a four wheel gear configuration. The maximum weight of a B787 is 482, 000 lbs.

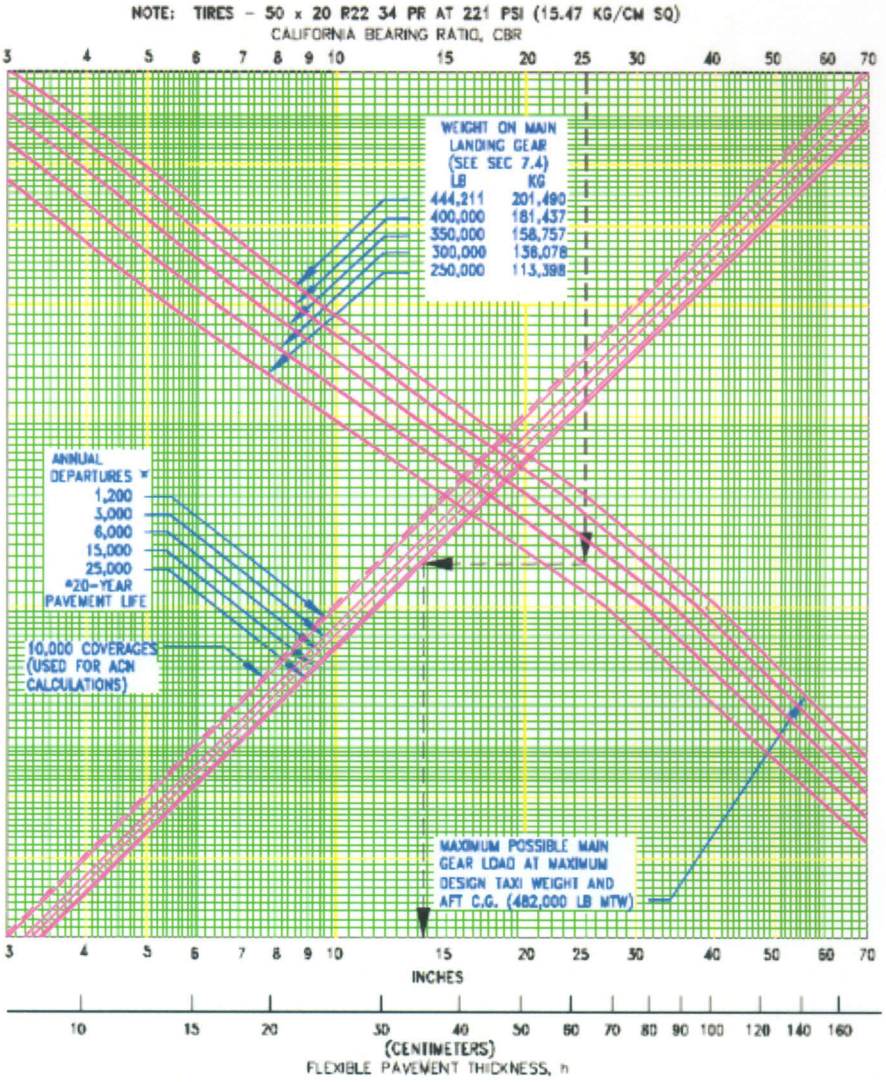

Figure 2.3: Boeing 787 CBR Design Curve (Boeing 2006)

This graph shows that for a subgrade with a CBR value of 25, a weight of 300 kips on the main landing gear, and an estimated annual departure rate of 25,000, it is predicted that there should be at least 14 total inches of stronger pavement layers above the top of the subgrade for 20 year life.

2.2.2 Equivalent Single Wheel Load

2.2.2.1 Background

As planes progressively grew in size, wheel arrangements went from single wheel to dual wheel, and on to dual tandem arrangements. The CBR method was extended using the concept of an Equivalent Single Wheel Load (ESWL), so that it could be used for design for aircraft that had larger weights and landing gears (Rodway 1995). This method is conducted by determining the maximum subgrade deflection caused by the multiwheel gearing and equating that to a single wheel causing similar deflection. With a single wheel loading established, rutting that would be caused by the single wheel loading is calculated using empirical formulas based on testing done through the early 1970's (Gervais et al 2003).

ESWL is a function of pavement depth. This method was developed in the 1950s, and used the single layer Boussinesq expression for deflection beneath and at offsets from a uniformly loaded circular area.

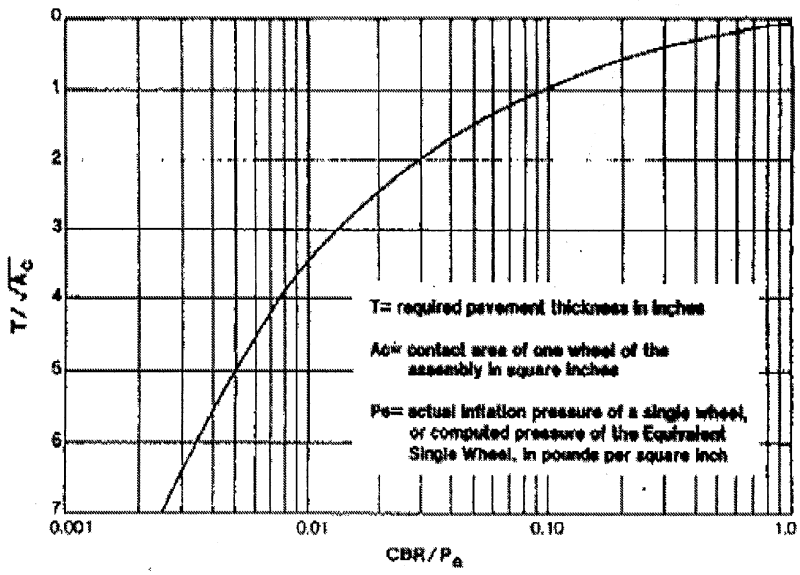

Figure 2.4: US Corps of Engineers CBR Curve (Rodway 1995)

Figure 2.4 above is from the US Army Corps of Engineers which relates load, pavement thickness and CBR. Both single and multiwheel test data have been combined to produce a single CBR curve by using the deflection based ESWL concept (Rodway 1995).

2.2.2.2 ESWL Shortfalls

This design method has many apparent inadequacies and is no longer relevant to airport pavement design. Due to the increasing number of wheels being used on modern aircraft, equating larger multiwheel gear configuration to a single wheel becomes exponentially inappropriate. This technique fails to recognize that larger wheel configurations can span large sections of pavement and can result in a nontraditional rutting pattern (Hayhoe, 1993).

When loading on a wheel reaches a certain threshold, the footprint of the load spreads, and can be more appropriately expressed as a compaction rather than a point load. Additionally, wheels with large enough loads actually create negative (upward) vertical strains and deflections at a radial distance proportional to the pavement depth and the actual load. When the negative strain is created and the radial distance to the negative strain lies under another wheel of the aircraft gearing, the deflection and strain under that wheel is actually reduced. This load distribution phenomenon is not considered when using this technique of deriving an equivalent single wheel load. The consequence of this major shortfall is large rutting depth over-predictions and the over-design of pavement structures. After the existence of multiwheel interactions was confirmed in the late 60's and early 70's, corrective measures were taken to

reduce the amount of over prediction made by the equivalent single wheel method. The correction factor that was used to account for these effects was called alpha factors, which will be discussed in the following section.

2.2.3 Alpha Factors

2.2.3.1 Background

Alpha factors, or load repetition factors, are determined by graphing the number of load repetitions against alpha curves that are based on the number of tires in a landing gear configuration (See Figure 2.5). This method replaced the LCN (Load Classification Number) system and its variations – referred to as ESWL systems. Both LCN and ESWL methods use the technique, similar to the CBR method, of deflection-based equivalent single wheel load (Gervais et al 2003).

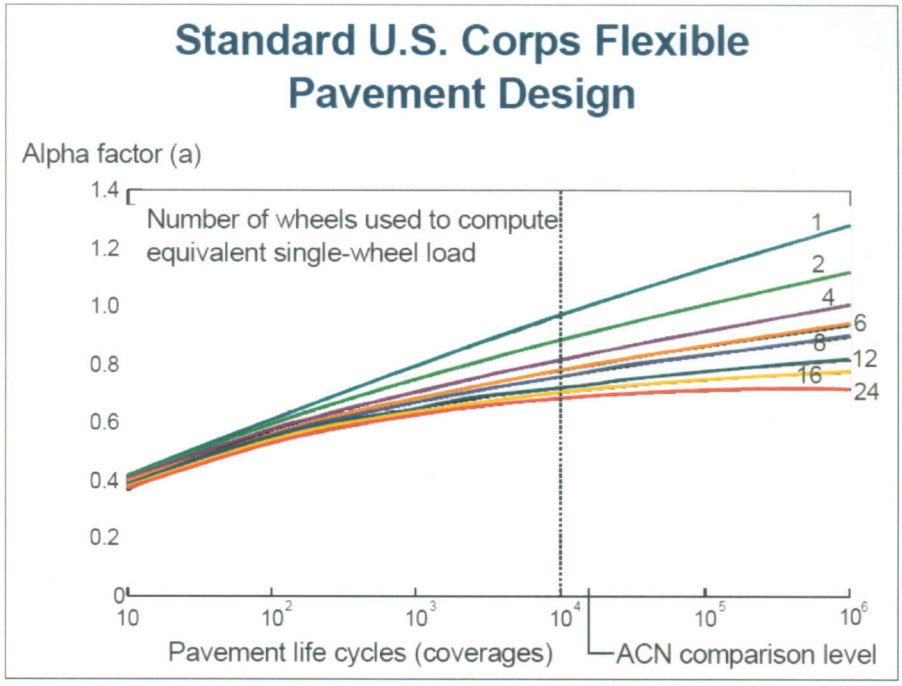

Figure 2.5: Alpha Factors versus Coverages (Gervais et al 2003)

Figure 2.5 shows that for any number of wheels and number of coverages, an alpha factor can be determined. For example, for 10,000 coverages, 24 wheels would have an approximate alpha factor of 0.7. This number means that the theoretical thickness of pavement calculated with the CBR method to support 24 wheel loading is reduced down to 70% of its value. This can be seen mathematically in equation 2.2.

$$t = a(A_c)^{.5}[-0.0481 - 1.1562\ (\log\frac{CBR}{P}) - 0.6414\ (\log\frac{CBR}{P})^2 - 0.473(\log\frac{CBR}{P})^3] \quad (2.2)$$

where t = pavement thickness, inches

a = alpha factor, index of desired pavement life as a function of number of wheels in main landing gear group

A_c= tire contact area (sq. inches), (single wheel load (lbs)/ tire inflation pressure (psi))

P = Equivalent Single Wheel Load (ESWL) lbs. (function of pavement thickness)

CBR= California Bearing Ratio, an index of subgrade soils strength *in situ*

This correction, however, is only a function of the number of tires used to calculate the ESWL. It is derived empirically from testing using only 1 to 6 wheels over relatively thin pavements with low CBR subgrades. This technique leaves out a lot of factors important to pavement design. The effects of the thickness of the pavements and the configuration of the wheel groupings are not considered by alpha factoring, only by the largest gear size on the main body. As discussed previously, the negative strains and deflections occur at a certain radius from each tire so the

configuration of the wheels and the interactions between them depend on the distance between the wheels and the depth of the pavement being loaded (Rodway 1995).

For specific applications, it is possible to test full-scale models of wheel configurations at varying depths and approximate the damage effects using an alpha factor specific to that particular setup. This has been done by the FAA for the most recently run four and six wheel configurations. This testing and analysis addresses current popular wheel configurations but it does not provide data for theoretical future wheel configuration. By simply adjusting a historic method without investigating the causes for the damage reduction, it becomes impossible to model other wheel configurations without testing and empirically deriving their effects.

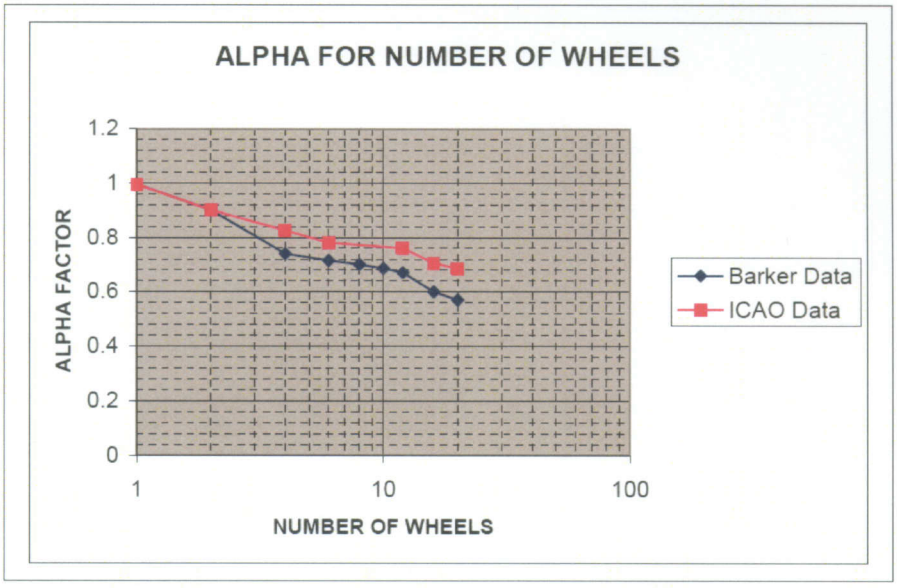

Figure 2.6: Revised Alpha Factors versus Coverages

The figure above show the revised alpha factors per the 1994 Barker Report in comparison to the original ICAO data (Gervais et al. 2003). With these alpha factors,

the CBR method can be used once again to design required pavement thickness. An iterative solution is required to solve equation (2.2) because thickness, t, is a function of P, the equivalent single wheel load (Gervais et al 2003).

2.2.4 ACN-PCN

2.2.4.1 Background

Due to its high importance for the management of airports, structural classification of airfield pavements has always been among the most interesting tasks of airport pavement engineering. Airport managers, aircraft manufacturers, and airline operators all require information to ensure that they can safely utilize both the aircrafts and the pavement to the maximum extent. Consequently, it is necessary to have a reliable classification system to report representative data for the bearing capacity of the pavements and the impact of the aircraft load on the pavement (Loizos 2004).

A single worldwide standard for expression of airfield pavement strength and aircraft pavement load intensity- the Aircraft Classification Number- Pavement Classification Number (ACN-PCN) system was announced in March 1981 by the International Civil Aviation Organization (ICAO). This system provided ways to express pavement load intensity of any aircraft and the load carrying capacity of any pavement (PCN) in a simple form that is technically satisfying, easy to use and understand (Gervais et al 2003).

The PCN is the number used by airport owners and operators to classify their pavement. This number is then compared to the ACN value of an individual aircraft. The ACN number expresses the loading effect of the aircraft on a specific pavement

type and standard subgrade. These values are based on static aircraft loads to the pavement surface, which makes them fairly conservative.

If the ACN of an aircraft is lower than the PCN of the airport pavement, the aircraft is guaranteed use of the airport. If an ACN value is higher than the airport's PCN, it is at the discretion of the airport owners and operators whether or not they will allow the aircraft access to their airport, knowing that the aircraft will likely damage the pavement surfaces (Loizos, 2004).

2.2.4.2 ACN Calculations

Aircraft classification number can be calculated in the following manner:

1. For the specific aircraft, the load on each main gear at maximum gross take-off weight is determined according to the percentage distribution of the most aft center of gravity
2. The number of coverages is set at 10,000 and corresponding load-repetition factor, a, (figure 2.5) is selected for a given number of wheels, n, to compute ESWL
3. Pavement thicknesses are determined for range of CBR values (3%, 6%, 10%, and 15%) according to the conventional FAA procedure (Eqn 2.2)
4. The ACN value is determined by the following expression (Livneh 2004):

$$ACN = \frac{\frac{t^2}{100{,}000}}{\frac{0.878}{CBR} - 0.01249} \qquad (2.3)$$

where t = pavement design thickness, in mm, calculated from Eqn 2.2 for specific CBR values at 10,000 coverages

CBR = one of specified values (3%, 6%, 10%, and 15%), as a percentage

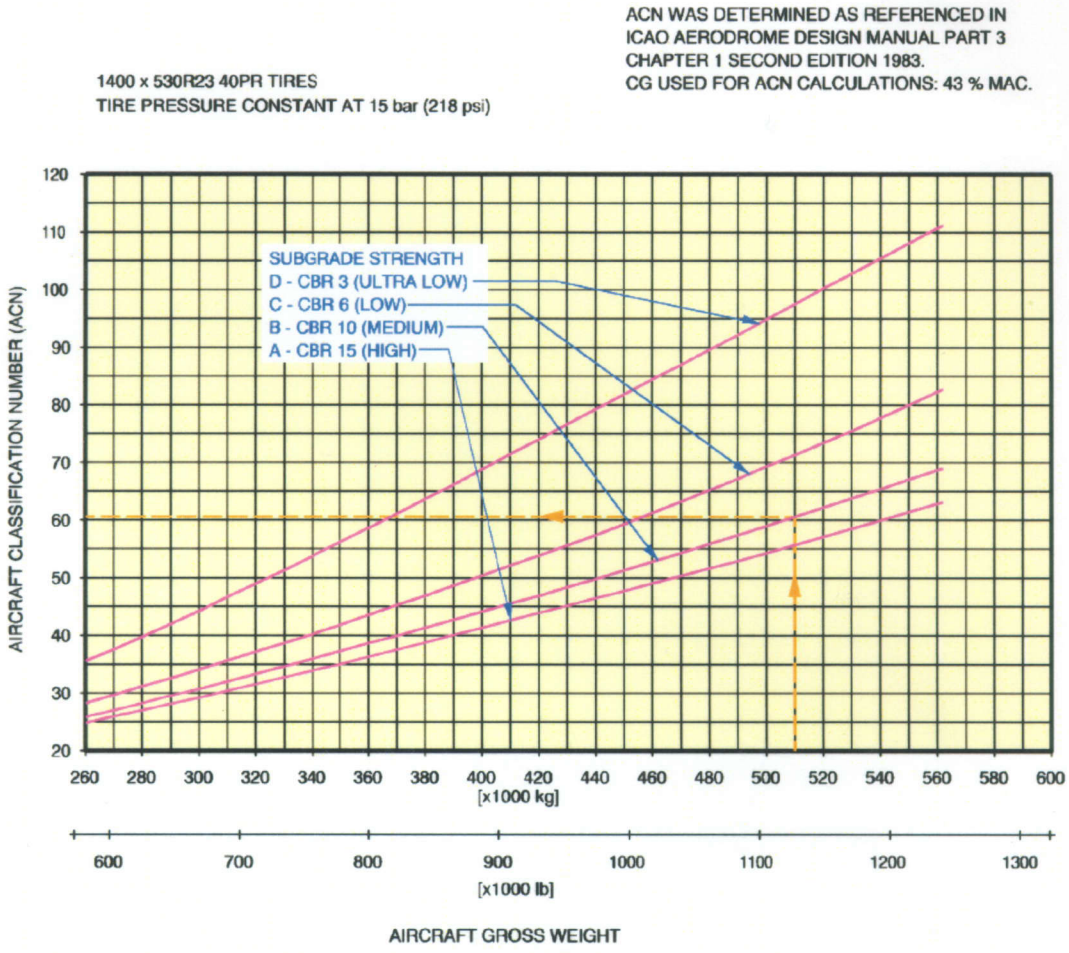

Figure 2.7: Airbus 380-800F Aircraft Classification Number (ACN) Chart (Airbus 2007)

Figure 2.7 shows the Aircraft Classification Number chart for the A380-800F with a gross weight of 510,000 kg. This graph shows that for a medium strength subgrade with CBR value of 10, the ACN value is 61.

2.2.4.3 PCN Calculations

2.2.4.3.1 PCN Description

There are two methods that airport authorities use to calculate pavement classification number. The first method, "Using" aircraft method, can be applied with limited knowledge of existing traffic and runway characteristics. This method is based on the aircraft currently and satisfactorily using the pavement, and there are no engineering methods or technical analysis employed to determine this type of PCN. The second method is known as the Technical evaluation method which requires much more in-depth knowledge of the pavement and its traffic (Stet and Verbeek 2004).

2.2.4.3.2 "Using" Aircraft Method

This method can be used when there is limited knowledge of the existing traffic and runway characteristics. The accuracy of this method is lower than the technical method; however, it can be determined more quickly and with minimal cost. Below are the two basic steps to determine a "Using" aircraft PCN:

1. Determine the airplane with the highest ACN in the traffic mix frequently using the runway. This is the critical airplane.
2. Assign the ACN of the critical airplane at commonly used load percentage as the PCN.

The pavement should be tentatively be rated at the PCN of step 2, assuming that the pavement is performing satisfactorily under current traffic. If the pavement is showing signs of distress, then this rating must be lowered at the discretion of the airport authority. If the rating is lowered, then one or more of the aircraft will have maximum ACN's that exceed the assigned rating. This may require a restriction in allowable gross weight for those aircraft or consideration of pavement strengthening.

2.2.4.3.3 Technical Evaluation Method

The "Using" aircraft method can be considered a close approximation. The technical evaluation method of determining PCN should be used when there is reliable knowledge of existing traffic and pavement characteristics or when heavier aircraft are expected.

Below are the steps required to determine PCN using the Technical evaluation method.

1. Determine the traffic volume in terms of type of aircraft number of operations of each aircraft that the pavement will experience over its life.
2. Convert that traffic into a single critical airplane equivalent.
3. Determine the pavement characteristics, including the subgrade CBR and pavement thickness.
4. Calculate the maximum allowable gross weight of the critical aircraft on that pavement.
5. Look up or calculate the ACN of the critical aircraft at this maximum allowable weight.
6. Assign the PCN to be the ACN of the critical aircraft at the allowable weight.

2.2.4.4 Conclusions

The design methods used previously have limitations as addressed in the earlier sections. To account for these deficiencies, there have been revised design tools developed or are in the process of being developed. Some of the design tools being developed include the layered elastic method, which will be discussed in the next section.

2.2.5 Layered Elastic Methods

2.2.5.1 Background

This method models the pavement structure as a system of horizontal layers. Each layer is assigned constant properties and is only allowed to deform elastically. Consequently the nonlinearity and stress-dependent load response of pavement materials cannot be directly represented. To some extent the response can be simulated by sub-layering the actual pavement layers and assigning different properties to each sub-layer. The method of sub-layering comes from having access to field data specifically deflections and strain, as well as using finite element modeling. The models can be used to predict theoretical load interactions for complex landing gear configurations, but will be limited by the accuracy of the assumptions. The US Army Corps of Engineers used layered elastic theory to develop design procedures for flexible aircraft pavements (Rodway 1995). In addition, the FAA uses this approach for performing thickness design of airport pavements using a computer program, LEDFAA 1.3.

2.2.5.2 LEDFAA

LEDFAA is a computer program for performing thickness design of airport pavements. It implements advanced design procedures based on layered elastic theory developed under the sponsorship of the Federal Aviation Administration (FAA). The computational core of the LEDFAA program is LEAF an improved layered elastic analysis program developed by FAA, replacing the JULEA program that ran in previous versions of LEDFAA.

The LEDFAA program is also primarily intended for use in designing airport pavements according to a standard procedure. It is not intended to be used to compare the damaging effects of different aircraft by running single aircraft designs or CDF computations, i.e., ACN type calculations (FAA 2004).

2.2.5.3 Airport Pavement Structural Design System (APSDS)

Another program that uses layered elastic design is called Airport Pavement Structural Design System (APSDS). The difference between this program and LEDFAA is that this one uses subgrade strains as the damage indicator and is computed for all points across a pavement, whereas single maximum values of the damage indicators are calculated in LEDFAA and previous methods. Using subgrade strains allows the user to suppress pass to coverage ratio and alter the degree of aircraft wander. Using subgrade strain as the damage indicator in this new design method reduces the predicted gear interaction. However some abnormal design results were produced by using vertical strain. The method predicts that adding fully loaded wheels can increase rather than decrease pavement life (Rodway et al 1999). The subgrade strain captures all the damage contributions from all the aircraft wheels

in all their wandering positions. The strains are then converted to damage using a performance model in the form:

$$N = \left(\frac{k}{\varepsilon}\right)^{b} \qquad (2.4)$$

where N is the predicted life (repetitions of ε)

k is a material constant

b is the damage exponent of the material

ε is the induced strain (dimensionless)

and accumulated using Miner's hypothesis. The parameters k and b are established through full-scale testing to failure. The Cumulative Damage factor (CDF) for the i-th loading can be defined as the number of repetitions (n_i) of a given response parameter divided by the maximum allowable repetitions (N_i) of the response parameter that would cause failure. The damage factor is given by summing the damage factors over all the loadings in the traffic spectrum.

$$CDF = \Sigma\left(\frac{n_i}{N_i}\right) \qquad (2.5)$$

Pavement is assumed to have reached its design life when CDF=1.

The benefit of this program is that the user can change all problem inputs such as aircraft mix, aircraft wander, numbers and weight, pavement layer thicknesses and material properties, and the performance model. This allows for the assessment of the sensitivity to each component input and to each design assumption.

2.2.5.4 Limitations of Layered Elastic Design (LED) Methods

The layered elastic design method used to interpret test results will be affected by the negative strain effects of the B747 and B777 for many of the wheel configurations and pavement structures of interest.

The load response of unbound granular pavement materials such as P209 and P154 is elasto-plastic and stress-dependent. The layered elastic method cannot take into account plastic behavior and cannot fully deal with stress dependence. An important limitation of the method is that elastic moduli must be constant within each horizontal layer. But stress diminishes with distance from the wheels so the modulus will also change with distance from the wheels. Consequently most of the modulus values used in the pavement model will be incorrect and therefore the strains and deflections calculated using the moduli must also be incorrect at most points.

To produce reasonable estimates of stresses or deflections measured at selected points in the pavement, linear elastic method tries to incorporate stress-dependence by sublayering materials and assigning moduli to each region.

Thus the layered elastic method uses a much-simplified representation of the pavement that is known to assume incorrect modulus values throughout much of the pavement. Vertical compressive strain at the subgrade level is the main focus of design methods based on estimating surface rutting. The critical strains occur in both FEDFAA and APSDS under the single gear loading.

The design method has serious limitations in that it assumes that all deformations are recoverable. It also assumes linear elastic over any stress range which is not true for granular materials. Linear elastic assumes all materials are

nonviscous, which the asphalt layer conforms to. Asphalt is both time and stress dependant.

2.3 Multi-wheel Multi-gear Interaction

It is extremely difficult to quantify the effects of multi-wheel multi-gear interactions. These effects vary by pavement thickness, load, tire size, temperature, and other minor factors. Accurate modeling of these effects may be nearly impossible due to the complexities introduced in multi-wheel multi-gear interactions. It is impossible to predict how each of these factors interacts with one another without testing every possible combination. Some of the minor factors of multi-wheel interactions are neglected to develop a practical model.

A computer modeling study done during the production of APSDS produced a model that approximated the size and shape of negative strains produced by both single wheels and single gears of the Boeing 777. It also discusses the use of vertical strains rather than vertical deflections because vertical deflections seem to over predict rutting as wheel loading increases.

Graphs showing the vertical strains created by single wheel loading and single gears are shown in Figures 2.8 and 2.9 respectively. These graphs are, however, only computer models and are therefore not able to be accepted as truth until they can be verified through field study (Rodway et al 1999).

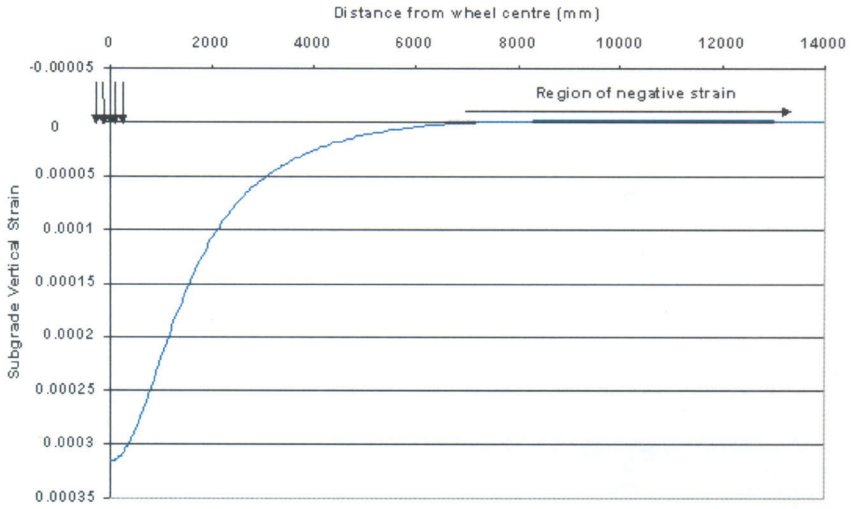

Figure 2.8: Subgrade Strain due to B777 Single Wheel on 2m 'FAA' Pavement

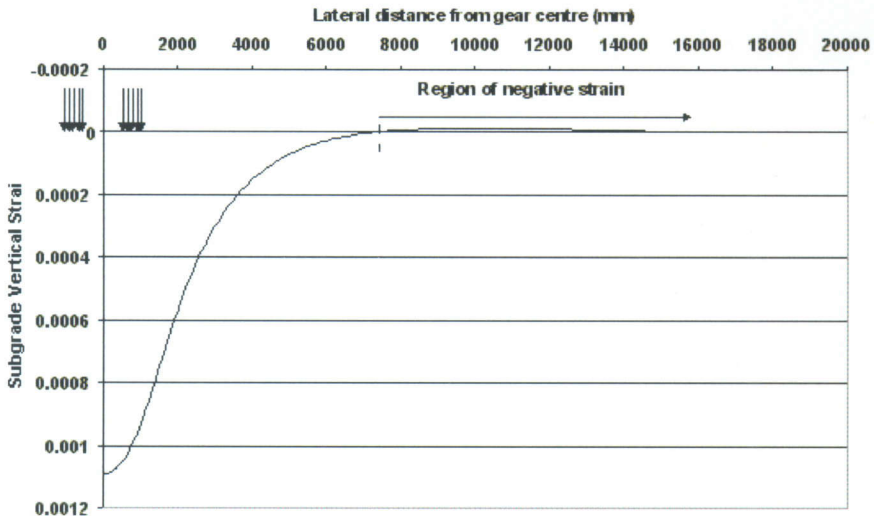

Figure 2.9: Subgrade Strain due to Single B777 Gear on 2m 'FAA' Pavement

Comparing figures 2.8 and 2.9 it can be seen that the subgrade strain increases in magnitude when using a single wheel versus a whole gear. The region of negative strain also changes with the two scenarios; a single wheel's region is closer to the centerline.

Wardle (2003) states that when calculating interactions between wheels and between wheel groups, some geometries result in a zone of negative strain generated

by one wheel or wheel group that falls beneath other wheels or wheel groups, which reduces strain. For a layered pavement structure, the horizontal distance from the load at which the computed subgrade strain becomes negative depends upon both the thicknesses and the stiffnesses of the pavement layers and subgrade. Therefore, adding fully loaded wheels or wheel groups to the model predicts a longer pavement life. This result seems counterintuitive; adding more loading should decrease the life of pavement instead of increasing it.

2.4 Effects of Wander on Pavements

The pass-to-coverage ratio (P/C) was an early attempt at a wander model used primarily due to its simplicity. The P/C ratio concept addresses the pattern of load distribution only at the pavement surface, which incorrectly implies that reduction in damage due to wander is equal for all pavement depths. However, testing has proven that wander is more beneficial for thinner pavements (Wardle, 1998).

Some alternatives to this approach might be the model used in the development of the Airport Pavement Structural Design System (APSDS). APSDS calculates subgrade strain distribution rather than a single maximum and is not based on the coverage concept. For tandem wheels, this model creates a strain graph with a single maximum rather than a double maximum plot similar to the shape of the wheels. Damage predicted using this model is single maximum rutting with significantly shallower ruts than the dual maximum rutting predicted with no wander.

This model seems promising and has been correlated to data obtained from relatively shallow test sections. For further progress and application to modern thicker pavements, this model should be calibrated to thicker pavement testing.

Donovan and Tutumluer (2007) summarized the effect of wander as a potential cause of more deformation in the subgrade than if the aircraft wheel loads traveled the same path consistently. In that paper, they called this effect on pavement the "anti-shakedown" effect which is the "shuffling" of the particles within the pavement system. They concluded that wander reduces the stability of the system.

2.5 Finite Element Modeling of Flexible Pavement

Three-dimensional finite element analysis tools are increasingly viewed as the best approach to answering certain fundamental questions about pavement performance (Chen et al., 1995, Cho. et al., 1996, Kuo et al., 1995), but the tedious processing and time required to accurately model pavement systems have hampered the use of these analyses. While two-dimensional axi-symmetric models can be utilized for a single wheel load analysis, such a constraint would lead to an inaccurate three-dimensional analysis, particularly for pavements subjected to multiple wheel loads and wander.

As stresses and strains are used more and more to predict pavement distresses, and thus the relative condition of the various layers in the pavement structure, the need for consideration of non-linear material behavior becomes increasingly important. Linear elastic approximations of unbound material behavior are no longer acceptable in pavement analysis. The stress state dependency of granular materials,

and strain based subgrade soil models must be considered for an accurate estimation of true pavement response (Nazarian and Boddspati, 1995).

Past flexible pavement models used multi-layer elastic analysis, which assumes static loading, whereas in reality pavements are subjected to both static and moving loads. The model used in the study conducted by Zaghloul and White (1993) incorporated an elasto-plastic model for the base, sub-base and subgrade and a visco-elastic model for the asphalt layer. Zaghloul and White (1993) researched the ability of three-dimensional dynamic finite element programs to predict the response of moving loads on pavement structures. The validation of their model was accomplished by testing the model's ability to predict deformations under static and dynamic load conditions. The final results showed that their model was capable of simulating truckloads and realistic deformation predictions were obtained.

2.5.1 Material Properties

2.5.1.1 Introduction

There are two material properties used within studies seen in later chapters. One is a plasticity model called the Drucker-Prager model which will be used for all layers of both low and medium strength flexible pavement sections. Also described is viscoelasticity, which will be used to describe the asphalt layer, P-401.

2.5.1.2 Drucker-Prager Model

The Drucker-Prager plasticity model is an isotropic elasto-plastic model based on a yield function

$$f(\sigma, \tau_Y) = F(\sigma) - \tau_Y \qquad (2.6)$$

with the pressure-dependent equivalent stress

$$F(\sigma) = \alpha I_1 + \sqrt{J_2} \qquad (2.7)$$

σ is the stress tensor, τ_Y is the yield stress under pure shear, and I_1 and J_2 are the first invariant and second deviatoric invariant of the stress tensor. The friction coefficient α is a positive parameter that controls the influence of the pressure on the yield limit, important for cohesive-frictional materials such as concrete, soils or other geomaterials. The flow rule is derived from the plastic potential

$$g(\sigma) = \alpha_\psi I_1 + \sqrt{J_2} \qquad (2.8)$$

where α_ψ is the dilatancy coefficient.

The extended Drucker-Prager models:

- are used to model frictional materials, which are typically granular-like soils and rock, and exhibit pressure-dependent yield (the material becomes stronger as the pressure increases);
- generally allow for volume change with inelastic behavior: the flow rule, defining the inelastic straining, allows simultaneous inelastic dilation (volume increase) and inelastic shearing (HKS 2006);

2.5.1.3 Viscoelasticity

2.5.1.3.1 Introduction

Viscoelasticity describes materials with both viscous and elastic characteristics. Viscous materials resist shear flow and strain linearly with time when a stress is applied. Elastic materials strain instantaneously when stretched and when the stress is

removed quickly return to their original state. Viscoelastic materials also exhibit time dependent strain.

2.5.1.3.2 Effect of Temperature on Viscoelastic Behavior

Viscoelastic properties change with increasing or decreasing temperature. In most cases, the creep modulus, defined as the ratio of applied stress to the time-dependent strain, decreases with increasing temperature. Generally speaking, an increase in temperature correlates to a logarithmic decrease in the time required to impart equal strain under a constant stress. In other words, it takes less energy to stretch a viscoelastic material an equal distance at a higher temperature than it does at a lower temperature.

2.5.1.3.3 Prony Series

ABAQUS, a general-purpose finite element code used for modeling in this study, uses a Prony series rheological model to characterize the relaxation master curve at a selected reference temperature (-20°C was used in this study), as described in equation 2.9. The Prony series rheological model consists of N-pairs of spring-dashpot assemblies, arranged in parallel.

$$E(\xi) = \sum_{i=1}^{N} E_i e^{-\xi/\lambda_i} \qquad (2.9)$$

where: $E(\xi)$ = relaxation modulus at reduced time ξ

E_i, λ_i = Prony series parameters for master relaxation modulus curve (spring constants or moduli and relaxation times for the Maxwell elements)

This function describes the relaxation modulus as a function of time at a single temperature, which is generally known as the reference temperature. The function defined at the reference temperature is called the master relaxation modulus curve. Relaxation moduli at other temperatures are determined by using the method of reduced variables (time-temperature superposition), which assumes that the mixture behaves as a thermo-rheologically simple material. Relaxation moduli at other temperatures are determined by replacing real time (i.e., time corresponding to the temperature of interest) with reduced time (i.e., time corresponding to the temperature at which the relaxation modulus is defined) according to the following equation (Bozhurt and Buttlar 2002):

$$\xi = \frac{t}{a_t} \qquad (2.10)$$

where:

ξ = reduced time

t = real time

a_T = temperature shift factor

In the next section, some of the material verification studies used in the finite element model will be described.

CHAPTER 3: MATERIAL VERIFICATIONS

3.1 Introduction

Material properties used in the Finite Element Model are critical to the accuracy of the model performance and behavior. Considerable effort during this study was spent on material verification and determination of suitable material models and properties for the various pavement materials that comprise the pavement system. The California Bearing Ratio (CBR) test was used to calibrate the model's material properties for the subbase, base and subgrade. The subgrade was tested to determine the elastic modulus that accurately depicts the real materials response to stress. The subbase and base have an assumed elastic modulus and the CBR test is used to find the corresponding friction and dilation angles. Viscoelastic and Drucker Prager material properties of the asphalt layer were calibrated with the results of the CBR tests. These simulations were used to identify the correct instantaneous elastic modulus and shift factor needed to allow the results to fit full-scale test data for viscoelasticity. They are also used to find the plasticity model parameters, which are a combination of elastic modulus, friction and dilation angle, and cohesion that will best fit the FAA Static Punch Test conducted March 2001. These verification studies will be further described in this section. In section 4.3, there is a comparison between the results of using viscoelasticity and the plasticity model.

3.2 California Bearing Ratio (CBR) Model

3.2.1 Background

The purpose of using California Bearing Ratio (CBR) test data is to determine the friction angle and dilation angle that will correspond to the given elastic modulus. Once the program is run, the amount of stress on the material after .1-inch penetration is determined and compared against material data sheets provided by the FAA.

3.2.2 Finite Element Model

The finite element model shown in figure 3.1 used for the CBR analysis has a diameter of 10 inches by 5 inches in depth. The element type chosen was quasi-three dimensional Fourier analysis elements (CAXA8R). These elements are used because of their ability to accurately predict the response of axially symmetric loaded models. The number of elements and nodes in the mesh are 185 and 6260 respectively.

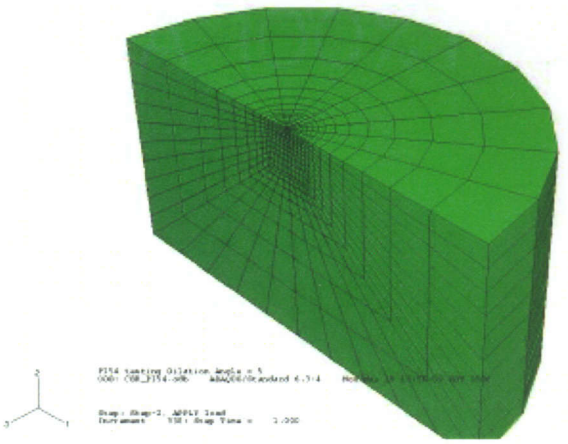

Figure 3.1: CBR Finite Element Mesh

To simulate the penetration of a piston onto a soil sample, a prescribed displacement was placed in the center of the mesh. This displacement was slowly incremented until it reached its final maximum of .2 inches. For this study, data was

taken at .1 inches of piston displacement. This study will be used to determine friction and dilation angle for the subbase, P-209 and base, P-154 materials. For each material type, every friction angle listed in table 3.1 is used with a dilation angle set to zero. The CBR value is calculated from each of these simulations and compared against the target CBR from the FAA material database. The friction angle that produces a lower CBR than the target is chosen as the friction angle. This friction angle now remains constant and the dilation angles of 0, 5 and 10 are inputted. The results of these CBR test simulations are compared once again to the target CBR value.

3.2.3 Material Properties Tested

Validation studies were conducted for each material type to verify the material properties. The material properties shown in Table 3.1 were taken from NAPTF laboratory testing.

Table 3-1: Material Properties for Material Verification

	Material			
Material Property	P-154	P-209	Dupont (Low)*	Dupont (Medium)*
Modulus, psi	20,000	40,000	3,000	11,000
Poisson's Ratio	0.35	0.3	0.45	0.45
Friction Angle	35,40,45,50	32,40,44,48,52	0	0
Dilation Angle	0,5,10	0,5,10	0	0
Cohesion, psi	6.4	5	**	**
Density, pcf	151	161	95	95

* Material Property values taken from Willis (2005).
** Stress-strain values were taken from Figure A.1 in the Appendix.

3.2.4 CBR Test Results

The results of the CBR testing are shown below.

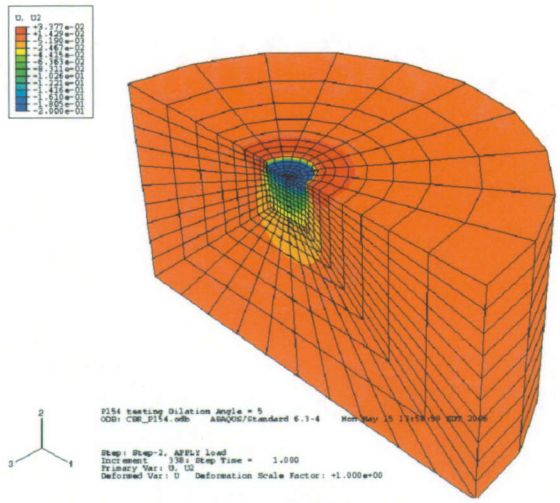

Figure 3.2: CBR Mesh after 0.2 inch Piston Penetration

Simulations were run for each of the friction angle values listed in table 3.1, while keeping dilation angle at zero. Table 3.2 shows the CBR results for base material P-209.

Table 3-2: Predicted vs. Measured CBR Values for P-209

Friction Angle	CBR at Displacement of .1 in
32	11.78
40	18.16
44	23.97
48	33.69
52	51.44
Target CBR:	44

Since dilation angle will only increase CBR by a few percent, the friction angle was determined to be between 48 and 52 degrees, which was averaged to 50 degrees. Using 50 degrees for the friction angle, dilation angles were varied to

determine CBR value close to that of the average value taken from the material data from the FAA.

Table 3-3: Predicted vs. Measured CBR Values for P-209 at a Friction Angle of 50

Dilation Angle	CBR at Displacement of .1 in
0	41.11
5	43.96
10	46.81
Target CBR:	44

Based on the above study, P-209 will now have a friction angle of 50 degrees, and a dilation angle of 5 degrees.

Table 3-4: Predicted vs. Measured CBR Values for P-154

Friction Angle	CBR at Displacement of .1 in
35	16.63
40	21.73
45	30.04
50	45.54
Target CBR:	33.1 - 40.6

A similar analysis was conducted for the P-154 subbase material. Table 3.4 summarizes the results of the study. From these results, a friction angle of 45 degrees was chosen. The dilation angle was changed to examine the sensitivity of the CBR values to the dilation angle.

Table 3-5: Predicted vs. Measured CBR Values for P-154 at a Friction Angle of 45

Dilation Angle	CBR at Displacement of .1 in
0	30.04
5	31.67
10	33.38
Target CBR:	33.1 - 40.6

Table 3.5 shows the results of the study, suggesting that the dilation angle should be 10 degrees, however a lower dilation angle was chosen of 5 degrees.

3.2.5 Conclusions of the Verification Studies using CBR Test Data

Table 3-6: Final Material Properties for P-209 and P-154

	Elastic Modulus (ksi)	Friction Angle	Dilation Angle
P-209	40	50	5
P-154	20	45	5

The results from the CBR modeling showed that the material properties being used were able to accurately capture the response of the material when subjected to the CBR test. Previous research conducted at Rowan suppressed dilation angle. This lead to the lack of upheaval seen in the pavement response, which is used to determine pavement failure.

3.3 Trench Model Background

FAA had completed an experiment in April of 2001 called the Static Punch test. Within this test, a trench was cut out of a medium strength subgrade flexible pavement section (MFC), and a 6-wheel B-777 gear configuration was placed approximately 20 inches away from the edge of the trench. The loading was gradually increased from zero to around 55 kips per wheel, and allowed to remain at this load for the remainder of the test. The deformation and force were recorded during the duration of the test. The results of this test help to verify the material properties for

the complete pavement structure, with material properties of each material ascertained through other FE models mentioned earlier. The goal of any model in finite element analysis is to have similar results to full-scale test data.

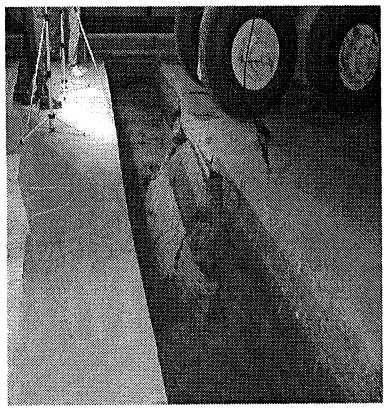

Figure 3.3: Picture of FAA's Static Punch Test 4/23/01

3.4 Viscoelasticity Model

3.4.1 Background

In order to describe the viscoelastic properties of asphalt, a Prony series expression is used. Table 3.6, taken from Bozhurt and Buttlar (2002), shows the starting point for this model. Even though the asphalt properties these numbers describe is one for highway surface layers and at a lower temperature than when full-scale testing was conducted at the NAPTF, it is still possible to use the data. For this study, it is assumed that for any type of asphalt the fraction of the total elastic modulus does not change for each spring constant. For example, the total elastic modulus for the PG 58-22 overlay mix is 3523.2 ksi and E_1=797.9 ksi. The fraction of the total modulus that E_1 has is approximately 26%; the same process is done for the other spring constants. A total elastic modulus can be assumed for the type of asphalt and can be divided among the spring constants by using the fraction previously calculated. The relaxation

times can be used as well, and will be altered using time-temperature superposition described previously in section 2.5.1.3.3.

Table 3-7: Prony Series Parameters for PG 58-22 Overlay Mix

Spring Constants (ksi)				
E_1	E_2	E_3	E_4	E_5
797.9	215.9	745.9	807.1	956.4
Relaxation Times, sec				
λ_1	λ_2	λ_3	λ_4	λ_5
8.1	101	826	6560	176087

3.4.2 Finite Element Model

Figure 3.4 shows the finite element model that was used to identify the instantaneous total elastic modulus as well as the shift factor required for the relaxation times to match the static punch test data from underneath the furthest wheel away from the trench. This wheel was chosen because it would have the least influence from the boundary conditions of the trench. It would almost act as if there was no trench at all.

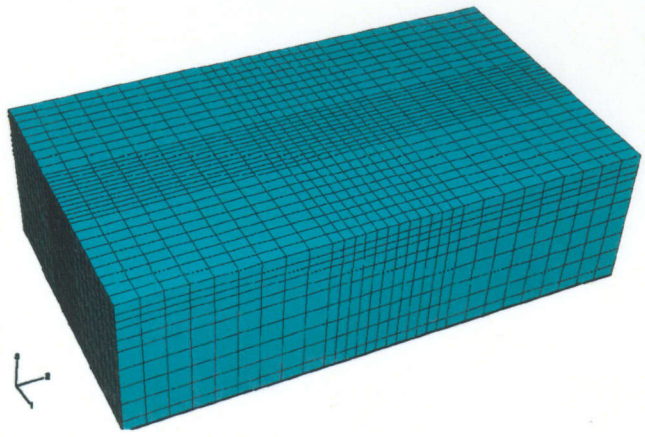

Figure 3.4: Viscoelasticity Finite Element Model

The dimensions of the model are 12 feet wide by 21 feet long by 6 feet deep, with an infinite layer of elements on the last 6 inches of pavement. The cross section matches that of a standard MFC pavement, which can be seen in figure 3.5. All the sides of the model are fixed in the x & y directions, and the bottom is fixed in the z-direction that is the vertical direction.

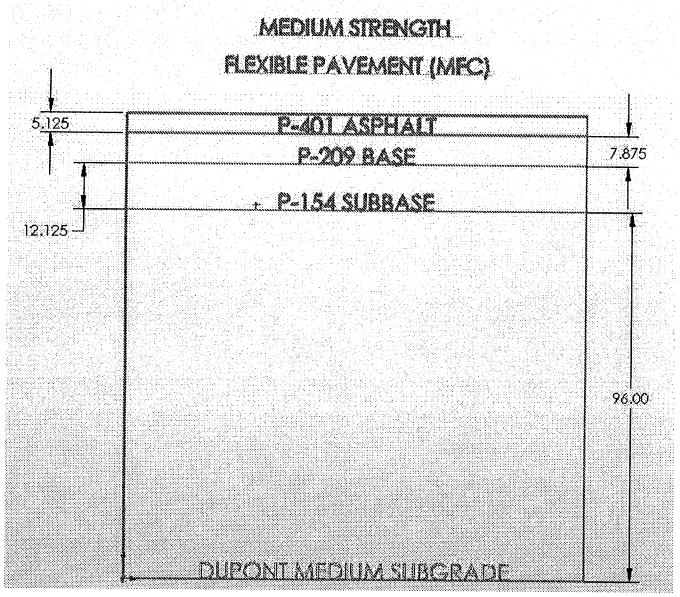

Figure 3.5: MFC Pavement Cross Section (dimensions in inches)

3.4.3 Material Properties

The only material properties that were varied throughout this study were in the P-401 layer (asphalt concrete); the other layer material properties remained constant, and are listed in Table 3.8.

Table 3-8: **Material Properties used in Viscoelastic Verification Model**

Material	Young's Modulus (ksf)	Friction Angle	Dilation Angle	Cohesion (ksf)	Density (kslug/ft$^{3)}$	Poisson's Ratio
P-209	5760	50	5	0.72	0.005	0.3
P-154	2880	45	5	0.9216	0.0047	0.35
Dupont Medium	1542	0.01	0.0067	2.52	0.0029	0.45

3.4.4 Loading

The loading of the model has a single wheel load directly in the center of the top surface, as seen in Figure 3.6. The load follows the same pattern as the FAA Static punch test described previously.

3.4.5. Results

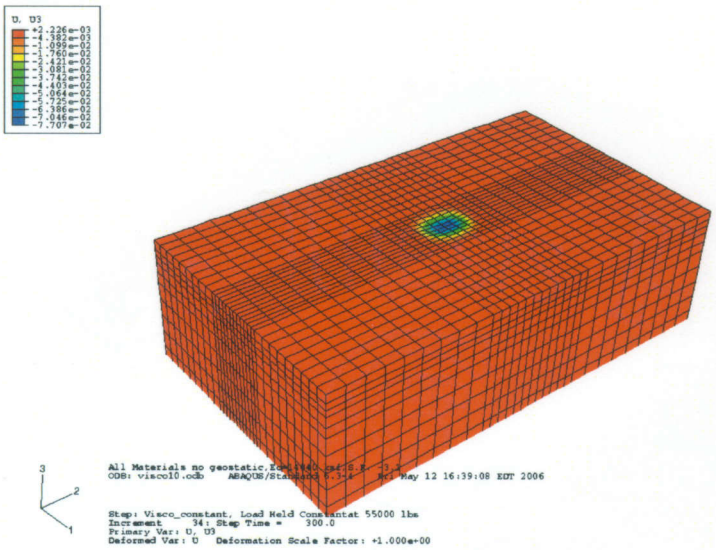

Figure 3.6: Viscoelasticity Model after Loading

After the program was run, the deflection versus time was compared to the full-scale testing data. The instantaneous elastic modulus as well as the shift factor for the relaxation times could be altered so that the simulation test data obtained could be matched up with the trench test data.

Figure 3.7 depicts the results of an initial elastic modulus value of 200 ksi and a shift factor of –3.3.

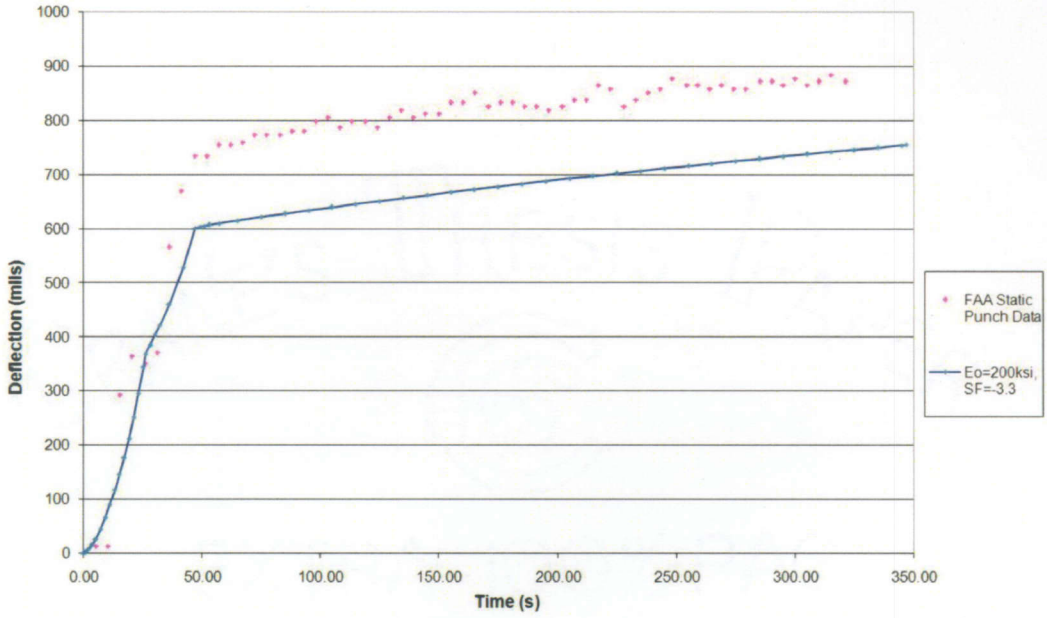

Figure 3.7: Viscoelasticity Verification: Deflection versus Time

When interpreting this graph, it can be seen that the material properties are too stiff to match the FAA data. However, when the elastic modulus value is lowered, the shift factor needs to be altered as well, even though it looks as if the slope of the line follows the deflection quite well. This model was run until the results almost matched perfectly to that of the FAA data (figure 3.8).

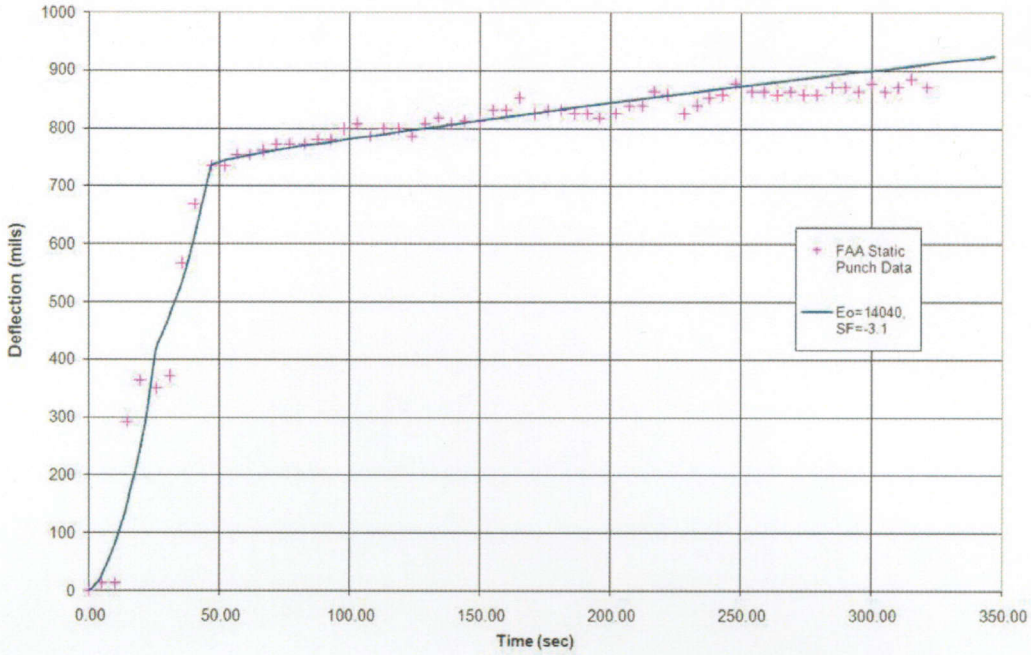

Figure 3.8: Viscoelasticity Verification: Deflection versus Time, Final Results

3.4.6 Viscoelasticity Conclusions

The table below shows the final Prony series parameters that describe the asphalt concrete's viscoelastic properties. These values will be used in chapter 4 section 3 static loading of LFC and MFC pavement.

Table 3-9: Prony Series Parameters for P-401 Asphalt Concrete

Spring Constants (ksf)				
E_1	E_2	E_3	E_4	E_5
3173	856	2976	3215	3805
Relaxation Times, sec				
λ_1	λ_2	λ_3	λ_4	λ_5
0.00643	0.08023	0.65612	5.2108	139.87

3.5 Drucker Prager Material Properties Testing for P-401

3.5.1 Model and Material Properties Tested

The determination of the Drucker Prager material properties for the asphalt layer, P-401 followed the same steps as that for the viscoelasticity model described earlier. The baseline material properties were established at 500 ksi for elastic modulus, friction angle of 20 degrees, dilation angle of 13.3 degrees, and cohesion of 80 psi. The subsequent variations changed only one property at a time to determine the effects of altering each one. Table 3.10 shows the properties for each test.

Table 3-10: Material Properties Tested

Test	Elastic Modulus (ksf)	Friction Angle	Dilation Angle	Cohesion (ksf)
DPtest1	72000	20	13.3	11.52
DPtest2	108000	20	13.3	11.52
DPtest3	72000	20	13.3	7.2
DPtest4	72000	20	5	11.52
DPtest5	72000	30	13.3	11.52
DPtest6	72000	20	5	3.6
DPtest7	72000	20	5	5.04
DPtest8	72000	20	5	4.32

Once run, the deflection versus loading was compared to the FAA Static punch test. Figure 3.9 shows the results from each model run.

3.5.2 Results

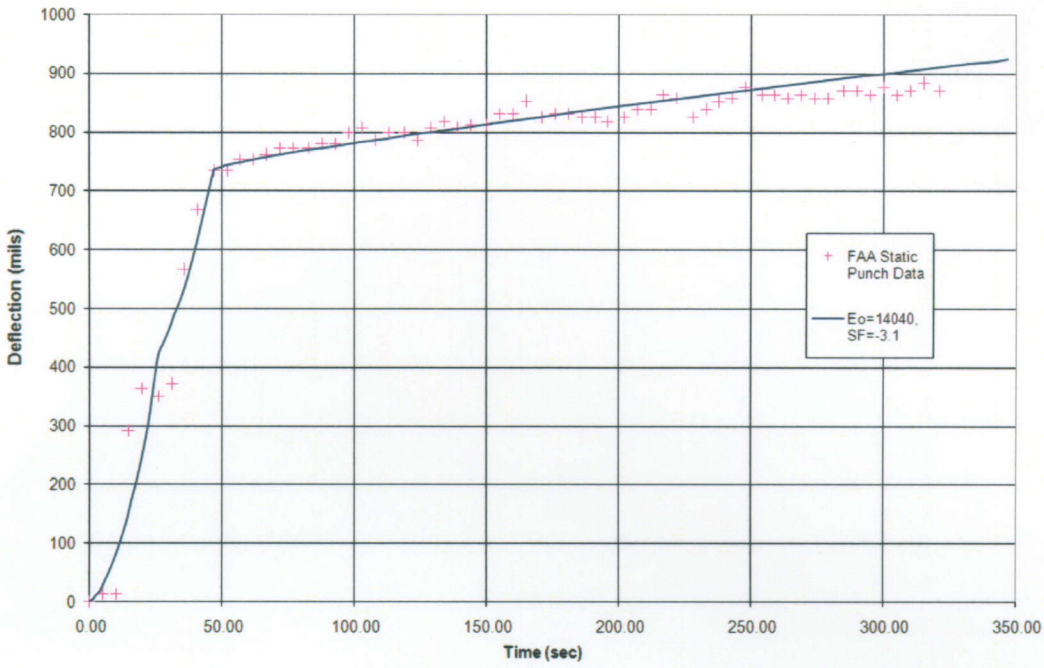

Figure 3.9: Drucker Prager Verification: Deflection versus Time, Final Results

3.5.3 Conclusions

The final material properties of the Drucker Prager testing for all the layers that are used in the main study are listed in Table 3.11.

Table 3-11: Final Drucker Prager Material Properties

Material	Young's Modulus (ksf)	Friction Angle	Dilation Angle	Cohesion (ksf)	Density (kslug/ft^3)	Poisson's Ratio
P-401 - Drucker Prager	72000	20	5	4.32	0.005	0.3
P-209	5760	50	5	0.72	0.005	0.3
P-154	2880	45	5	0.9216	0.0047	0.35
Dupont Medium	1542	0.01	0.0067	2.52	0.0029	0.45
Dupont Low	432	0.01	0.0067	4.608	0.003	0.45

3.6 Material Verification Conclusions

From studying the graphs in Figure 3.9, it can be concluded that the material properties chosen from these material verification studies, do predict the shape of the response similar to that of the full scale testing done at the FAA tech center. From the conclusion of these studies, it is now possible to move onto the main study of this thesis.

CHAPTER 4: MAIN STUDY

4.1 Introduction

The main purpose of this chapter is to determine the effects of wander and wheel configuration on conventional base, flexible pavement. To do this, material properties were tested and matched to actual data, which can be seen in chapter 3 verification studies. Chapter 3 verification studies calibrated plasticity properties of each layer of the pavement as well as the viscoelastic properties of the asphalt layer. Table 4.1 and 4.2 list the material properties used for the various layers of low (LFC) and medium (MFC) strength flexible pavements, which will be used for analysis in the upcoming sections. Table 4.1 contains all the properties needed for the Drucker Prager plasticity model. Table 4.2 uses the Prony series to describe the degradation of the elastic modulus of a viscoelastic material for the surface asphalt layer.

Table 4-1: Drucker Prager Material Properties

Material	Young's Modulus (ksf)	Friction Angle	Dilation Angle	Cohesion (ksf)	Density (kslug/ft^3)	Poisson's Ratio
P-401 - Drucker Prager	72000	20	5	4.32	0.005	0.3
P-209	5760	50	5	0.72	0.005	0.3
P-154	2880	45	5	0.9216	0.0047	0.35
Dupont Medium	1542	0.01	0.0067	2.52	0.0029	0.45
Dupont Low	432	0.01	0.0067	4.608	0.003	0.45

Table 4-2: Prony Series (Viscoelastic) Material Properties for the P-401 Layer

Spring Constants (ksf)				
E_1	E_2	E_3	E_4	E_5
3173	856	2976	3215	3805
Relaxation Times, sec				
λ_1	λ_2	λ_3	λ_4	λ_5
0.00643	0.08023	0.65612	5.2108	139.87

These properties are used in two different sets of simulations. The first set of simulations consider one, four, and six wheel loads on both LFC and MFC pavements

to test the effects of wheel configuration. Within this set, the pavement sections use Drucker-Prager, viscoelastic and linear elastic material properties for the asphalt (P-401) layer and linear elastic material model for all layers. These results are compared to study the effect of using viscoelastic, Drucker Prager and linear elastic material properties. The second set of simulations tests the effects of both wheel configuration and wander. These simulations use the same material model for the pavement structure, namely the Drucker Prager; however the loading is different. One of the subsets utilizes only one wheel with and without wander and the other is a four wheel configuration with and without wander. The first comparison is one wheel with and without wander. Only one wheel is used because it will isolate the effects of wander by eliminating the effects of wheel configuration. The second comparison is four wheels with and without wander. This test combines both the effect of wheel configuration and wander under quasi-static loading. The third comparison uses the data from one and four wheels with and without wander to investigate how plastic and elastic strain in the subgrade increases as the number of cycles increase. The last comparison uses the results from one and four wheels without wander to investigate rutting and the contribution of each layer to the total permanent deformation. Due to the limitations of computing power available presently, Drucker Prager material properties for the asphalt concrete layer (P-401) are used in the second set of simulations.

4.2 Static Wheel Configuration Models

4.2.1 Background

One, Four and Six wheels are statically loaded onto both low and medium strength pavement with viscoelastic properties for the asphalt layer. Static loading in this case means that the load remains on the same footprint through the simulation, not that the load remains constant. These programs are then run again with Drucker Prager plasticity properties for the asphalt layer. The entire model afterwards is then modeled as linear elastic to allow for comparison as to the benefits and drawbacks for each material property model. The purpose of these simulations is to investigate the effects of wheel configuration on LFC and MFC pavement. The loading mimics that of the static punch test; Geostatic forces are also programmed into the simulations to estimate the amount of settlement of the pavement after construction. After the program finished, various parameters such as stress, deflection, and strain were taken along the line of the loading at different depths of the pavement structure.

4.2.2 Loading

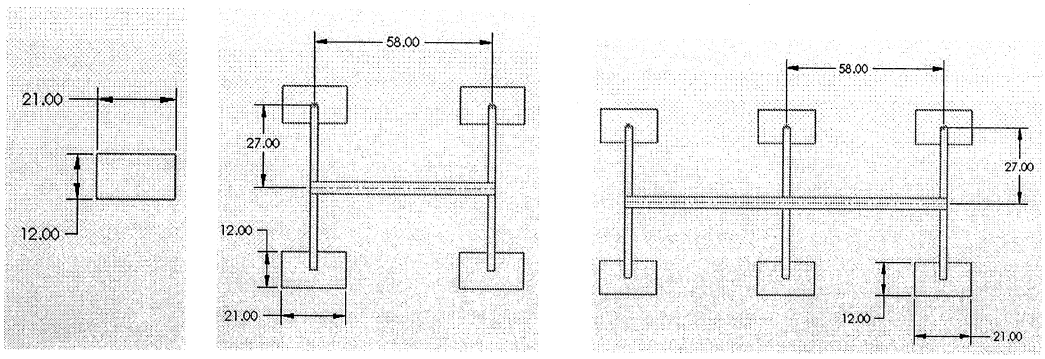

Figure 4.1(a), (b) and (c): One, Four and Six Wheel Footprints used in Main Study Simulations

Figure 4.1a, b, and c display the dimension, in inches, used to simulate the wheel footprints of one, four and six wheel configurations. These wheel configurations are used throughout this chapter for aircraft loading.

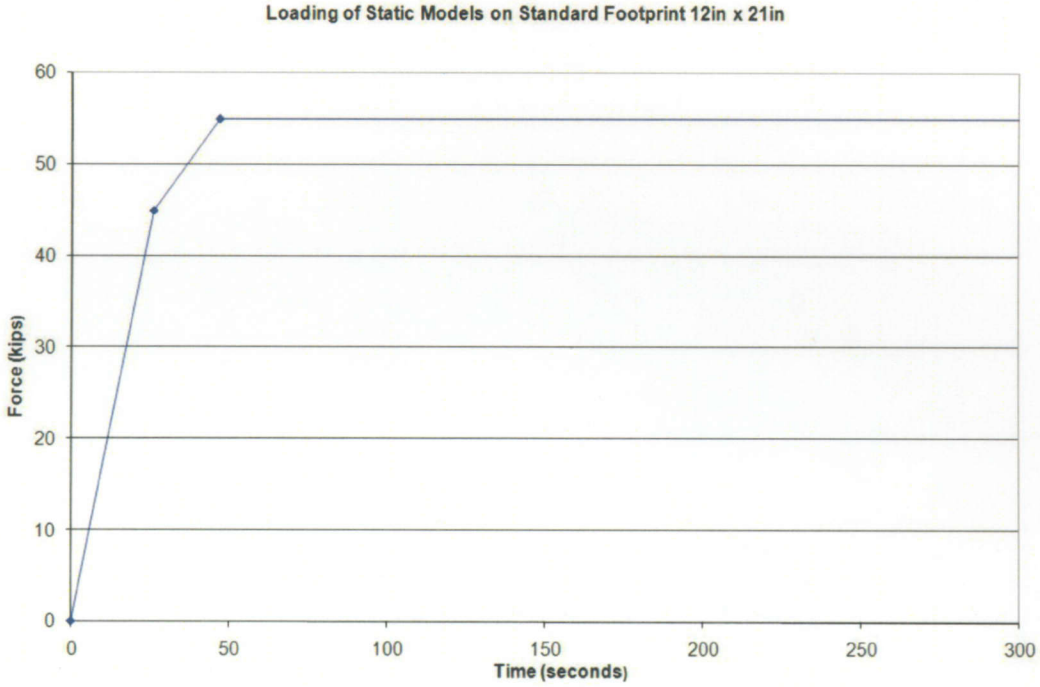

Figure 4.2: Loading on Static Models

Figure 4.2 shows the loading for the static models. The force is distributed over a standard footprint size of 12 inches by 21 inches. The maximum loading for these models is 55 kips, which is the same loading as the static punch test. Even though this loading is only in two steps, it is enough to see plastic deformation. Drucker-Prager model is only stress dependent, so when the model reaches its maximum loading, any permanent deformation can be seen. Since Viscoelasticity is time dependent, the maximum loading is held for some time to allow for permanent deformation to occur.

4.2.3 FE Model

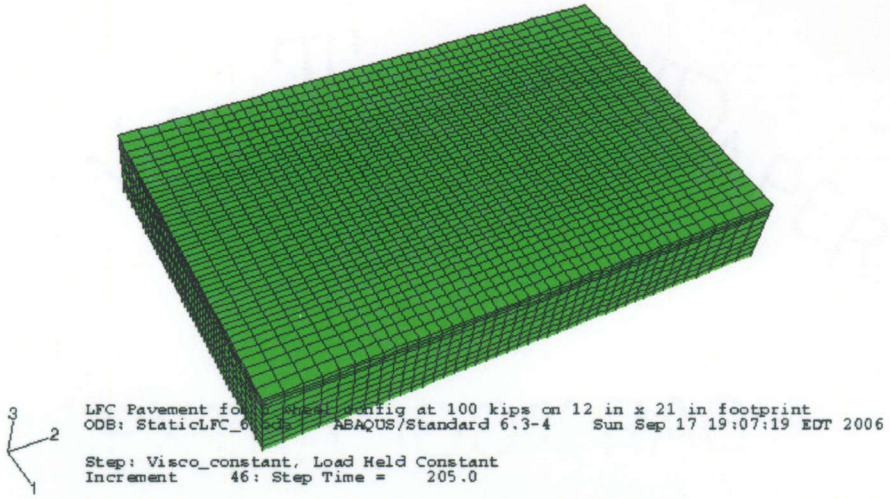

Figure 4.3: LFC Pavement used in Static LFC Simulation

Figure 4.3 shows the finite element model used in the static loading of LFC pavement under one, four and six wheel configurations. The cross section of the pavement structure is shown in figure 4.4. There are 16,632 C3D8R elements, which are three dimensional, eight noded reduced integration finite elements, and 21,285 nodes. There are also 1848 of CIN3D8 elements along the bottom layer of the model, which are three dimensional infinite elements with eight nodes. Infinite elements were used to reduce the size of the model to save memory and run time.

P-401 Asphalt	Layer 1 (5 in)
P-209 Base	Layer 2 (4 in)
	Layer 3 (4 in)
P-154 Subbase	Layer 4 (9.25 in)
	Layer 5 (9.25 in)
	Layer 6 (9.25 in)
	Layer 7 (9.25 in)
Dupont Low Subgrade	Layer 8 (8 in)
	Layer 9 (8 in)
	Infinite Element Layer (6 in)

Figure 4.4: Cross Section of LFC Pavement

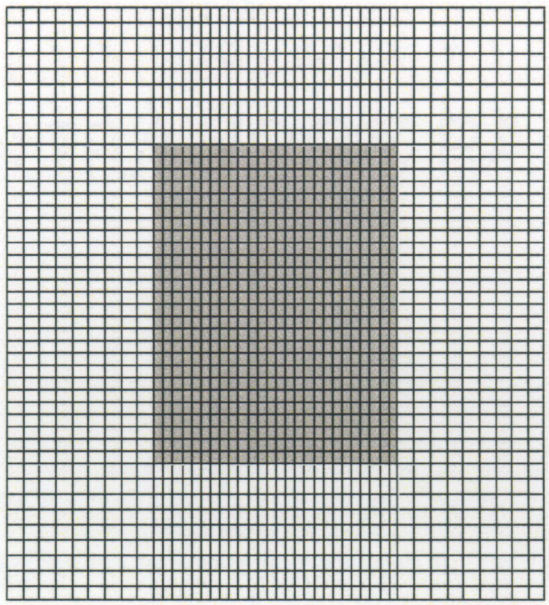

Figure 4.5: Element Dimensions used in Static LFC and MFC Pavements

Figure 4.5 shows the top surface of the finite element model used in the static LFC and MFC pavements. The highlighted center section has elements with dimensions of six inches by 10.5 inches, which translates to four elements comprising each wheel footprint.

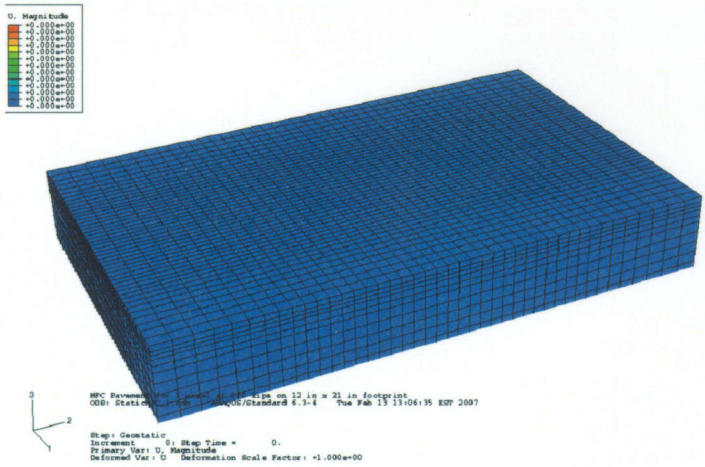

Figure 4.6: MFC Pavement used in Static MFC Simulation

Figure 4.6 shows the finite element model used in the static loading of MFC pavement under one, four and six wheel configurations, the cross section for which can be seen in figure 4.7. There are 16,632 C3D8R elements, which are three dimensional, eight noded reduced integration finite elements. There are also 1848 CIN3D8 elements along the bottom layer of the model, which are three dimensional infinite elements with eight nodes.

P-401 Asphalt	Layer 1 (5.125 in)
P-209 Base	Layer 2 (3.9 in)
	Layer 3 (3.9 in)
P-154 Subbase	Layer 4 (6 in)
	Layer 5 (6 in)
Dupont Medium Subgrade	Layer 6 (10.25 in)
	Layer 7 (10.25 in)
	Layer 8 (10.25 in)
	Layer 9 (10.25 in)
	Infinite Element Layer (6 in)

Figure 4.7: Cross Section of MFC Pavement

4.2.4 Results

Figure 4.8, shows the von Mises stress after loading of six wheels on LFC pavement, while using viscoelastic properties in the asphalt layer. The line shown in that figure is where data was extracted from the output files.

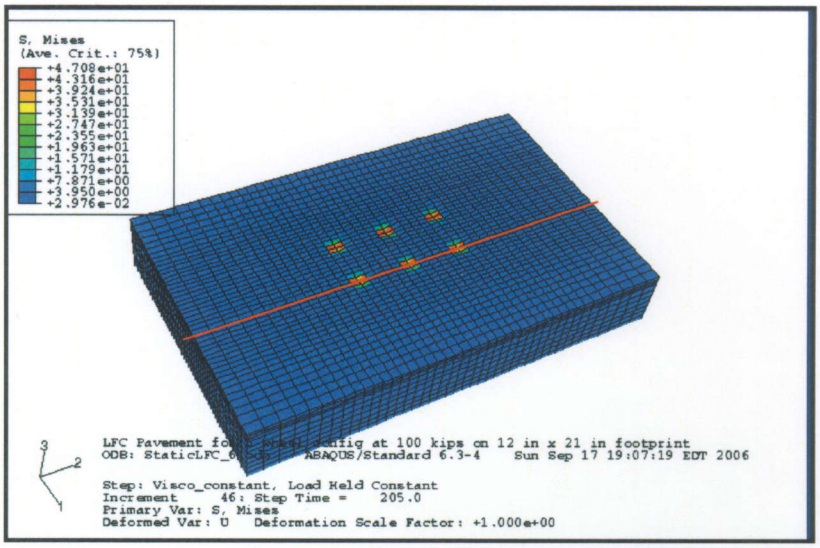

Figure 4.8: Static Model of LFC Pavement using Six Wheel Configuration Loading

The data that was collected for this simulation was taken while the pavement was still loaded at 55 kips and at 300 seconds. The results section will be formatted in the following manner. The deflection in the asphalt layer will be discussed first. The pavement type, either low or medium strength flexible pavement, will further divide the section and each graph of the material property models showing the pavement responses will be presented. Vertical stress and vertical plastic strain in the subgrade will be discussed second and third respectively and will be subdivided in the same manner as deflection in the asphalt layer.

4.2.4.1 Deflection in the Asphalt Layer

Deflection in the asphalt layer is an important pavement response to monitor because it is used as the failure criteria for flexible pavement. Permanent deformation in the asphalt layer is limited to 1 inch of surface upheaval adjacent to the traffic lane (Hayhoe and Garg 2002). The purpose of this section is to find which wheel

configuration will lead to the pavement failing more quickly by imparting more deformation in the asphalt layer.

4.2.4.1.1 Deflection in the Asphalt Layer: LFC Pavement

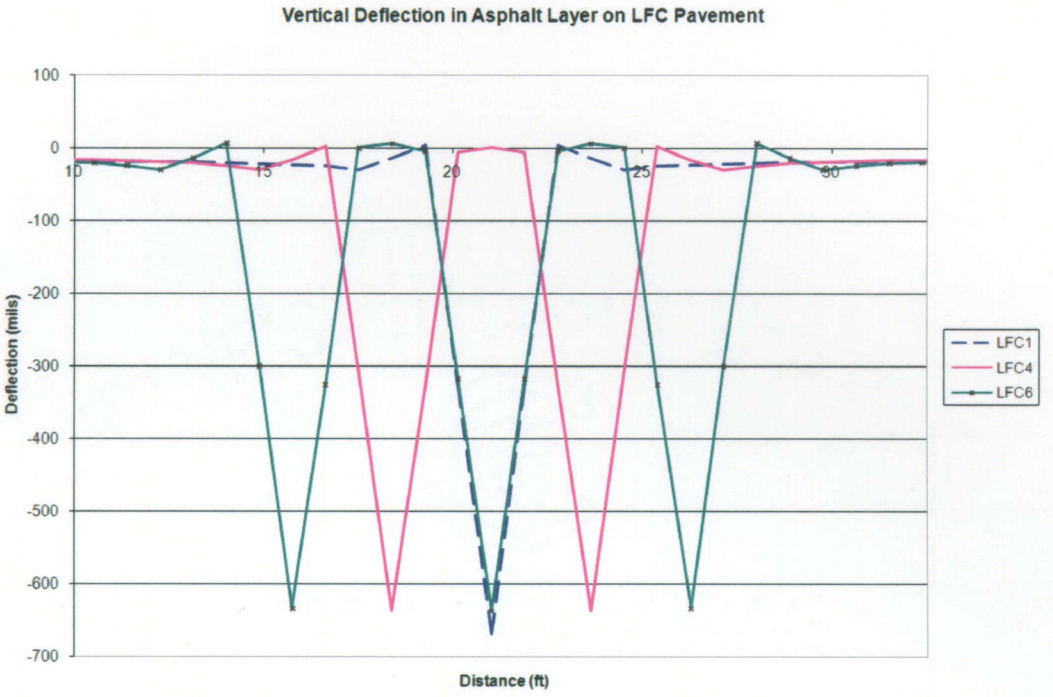

Figure 4.9: LFC Pavement with Viscoelastic Properties - Deflection in Asphalt Layer

Figure 4.9 shows the vertical deflection of the asphalt layer under the line of loading from one, four, and six wheel configurations. From analyzing the figure above, several observations can be made. When comparing one and four wheels to six, one wheel's maximum upheaval is 58% of six wheels and four wheels is 43% of six wheels. Also the one wheel gear configuration has a 5% higher maximum deflection as compared to the other two wheel configurations.

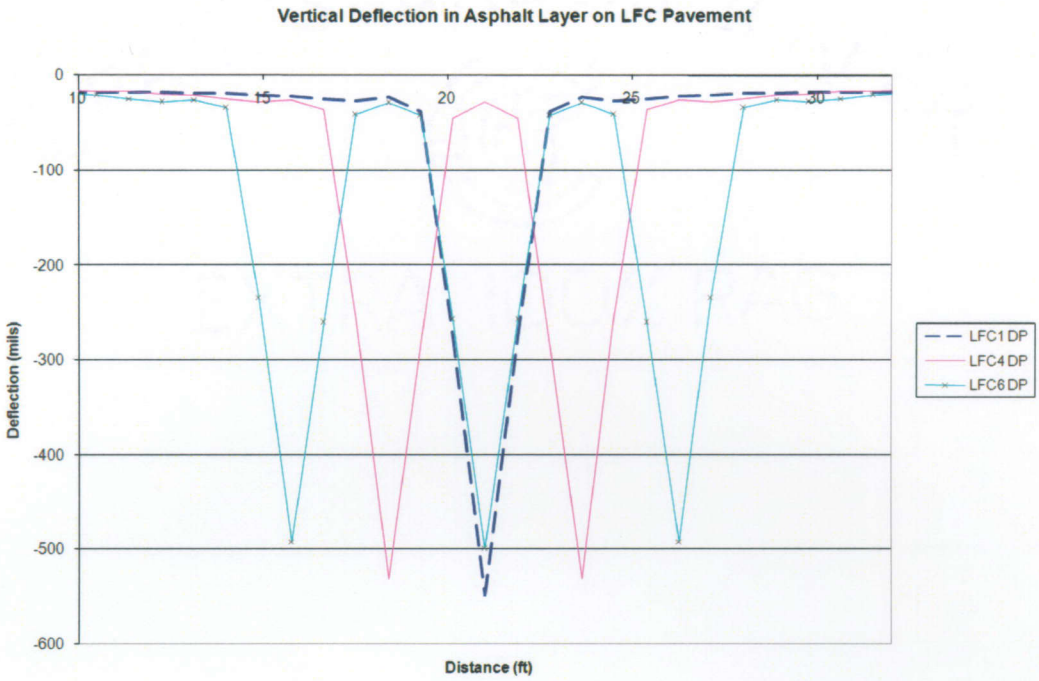

Figure 4.10: LFC Pavement with Drucker Prager Properties- Deflection in Asphalt Layer

Figure 4.10 shows the deflection in the asphalt layer on LFC pavement using Drucker Prager for all layers. Six wheel configuration upheaval is 10% higher than one wheel's upheaval and is equal to four wheel upheaval. Also one wheel has 10% higher maximum deflection compared to six wheels and four wheels is 6% higher than six wheels.

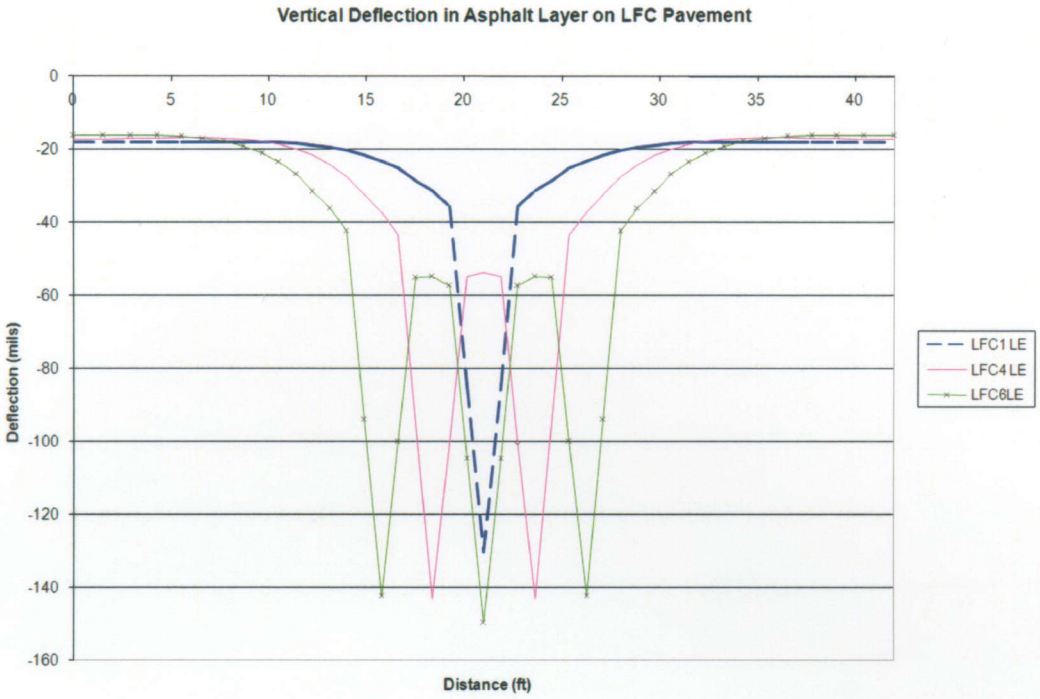

Figure 4.11: LFC Pavement with Linear Elastic Properties-Deflection in Asphalt Layer

Figure 4.11 shows the vertical deflection in the asphalt layer assuming that all the pavement layers are purely linear elastic. The graph above does not predict any upheaval in any of the wheel configurations. The maximum deflection is predicted to be greatest under six wheels. In comparison four wheels is 4% lower than six and one wheel is 13% lower.

4.2.4.1.2 Deflection in the Asphalt Layer: MFC Pavement

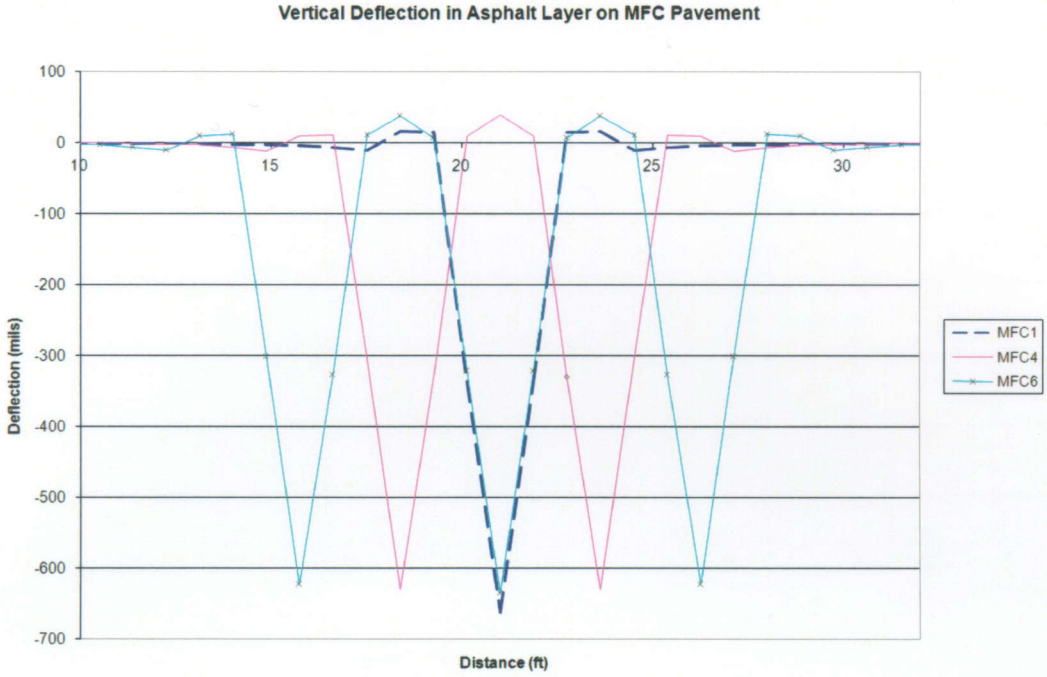

Figure 4.12: Vertical Deflection on Top Surface on MFC Pavement

Figure 4.12 shows the vertical deflection of the asphalt layer for one, four, and six wheel configurations on MFC pavement using viscoelastic properties for the asphalt layer. One wheel's upheaval is 46% of six wheel upheaval and 106% of six wheels upheaval is equal to the four wheel upheaval. Also, one wheel has a 4% higher maximum deflection as compared to the other two wheel configurations.

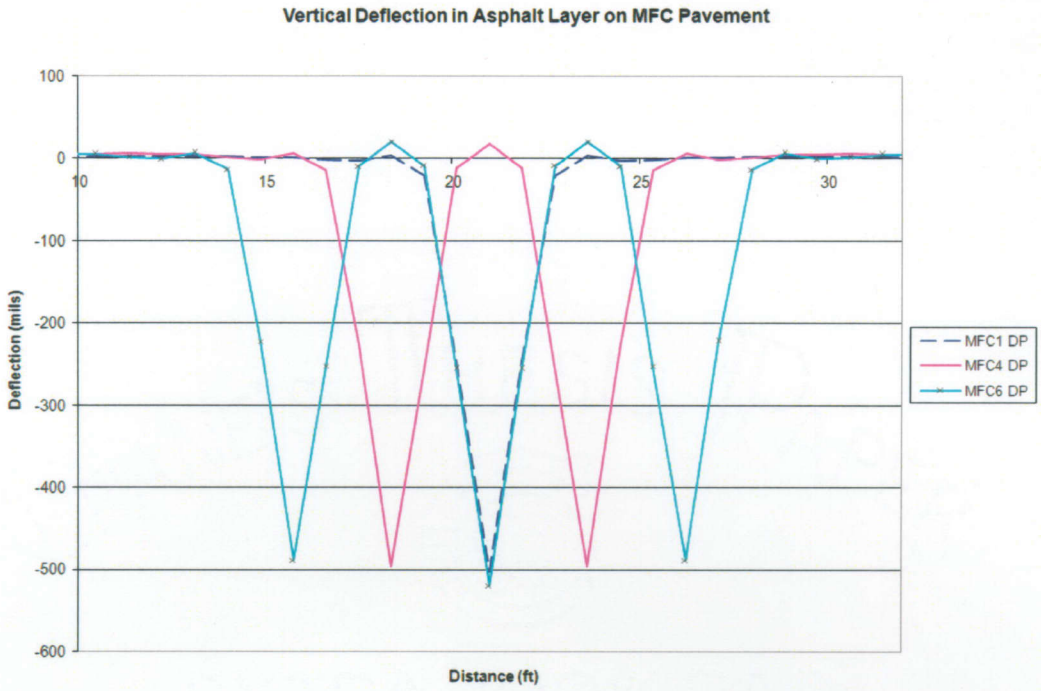

Figure 4.13: MFC Pavement with Drucker Prager Properties- Deflection in Asphalt Layer

Figure 4.13 shows the comparison of deflection in the asphalt layer on MFC pavement under one, four and six wheel loading. Six wheel configuration's upheaval is 82% higher than one wheel's upheaval and only 12% higher than four wheels. Also six wheels have 5% higher maximum deflection as compared to one wheel and is 3% higher than four wheels.

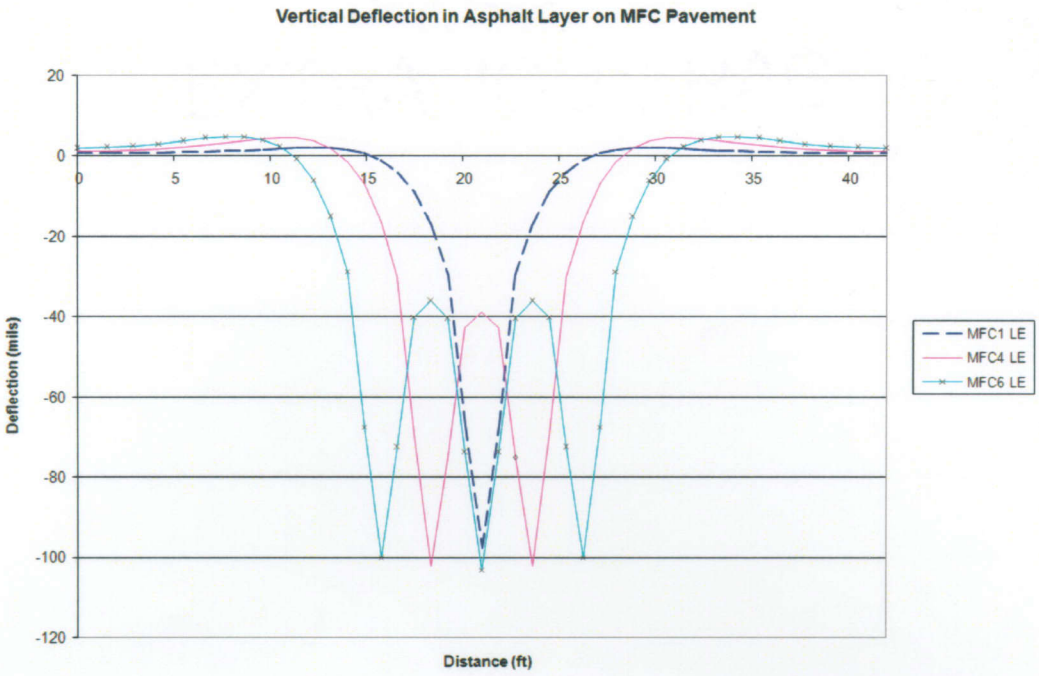

Figure 4.14: MFC Pavement with Linear Elastic Properties- Deflection in Asphalt Layer

Figure 4.14 shows the vertical deflection in the asphalt layer assuming that all the pavement layers are purely linear elastic. The graph above does not predict any upheaval in any of the wheel configurations. The maximum deflection is predicted to be greatest under six wheels. One wheel is 95% of six wheel maximum deflection and four wheel configuration is only 1% less than six wheels.

4.2.4.2 Vertical Stress in the Subgrade Layer

From section 2.2.1 on the CBR method, it is assumed that the way in which failure of a pavement occurs is by overstressing the subgrade which causes surface rutting. In this section various wheel configurations are analyzed on different pavement structures which will allow the amount of stress imparted on the subgrade to be estimated.

4.3.4.2.1 Vertical Stress in the Subgrade Layer: LFC Pavement

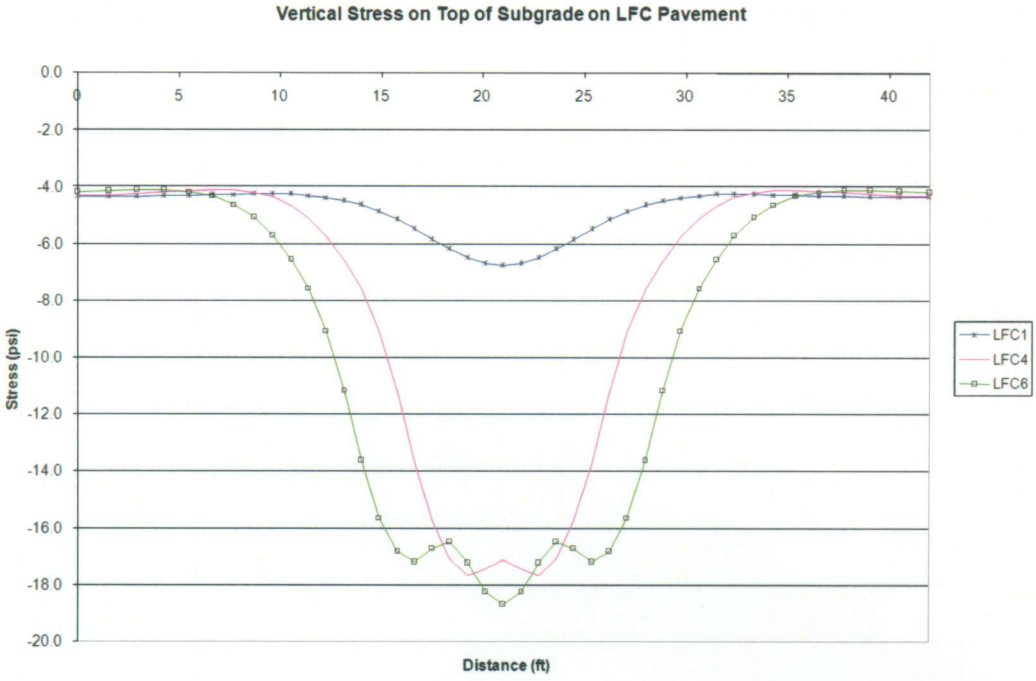

Figure 4.15: LFC Pavement with Viscoelastic Properties- Vertical Stress in Subgrade

Figure 4.15 shows the comparison of the different wheel configuration on LFC pavement with regards to vertical stress in the subgrade layer using viscoelasticity in the asphalt layer. From this graph, one wheel imparts only 36% of stresses generated by the six wheel configuration and four wheels impart 95% of six wheels.

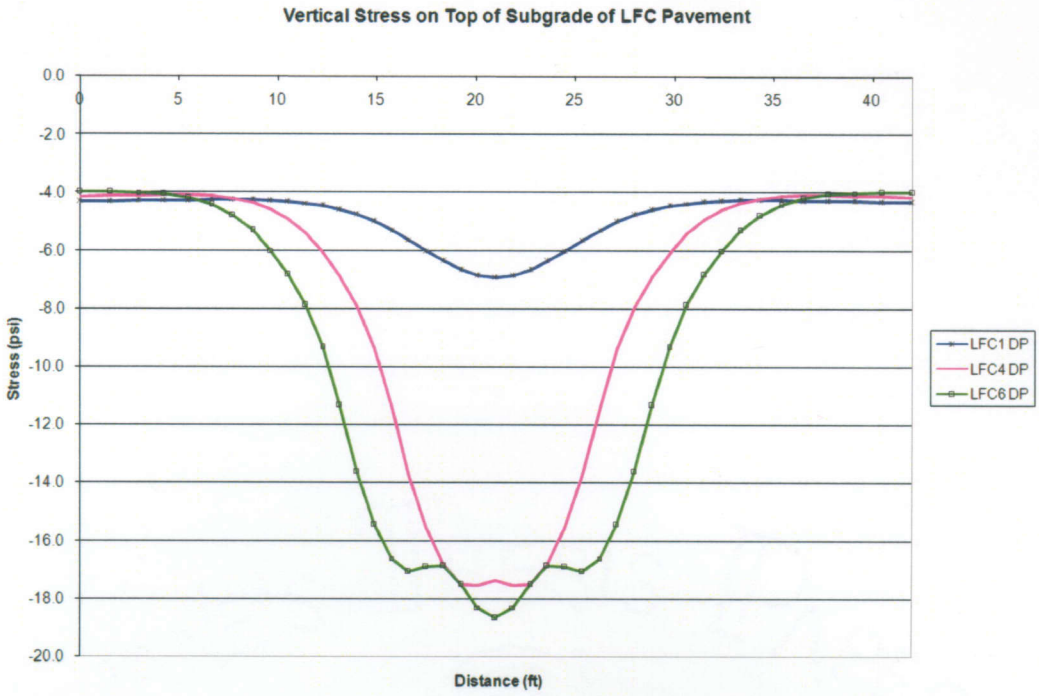

Figure 4.16: LFC Pavement with Drucker Prager Properties- Vertical Stress in Subgrade

Figure 4.16 shows the vertical subgrade stress under different wheel configuration on LFC pavement using Drucker Prager in the asphalt layer. In analyzing this graph, one wheel imparts only 37% of six wheel configuration and four wheels impart 94% of six wheels.

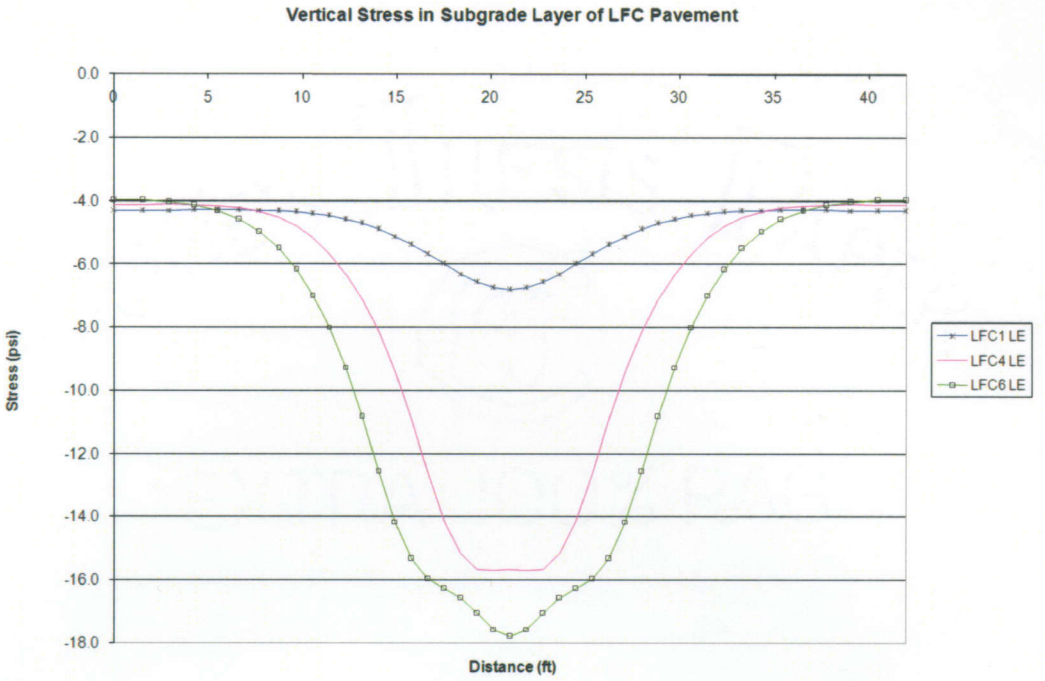

Figure 4.17: LFC pavement LE- Vertical Stress in Subgrade

Figure 4.17 shows the comparison of vertical stress in the subgrade under the different wheel configuration on LFC pavement. From this graph, one wheel imparts only 38% of six wheel configuration and four wheels impart 88% of six wheels.

4.2.4.2.2 Vertical Stress in the Subgrade Layer: MFC Pavement

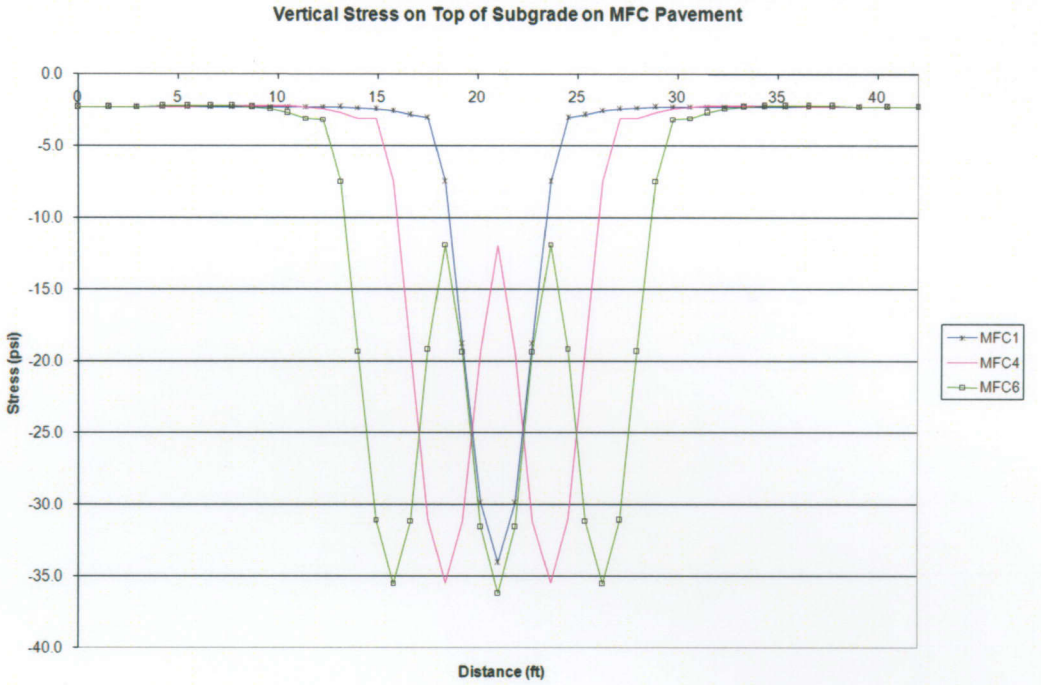

Figure 4.18: Vertical Subgrade Stress on MFC Pavement

Figure 4.18 displays the vertical stress in the subgrade from one, four and six wheel configurations on MFC pavement. This figure shows that one wheel imparts 94% of six wheel configuration and four wheels impart 98% of six wheels.

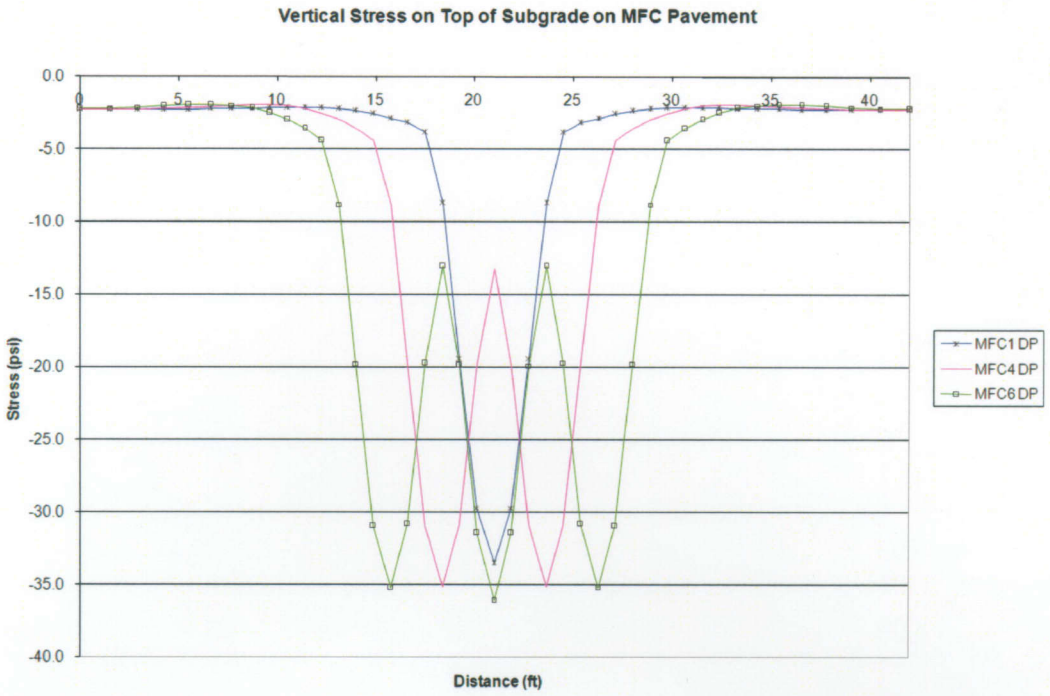

Figure 4.19: MFC Pavement with Drucker Prager Properties- Vertical Stress in Subgrade Layer

Figures 4.19 shows the comparison of one, four, and six wheel configuration on MFC pavement with respect to vertical stress in the subgrade layer using Drucker Prager properties in all layers. Six wheels impart 7% more stress than one wheel and 3% more stress than four wheels.

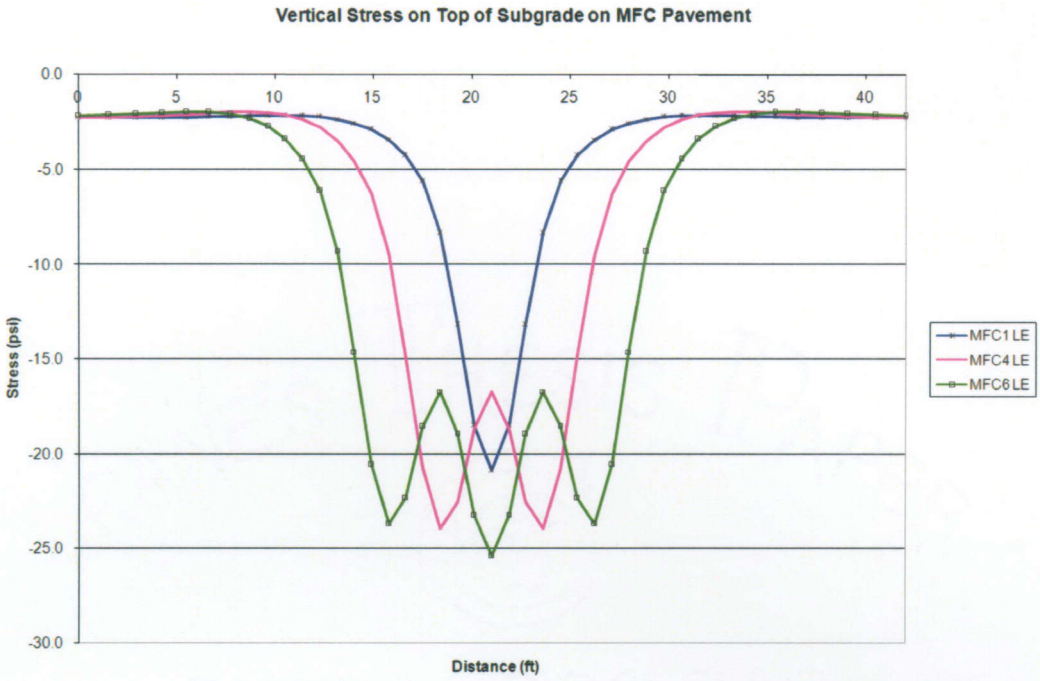

Figure 4.20: MFC pavement LE- Vertical Stress in Subgrade

Figure 4.20 is the comparison of the vertical stress in the subgrade under the various wheel configurations on MFC pavement assuming linear elastic material properties in each layer. Approximately 6% more stress is transmitted to the subgrade with six wheels than four wheels, and one wheel imparts only 82% of the total stress that six wheels does.

4.2.4.3 Vertical Plastic Strain in the Subgrade Layer

Vertical plastic strain is another way to determine failure of a pavement. When a pavement is overstressed, it causes permanent deformation which can be measured. It is important to note, however, that plastic strain in the subgrade can only be compared between the two models that use viscoelasticity and Drucker Prager material properties for the asphalt layer, due to the inherent nature of the linear elastic model.

4.2.4.3.1 Vertical Plastic Strain in the Subgrade Layer: LFC Pavement

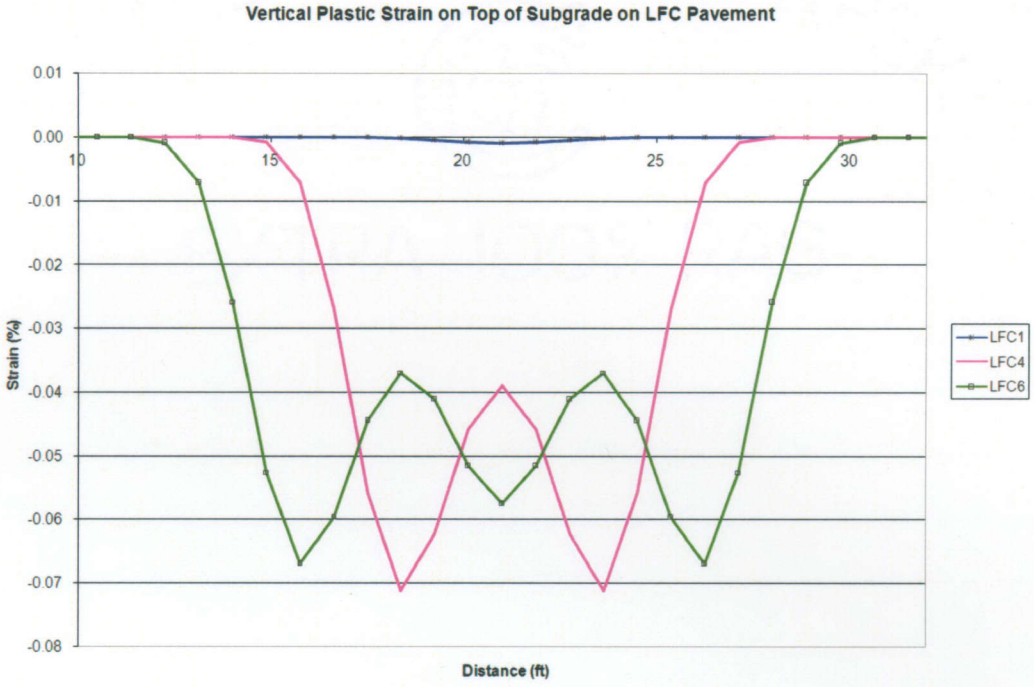

Figure 4.21: LFC Pavement with Viscoelastic Properties: Vertical Plastic Strain on Top of Subgrade

Figures 4.21 shows the plastic strain in the low strength subgrade under the three types of wheel configurations using viscoelasticity in the asphalt layer. One wheel shows the least amount of strain in the subgrade with approximately only 1% of six wheels and four wheels impart 6% more plastic strain into the subgrade than six wheels.

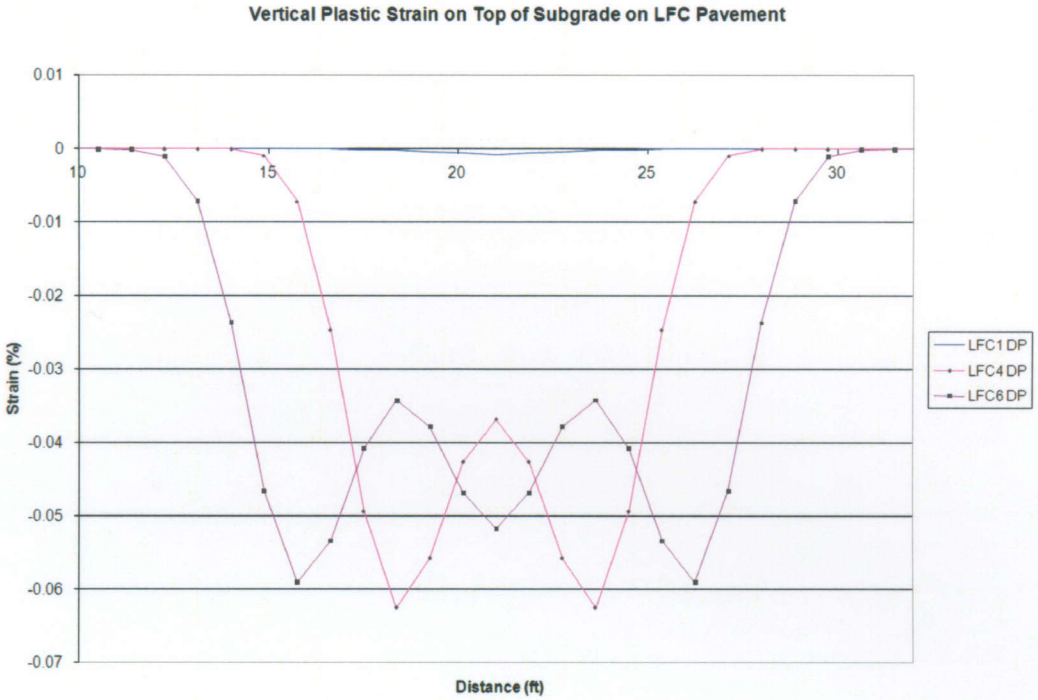

Figure 4.22: LFC Pavement with Drucker Prager Properties: Vertical Plastic Strain on Top of Subgrade

Figures 4.22 shows the plastic strain in the low strength subgrade under the three types of wheel configurations using Drucker Prager in all layers. One wheel is predicted to produce the least amount of strain in the subgrade with only 1% of six wheels and four wheels impart 6% more plastic strain into the subgrade than six wheels.

4.2.4.3.2 Vertical Plastic Strain in the Subgrade Layer: MFC Pavement

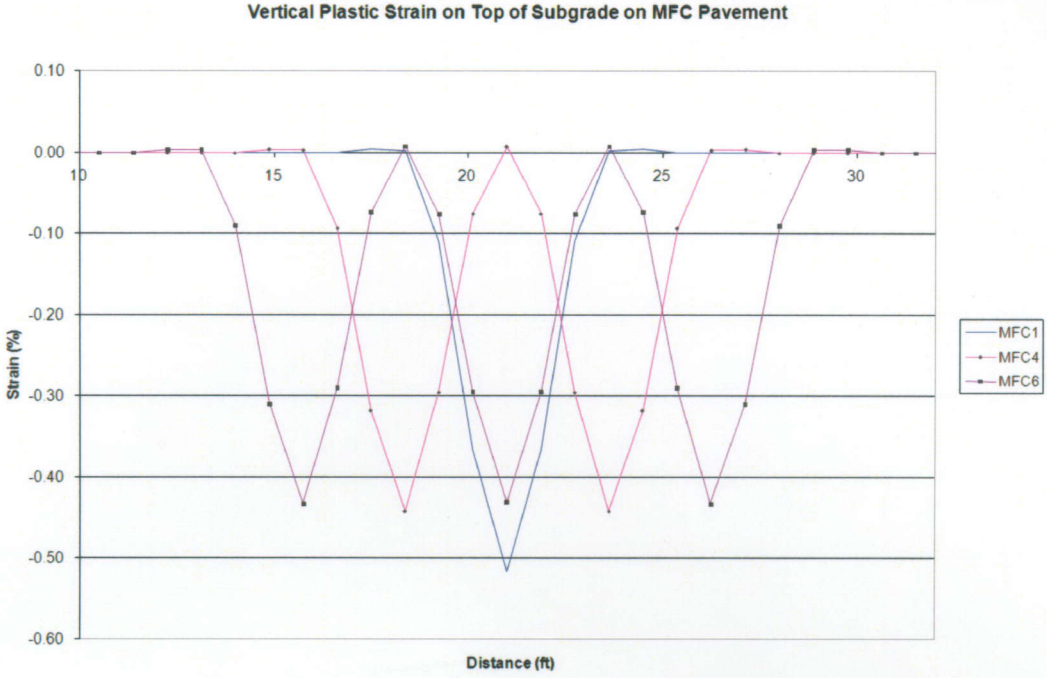

Figure 4.23: Vertical Plastic Strain in Subgrade on MFC Pavement

Figures 4.23 shows the plastic strain under various the three types of wheel configuration on MFC pavement using viscoelasticity in the asphalt layer. One wheel is predicted to cause 19% more plastic strain than six wheels and four wheels impart 2% more plastic strain into the subgrade than six wheels.

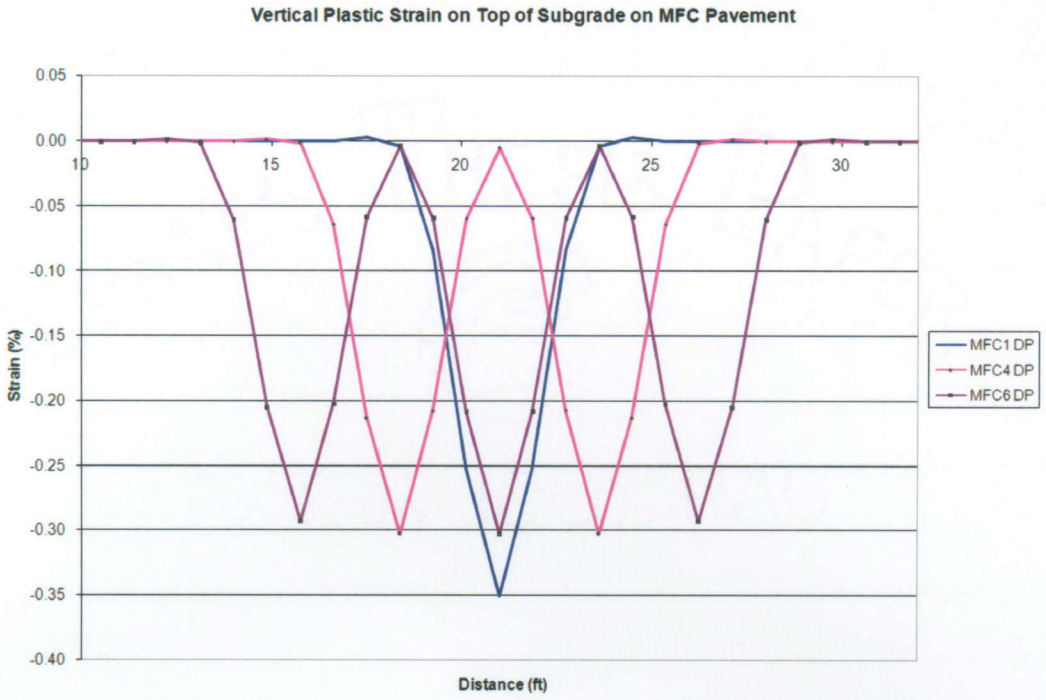

Figure 4.24: MFC Pavement with Drucker Prager Properties: Max Plastic and Elastic Strain in Subgrade and Asphalt Layers

Figure 4.24 shows the plastic strain in the subgrade on MFC pavement using Drucker Prager in all layers. One wheel is predicted to cause 16% more plastic strain than four and six wheels.

4.2.5 Impact of Material Model

In determining the effects of trafficking on pavement several responses are measured, such as deformation in the asphalt layer, vertical stress and plastic strain in the subgrade. The previous section three material models were tested to determine which material properties would give the data needed to predict pavement damage and possibly pavement failure. The first material model used a plasticity model for the lower three layers and viscoelasticity in the asphalt layer. Viscoelasticity can account

for how asphalt behaves when temperature rapidly changes and is heavily time dependent when it comes to loading. One problem with this material property is that it does not produce plastic deformation in that layer. This material property also causes simulations to run for long periods of time and takes a lot of memory. The second model uses the Drucker Prager plasticity model for all the layers. This model is able to determine plastic deformation in any layer and runs more quickly than viscoelasticity. This model, however, assumes that the asphalt layer is only stress dependent, not time or temperature dependent. The final material model assumes that every layer is linear elastic. This model does cause the simulation to run the quickest out of all three models. The drawback of this model is that permanent deformation is not calculated in any of the layers. Considering all the positive attributes and the drawbacks of each model, Drucker Prager was chosen to be used for the asphalt layer. This model was chosen because it can predict permanent deformation in all the layers, and it runs in a relatively short time.

4.2.6 Impact of Wheel Configuration and Structure

This section tested wheel configuration effects on flexible pavement. Several conclusions can be drawn from this section of the main study. When modeling LFC pavement with a viscoelastic asphalt layer, comparing one, four, and six wheel configuration shows that one wheel produces the least amount of deflection in the asphalt layer. Four and six wheel configuration have similar pavement responses, with the maximum subgrade stress under the middle wheel of the six wheel configuration. When considering MFC pavement with viscoelastic asphalt layer,

wheel configuration does not make a significant difference. The upheaval on the outside and in between each wheel is very close to identical.

While analyzing the results from this section, it is evident that pavement structure has an effect on the pavement response. For medium strength subgrade, even though the subgrade is stronger, higher deflections, greater stresses and greater plastic strain in the subgrade are seen in comparison to low strength flexible pavement. This can be attributed to the lower thickness of pavement above the subgrade; with less pavement thickness, the stress cannot spread out and reduce in magnitude.

4.3 Wander Models

4.3.1 Introduction

The next study investigates both the effects of wander and wheel configuration on flexible pavement structure. One and four wheels are tested with and without wander. Comparing one wheel to four wheels without wander investigates the effects of quasi-static loading on LFC2 pavement. LFC2 pavement was chosen for two reasons. First LFC pavement shows effects of loading quicker than MFC would. Second, a recent study conducted by the NAPTF has real scale testing data which could be used to compare FE data. The second comparison is one wheel with and without wander. Only one wheel is used because it will isolate the effects of wander by eliminating the effects of wheel configuration. The last comparison is four wheels with and without wander. This test combines both the effect of wheel configuration and wander under quasi-static loading.

Figure 4.25 below shows the abbreviated wander pattern that was used for single wheel wander and figure 4.26 is the wander pattern used for the four wheel simulation.

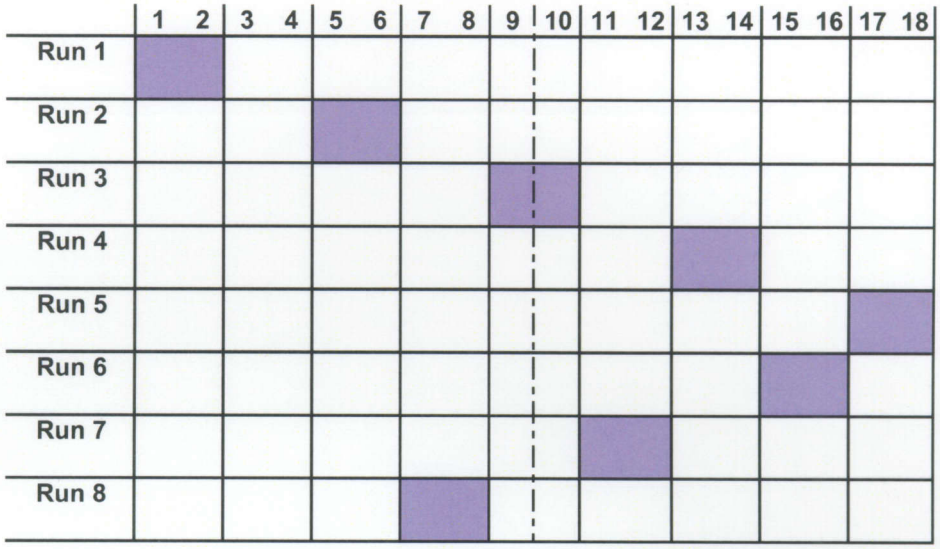

Figure 4.25: Abbreviated Wander Pattern for Single Wheel

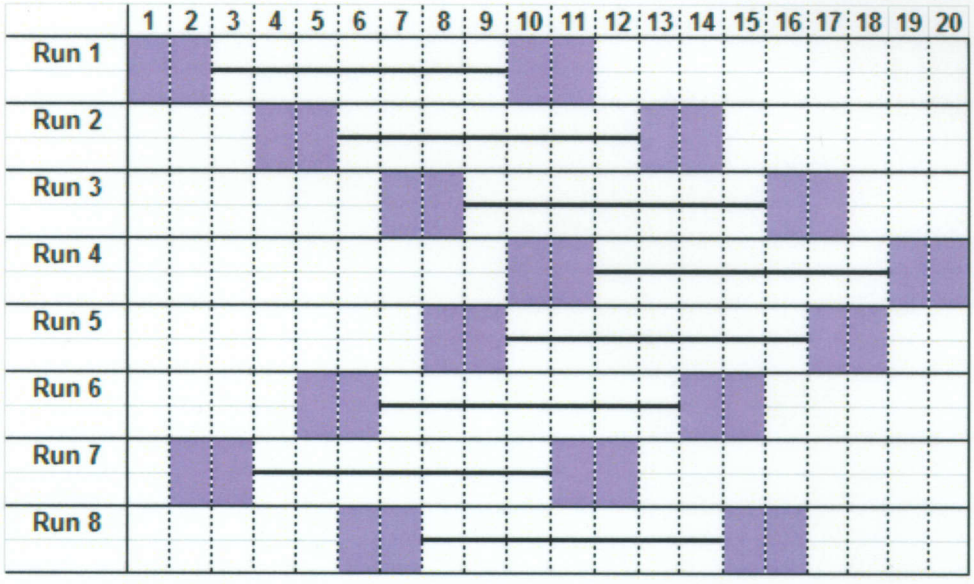

Figure 4.26: Abbreviated Wander Pattern for Four Wheels

The wander pattern mimics the standard distribution that the FAA uses in testing; however instead of 66 runs down and back, this model only uses eight due to time and memory constraints.

4.3.2 Loading

Each wheel has a load of 55 kips on a standard wheel footprint of 12 inches by 21 inches. The loading pattern is shown in figure 4.27 for the four wheel configuration. One wheel with and without wander follows the same progression. This loading simulates a moving load by ramping up and down the loading on each one of the footprints in each step. This loading moves down and back across the pavement for eight cycles.

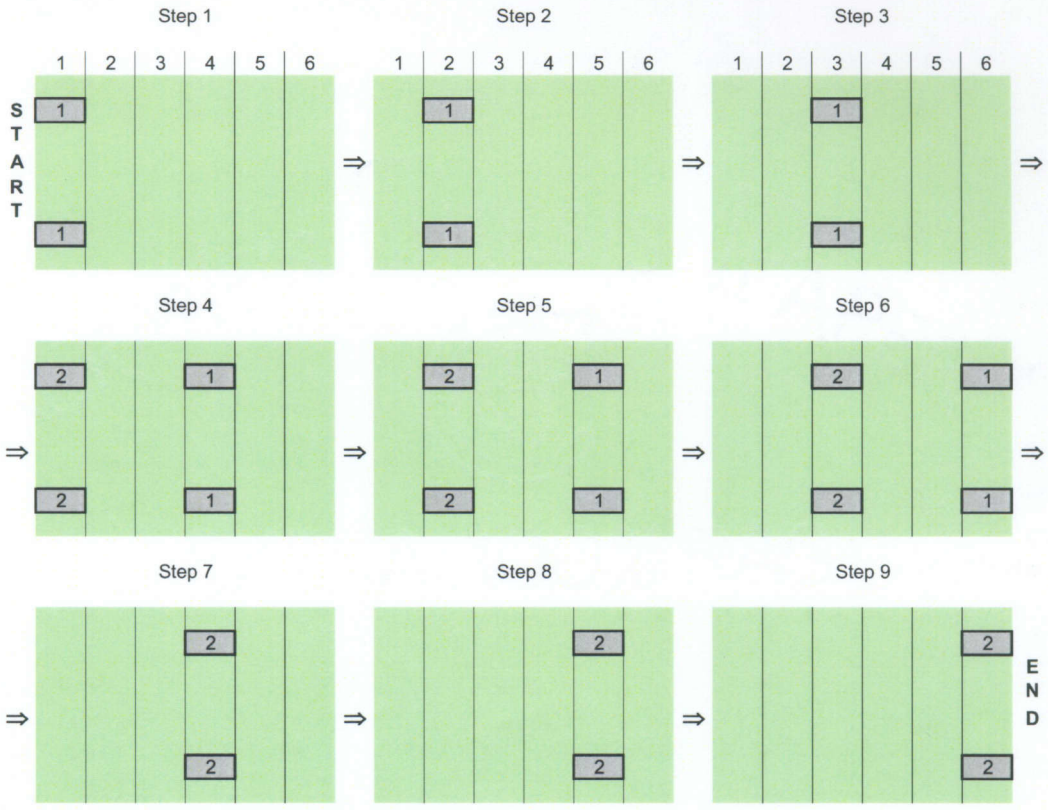

Figure 4.27: Loading Pattern Used for Four Wheel Configuration

4.3.3 Finite Element Model

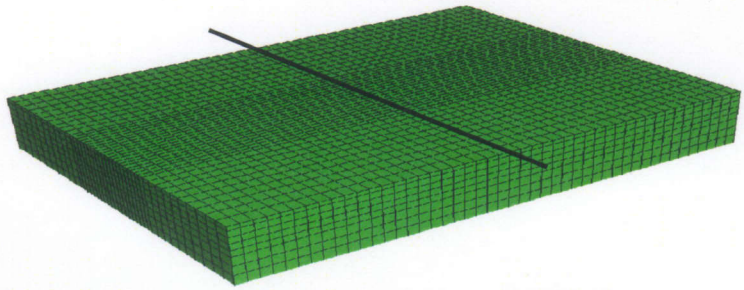

Figure 4.28: LFC2 Pavement Section for Wander Models

The overall dimensions are 30 feet by 40 feet by 6 feet deep. The material properties for this model can be seen in table 4.1, which describe the Drucker Prager plasticity model. The model contains 12880 C3D8R and 1840 CIN3D8 elements, and 17343 nodes. The elements from the center section of the model above have dimensions of 10.5 inches long by 6 inches wide. The line shown in figure 4.28 is where data was extracted from the output files. Figure 4.29 below shows the thickness of each layer of elements in the LFC2 pavement.

P-401 Asphalt	Layer 1 (5 in)
P-209 Base	Layer 2 (8 in)
P-154 Subbase	Layer 3 (8 in)
	Layer 4 (8 in)
	Layer 5 (8 in)
Dupont Low	Layer 6 (11.5 in)
	Layer 7 (11.5 in)
	Inf Layer (12 in)

Figure 4.29: Cross Section of LFC2

4.3.4 Results

The data from this section was taken from the model after the loading was taken off the pavement. The results show the permanent effects of trafficking, which are

deformation in the asphalt layer, and vertical residual stress and plastic strain in the subgrade. The data was taken along the line shown in Figure 4.28.

4.3.4.1 One Wheel with and without Wander

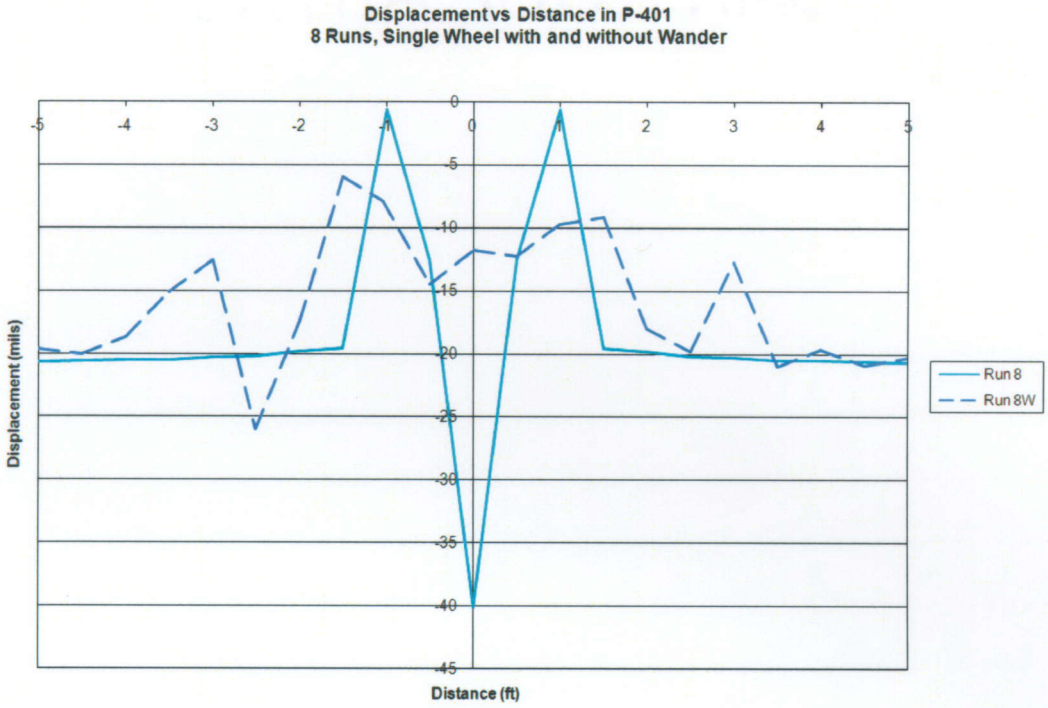

Figure 4.30: One Wheel with and without Wander: Vertical Deflection in Asphalt Layer After 8 Cycles

Figure 4.30 compares the vertical deflection in the asphalt layer between one wheel with and without wander. The one wheel without wander causes 71% larger deflection than one wheel with wander. The upheaval is 28% larger for one wheel without wander than with wander.

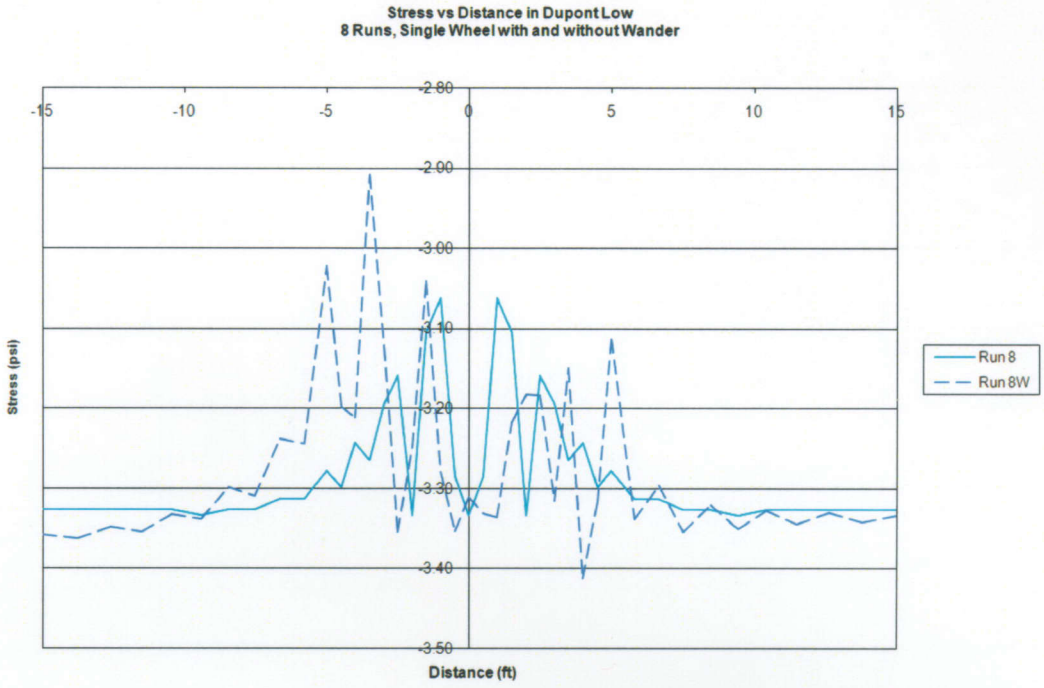

Figure 4.31: One Wheel with and without Wander: Vertical Stress in Subgrade Layer After 8 Cycles

Figure 4.31 shows the vertical stress in the subgrade layer under one wheel with and without wander. From analyzing the results, the maximum stress imparted into the subgrade is 2% higher with wander.

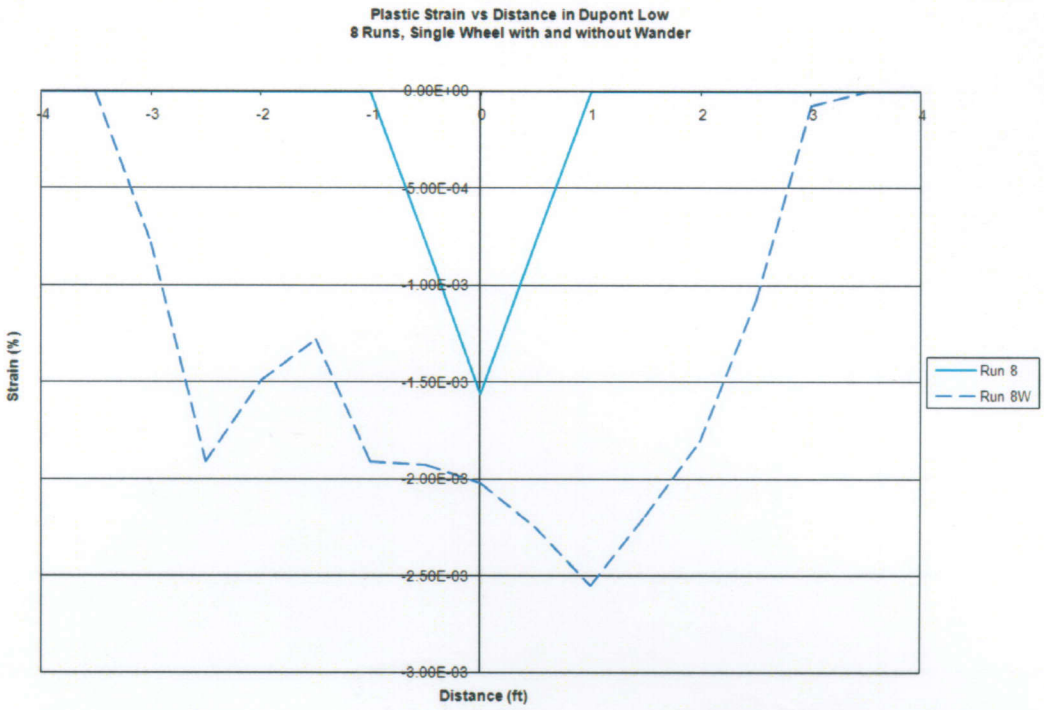

Figure 4.32: One Wheel with and without Wander: Plastic Strain in Subgrade Layer After 8 Cycles

Figure 4.32 shows the plastic strain in the subgrade layer under one wheel with and without wander. One wheel with wander imparts 39% more permanent strain to the subgrade than a single wheel without wander.

4.3.4.1.1 Impact of Wander: One Wheel with and without Wander

Wander effects can be summarized in the following manner. In the asphalt layer, one wheel without wander causes more deflection and upheaval. In the subgrade, wander causes more stress to be transmitted which leads to a greater amount of plastic strain. With wander, the amount of damage seen in the subgrade is distributed over a larger area.

4.3.4.2 Four Wheels with and without Wander

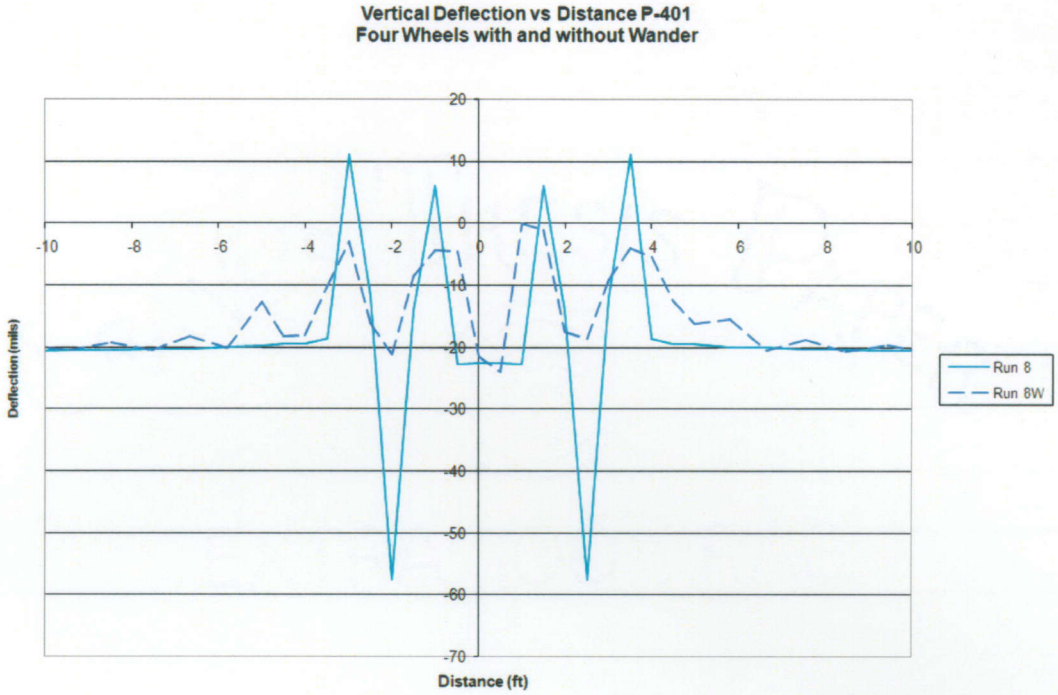

Figure 4.33: Four Wheels with and without Wander: Deflection in Asphalt Layer after 8 Cycles

Figure 4.33 displays the deflection in the asphalt layer for four wheels with and without wander. Similar to one wheel with and without wander, the four wheels without wander cause 58% more deflection and 34% more upheaval in the asphalt layer. The deflection basin for four wheels with wander is also wider than for the case with no wander.

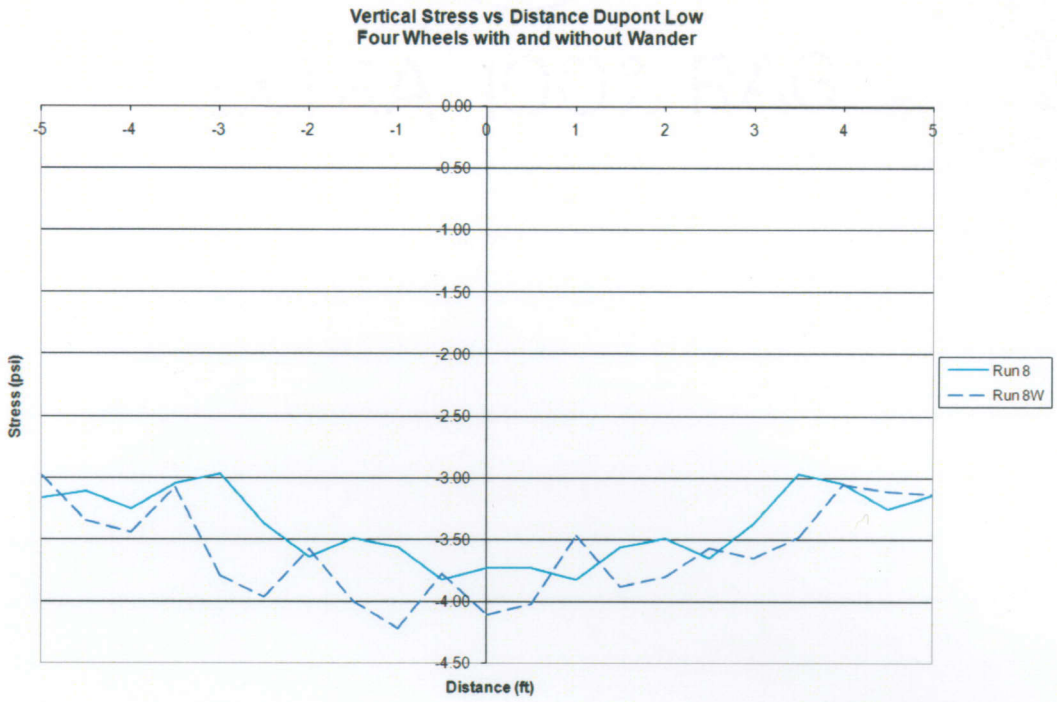

Figure 4.34: Four Wheels with and without Wander: Stress in Subgrade Layer after 8 Cycles

Figure 4.34 shows the vertical stress in the subgrade layer under four wheels with and without wander. The stress imparted by four wheels with wander cause 9% more stress in the subgrade than without wander.

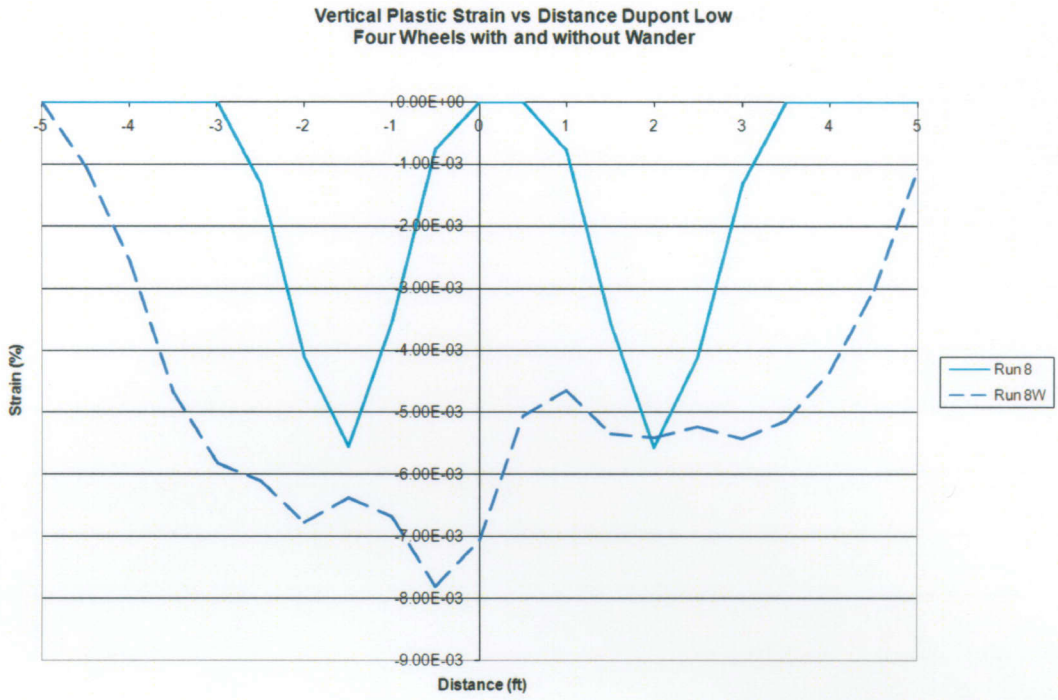

Figure 4.35: Four Wheels with and without Wander: Plastic Strain in Subgrade Layer after 8 Cycles

Figure 4.35 displays the plastic strain in the subgrade layer of four wheel configuration with and without wander. Four wheels with wander cause 29% more permanent strain in the subgrade.

4.3.4.2.1 Impact of Wheel Configuration and Wander: Four Wheels with and without Wander

Wander effects summarized earlier with one wheel with and without wander can be seen in this section as well. Deflection and upheaval in the asphalt is greater without wander than with wander. In the subgrade, wander causes more stress to be transmitted which leads to a greater amount of plastic strain. The wheel configuration effects can be seen as well. Wheel configuration causes the difference in deflection to

go up and the upheaval to go down. It also allows for greater vertical stress and plastic strain to be imparted to the subgrade.

Donovan and Tutumluer (2007) describe the effect of wander as the potential cause of more deformation than if the aircraft wheel loads traveled the same path consistently. They attribute wander's damage to the "anti-shakedown" effect, which is the "shuffling" of the particles within the pavement system. They state that wander actually reduces the stability of the system.

The next section will use the results from the wander study to investigate rutting of the flexible pavement section.

4.3.4.3 Rutting Results

The results from one and four wheels without wander are analyzed further to investigate how rutting develops after each trafficking run and the amount of deformation can be attributed to each of the layers. Rutting data is the permanent deflection seen in the asphalt layer; for this study, the data is taken across the pavement in the same location as shown in figure 4.28.

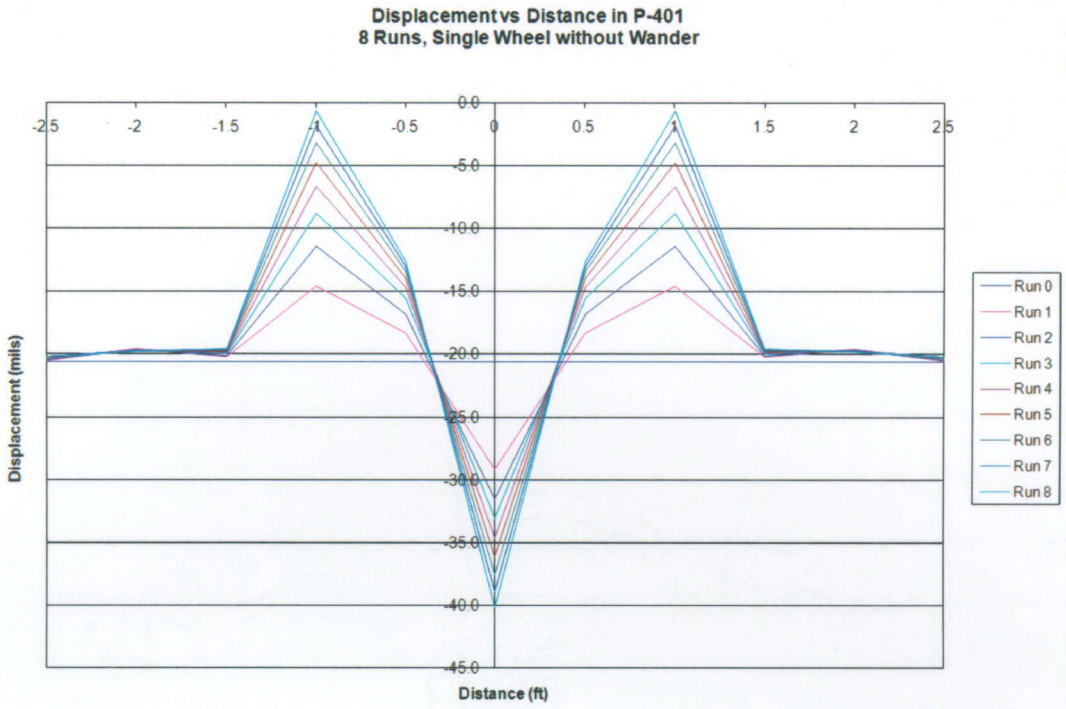

Figure 4.36: Single Wheel without Wander: Deflection of Asphalt Layer vs. Run

Figure 4.36 shows how the deflection of the asphalt layer changes with each run of trafficking with only one wheel without wander. Run 0 shows the initial deflection after geostatic forces are applied. As each run occurs, the maximum deflection and upheaval increases. Upheaval occurs at approximately one foot from the center of the loading footprint. The rate of rutting and upheaval will be analyzed in the following graphs.

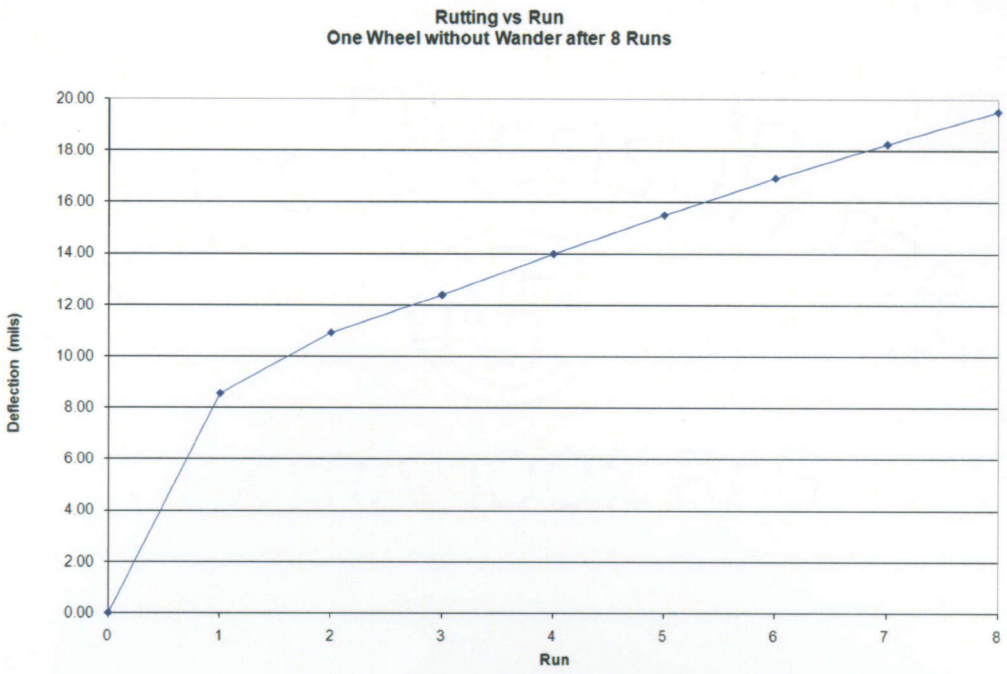

Figure 4.37: Single Wheel without Wander: Rutting vs. Run

Figure 4.37 shows the amount of maximum deflection, which increases with each run of trafficking under one wheel of loading on LFC2 pavement. Rutting is not linear, but rather slowly tapering off as the cycles increase.

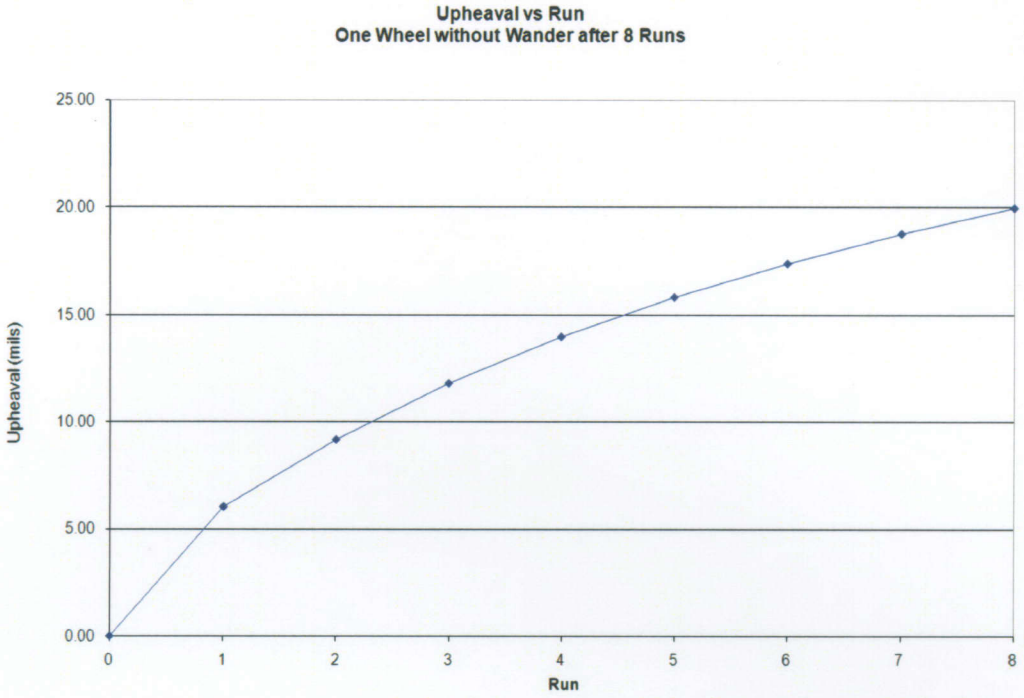

Figure 4.38: Single Wheel without Wander: Upheaval vs. Run

Figure 4.38 shows the amount of upheaval, which attenuated with each run. This like rutting, shows that upheaval slowly tapers off as each run occurs.

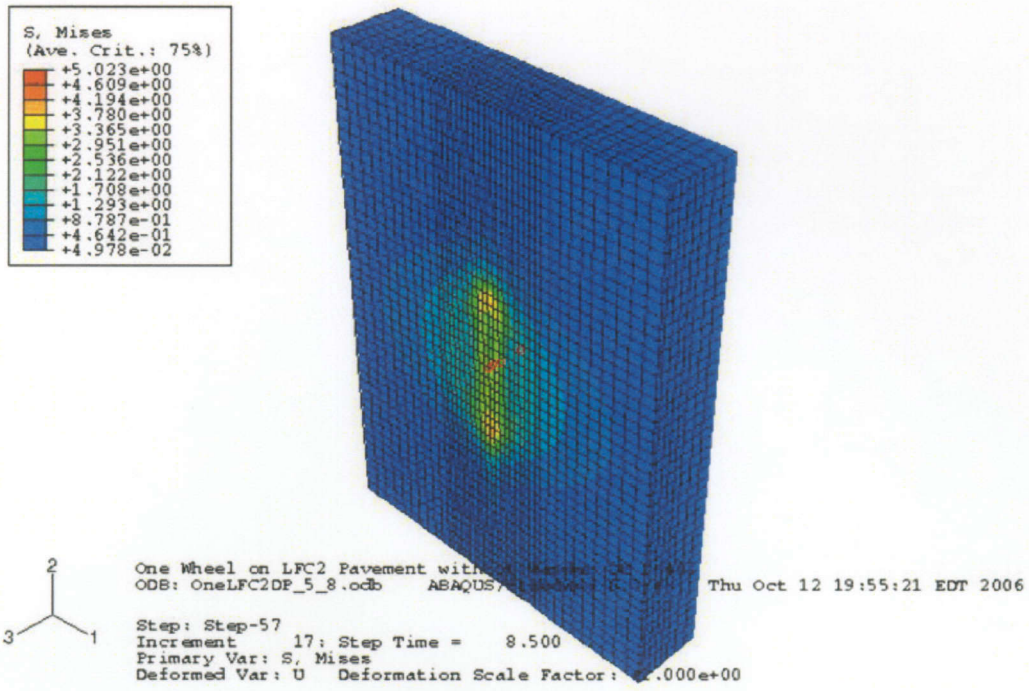

Figure 4.39: Wander Study LFC2 Pavement Section

To determine the amount of deflection attributed to each of the layers, data was taken at the point shown in figure 4.39. This is under the wheel loading of 55 kips.

Table 4-3: One Wheel without Wander: Deflection in each Layer after 8 Runs

Total Deflection (mils)	Dupont Low (mils) [% of total]	P-154 (mils) [% of total]	P-209 (mils) [% of total]	P-401 (mils) [% of total]
-57.56	-17.31 30.1%	-5.09 8.8%	-11.47 19.9%	-23.69 41.2%

Table 4.3 shows the total deflection and the amount each layer contributes after 8 runs under one position of loading. From this table it can be summarized that asphalt contributes most to deformation with 41% and the subgrade is second with 30%. This analysis is repeated for four wheels without wander.

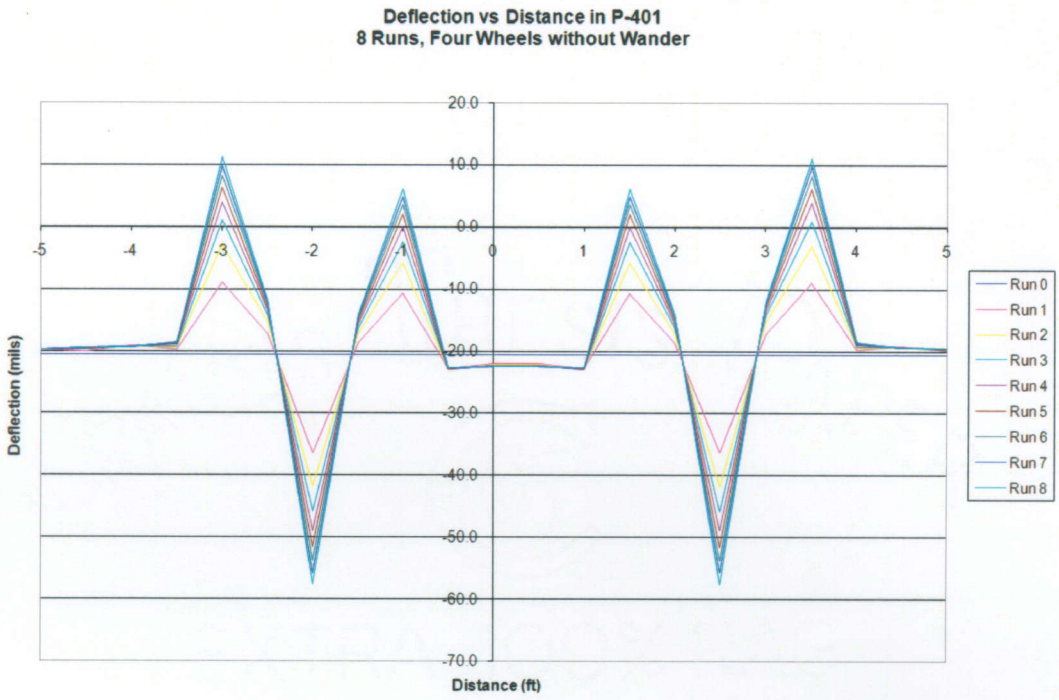

Figure 4.40: Four Wheels without Wander: Deflection of Asphalt Layer vs. Run

Figure 4.40 shows the deflection of the asphalt layer after each run under four wheels without wander. Run zero is the baseline deflection after geostatic forces are considered. Upheaval, outside the wheels and in between wheels, can be seen at one foot away from the center of the loading surface.

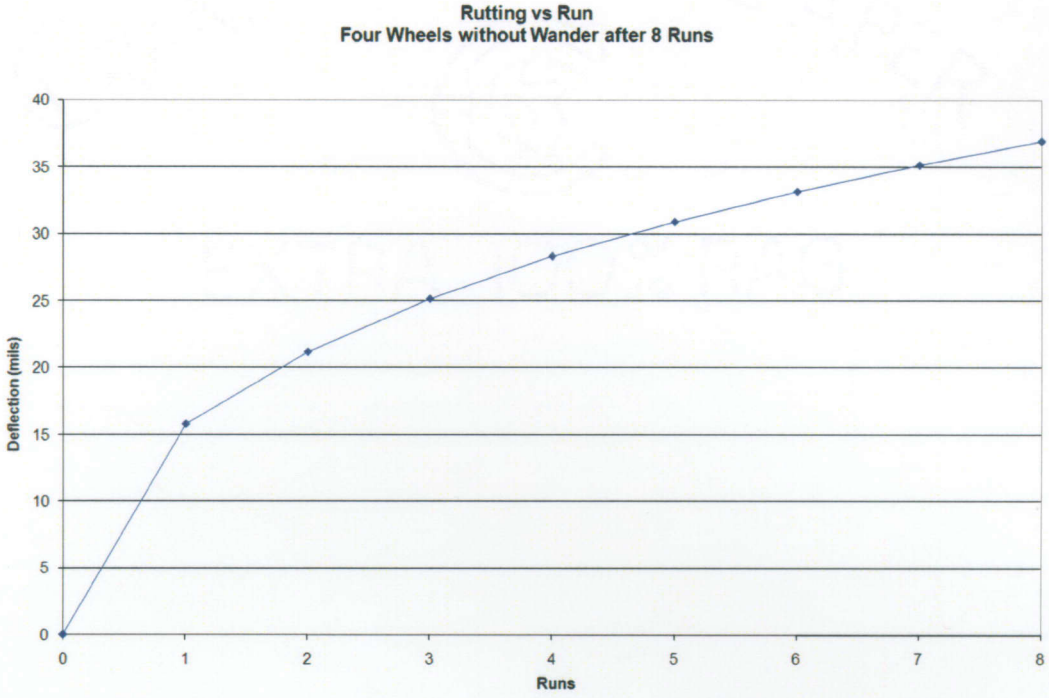

Figure 4.41: Four Wheels without Wander: Rutting vs. Run

The figure above shows the rate of rutting for four wheels without wander. Similar to one wheel rutting, four wheels exhibits a decaying rate of rutting attenuation; with each run, less permanent deformation is added. The difference in rut accumulation can be attributed to a few different factors, such as consolidation, dilation and shear flow of the pavement materials.

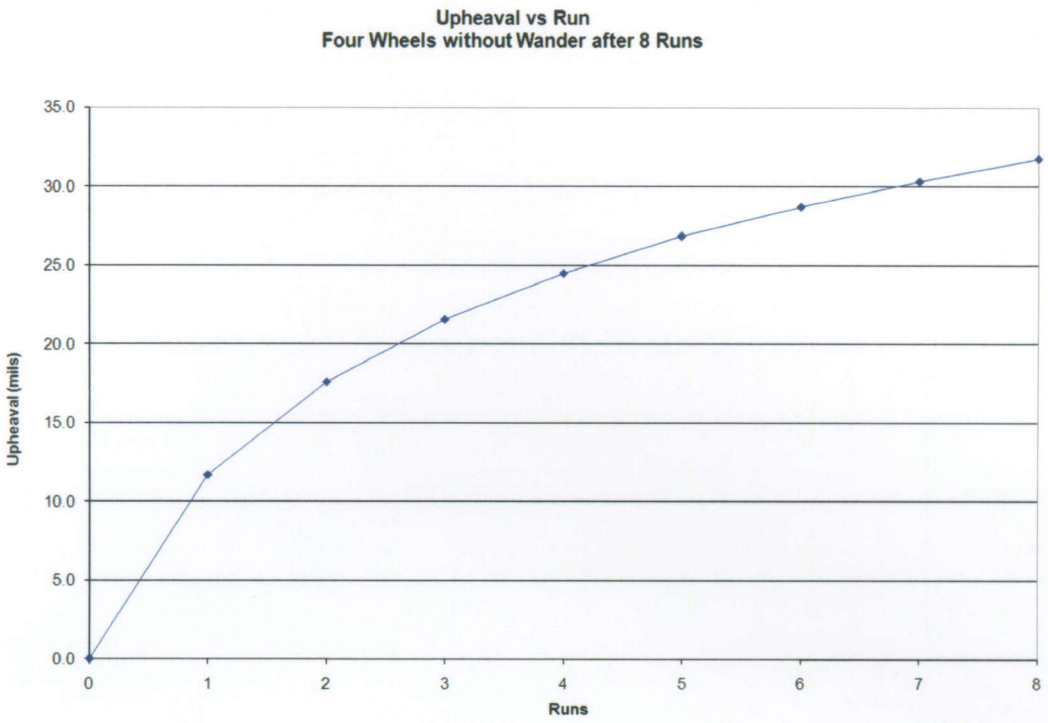

Figure 4.42: Four Wheels without Wander: Upheaval vs. Run

Figure 4.42 shows the outside upheaval produced under four wheels without wander. Once again, the upheaval increases is similar to what was seen earlier with one wheel; the amount of upheaval for each run increases by a smaller amount each time.

Table 4-4: Four Wheels without Wander: Deflection in each Layer after 8 Runs

Total Deflection (mils)	Dupont Low (mils) [% of total]	P-154 (mils) [% of total]	P-209 (mils) [% of total]	P-401 (mils) [% of total]
-67.64	-18.78 27.8%	-5.56 8.2%	-11.56 17.1%	-31.74 46.9%

Table 4.4 shows the permanent deformation and the percent of the overall deformation in each layer under four wheels. This table shows that the asphalt produces the most deflection with 47% and the subgrade second with 28%.

4.3.4.3.1 Rutting Summary

Rutting and upheaval show the same characteristic of decaying attenuation rate. Each run produces a diminishing increase in rutting and upheaval. These results indicate that pavement is showing signs of consolidation. If rutting and upheaval rates were accelerating, then the pavement would be showing signs of structural failure. From analyzing the percent contribution of each layer, it is evident from either one or four wheels after 8 runs that the asphalt layer contributes the most to the overall deformation with 41-47% and the subgrade contribution ranges between 28-30% of the total deformation for the pavement structures analyzed.

4.3.4.4 Plastic and Elastic Accumulation

This next section studies how plastic and elastic strain in the subgrade under four wheels with and without wander changes after each run.

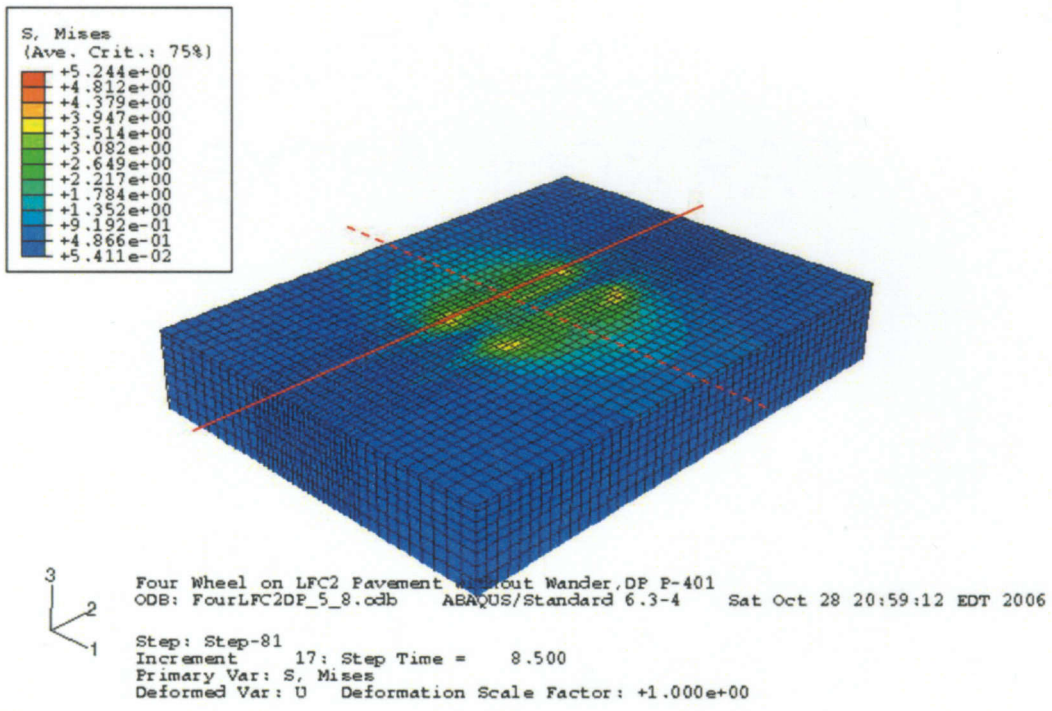

Figure 4.43: Wander Study LFC2 Pavement Section

The data was taken along the point shown in figure 4.43. This point is the intersection of the centerline beneath the four wheels without wander. The initial elastic and plastic strain of run zero is not included in the trendline regression.

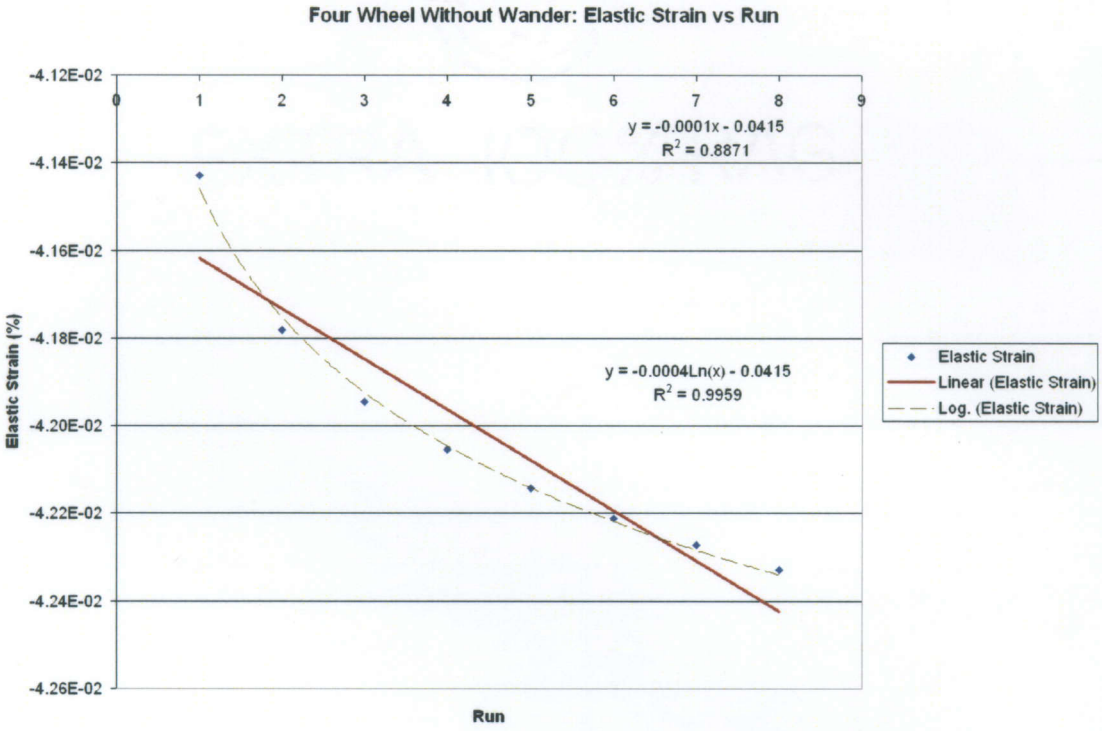

Figure 4.44: Elastic Strain vs. Run: Four Wheels without Wander

Figure 4.44 shows the elastic strain in the subgrade after each run for four wheels without wander. The increase in elastic strain starting at the first run is best described as a log function, which means that the rate of increase of elastic strain is gradually declining.

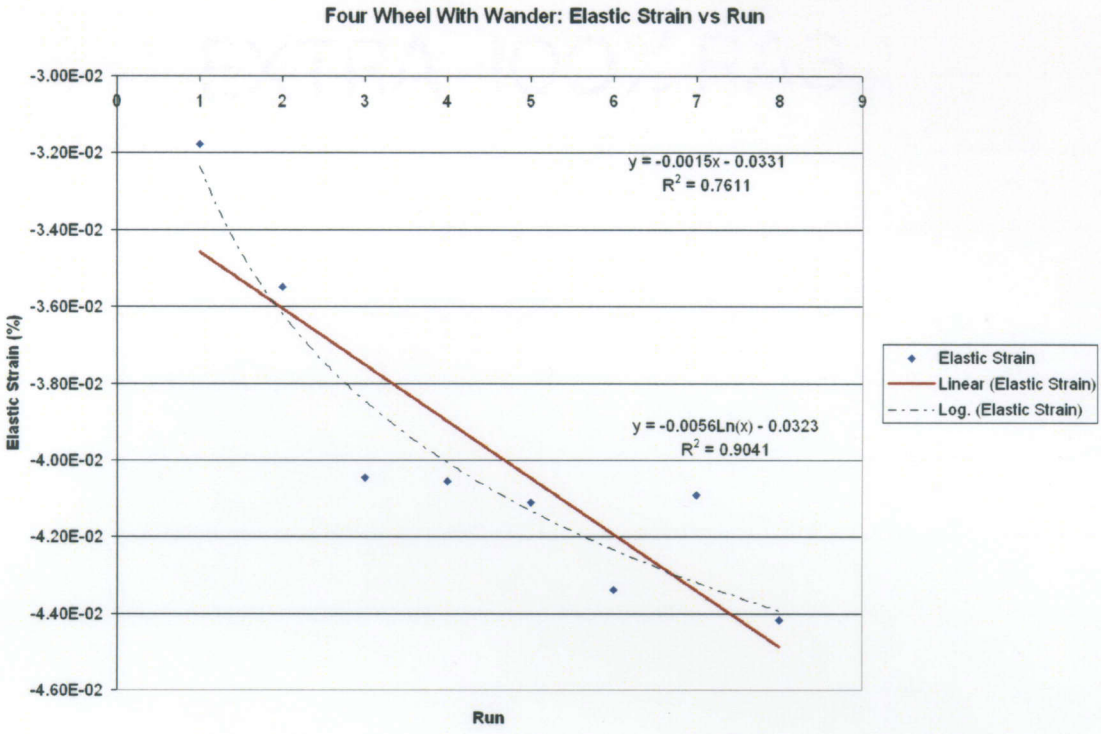

Figure 4.45: Elastic Strain vs. Run: Four Wheels with Wander

Figure 4.45 shows the elastic strain in the subgrade after each run for four wheels with wander after 8 runs. As with four wheels without wander, the elastic strain can best be described as a log function, which means the elastic strain increases at a logarithmic rate for each subsequent run.

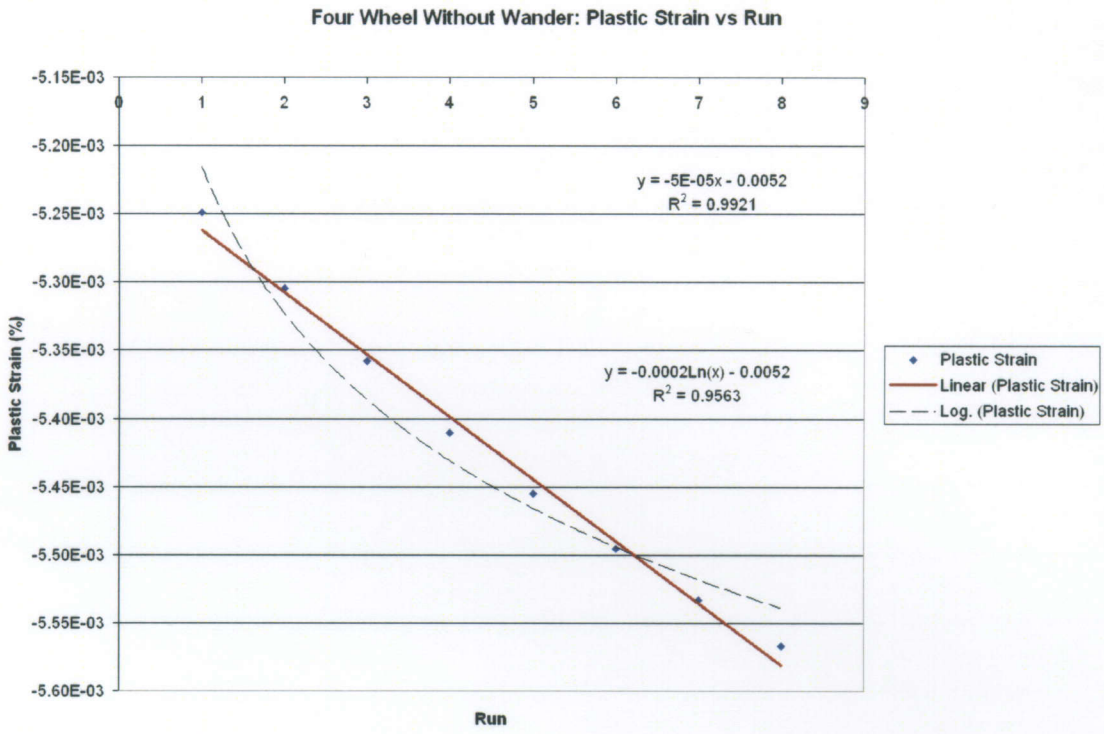

Figure 4.46: Plastic Strain vs. Run: Four Wheels without Wander

Figure 4.46 shows the plastic strain in the subgrade under four wheels without wander. Plastic strain increase with each run can be estimated with a linear equation. This means that the permanent deformation will continue to increase at the same rate with each subsequent run.

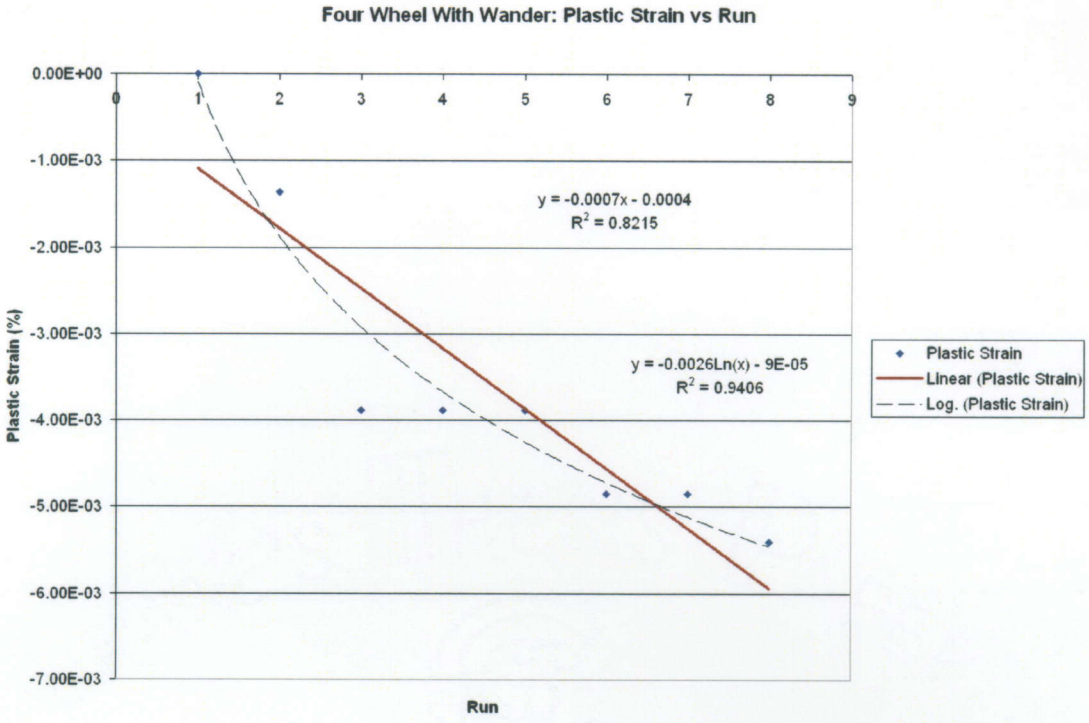

Figure 4.47: Plastic Strain vs. Run: Four Wheels with Wander

The figure above shows the plastic strain in the low strength subgrade of LFC2 pavement under four wheels with wander. The plastic strain increase with each run can be described by a log function that tapers off with each run. This implies that wander causes less permanent strain in the subgrade.

4.3.4.4.1 Plastic and Elastic Strain Accumulation Summary

Elastic strain increases in the subgrade for four wheels with and without wander is similar. Elastic strain increase can be attributed to consolidation within the pavement. As permanent deformation increases, the amount of increase of elastic strain becomes smaller. This is why a decay function, such as a log function, describes the rate of elastic strain increase. There is a clear difference with plastic strain; wander allows for less damage to be imparted to the subgrade.

The next section is a comparison of the trends learned in the wander study to full scale testing done at the NAPTF.

4.3.4.5 Comparison with Full-scale Testing Results

Four and Six wheel configurations tested over several wander cycles under 45 kip per wheel loading on MFC pavement were conducted by the NAPTF. Several conclusions from this study are shown below. Also, where possible, a comparison to data collected in the main studies is presented. It is difficult to compare directly the results from the simulated wander models for several reasons. First, the number of wander cycles completed in the full-scale testing far exceeds the passes in the simulation. Also the pavement structure is different; the simulation uses the LFC2 pavement structure whereas the full-scale testing uses the MFC structure. Taking these differences into account a general comparison can still be done.

Following conclusions were drawn from the full scale studies conducted at NAPTF (Hayhoe and Garg 2002):

- Permanent deformation as evidenced by unrecovered vertical strains in the subgrade (and in aggregate layers) was a significant component in the total response of the pavement structure during the traffic tests.
- Recovered strains are very weakly dependent on the path of previously applied loads, whereas unrecovered strains are very strongly dependent on the path of previously applied loads.

- Vertical elastic strain at the top of the subgrade due to the four-wheel loading is predicted to be slightly higher than that due to the six-wheel loading.

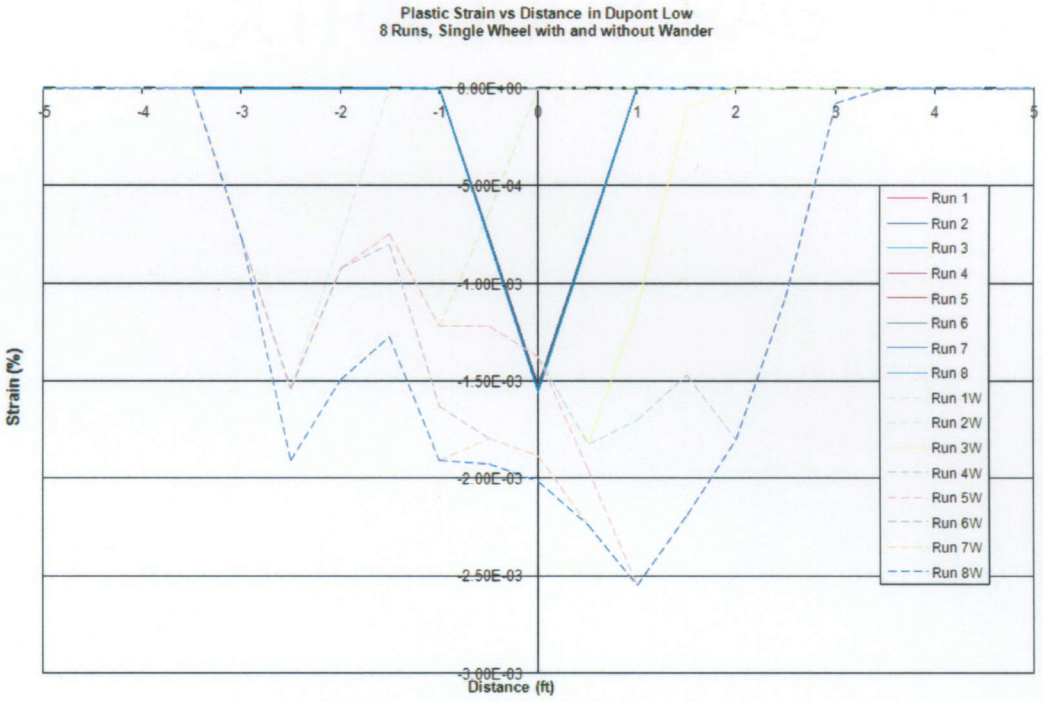

Figure 4.48: One Wheel with and without Wander: Plastic Strain in Subgrade Layer (LFC2)

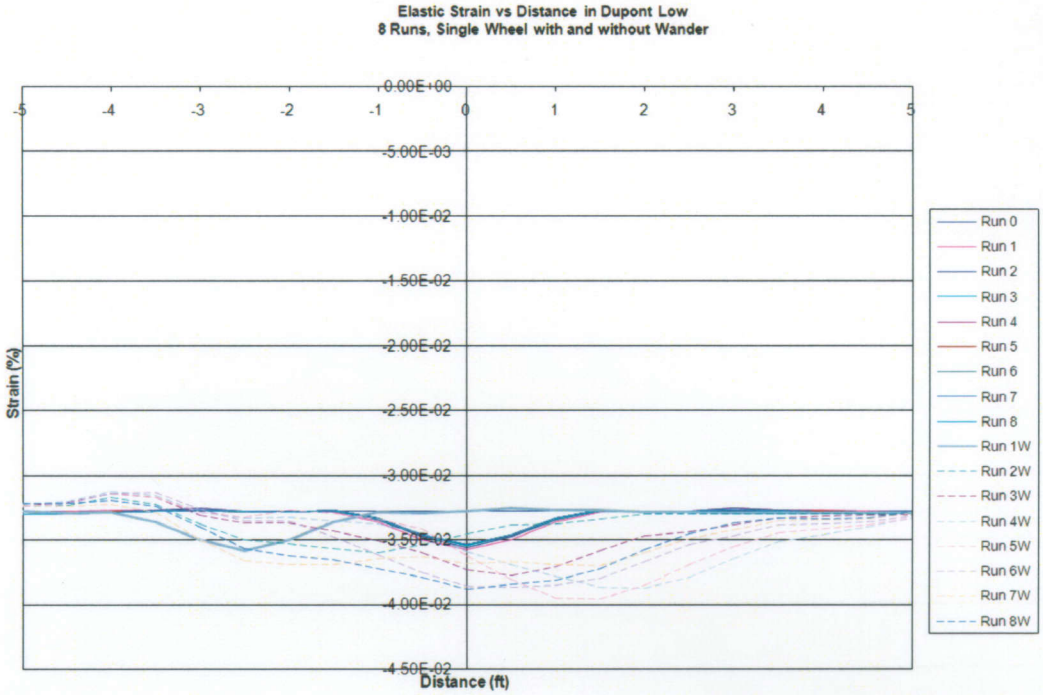

Figure 4.49: One Wheel with and without Wander: Elastic Strain in Subgrade Layer (LFC2)

Figures 4.48 and 4.49 show plastic strain and elastic strain for all eight runs on LFC2 pavement on top of the subgrade layer with and without wander. In comparing the conclusions from Hayhoe and Garg (2002) with results in the main study, the results fit pretty well with some of the conclusions. Figure 4.48 and 4.49 show that after each pass of the landing gear both recovered and unrecovered strains increase in magnitude. Also it is evident that the unrecovered (plastic) strain is highly dependent on previous path. The plastic strain has peaks where the loading had taken place, whereas elastic strain remains quite level after each pass has occurred.

4.4 Chapter Conclusions

The material properties presented in this paper fit the FAA data well. The option of using viscoelasticity depicts how asphalt would act; however due to memory

constraints, it could not be used in quasi-static or dynamic modeling. Considering all the positive attributes and the drawbacks of each model, Drucker Prager was chosen to be used for the asphalt layer. This model was chosen because it can predict permanent deformation in all the layers, and it runs in a relatively short time.

In this chapter, wheel configuration effects were tested on flexible pavement. Several conclusions can be drawn from this section of the main study. When modeling LFC pavement with a viscoelastic asphalt layer, comparing one, four, and six wheel configuration shows that one wheel produces the least amount of deflection in the asphalt layer. Four and six wheel configuration have similar pavement responses, with the maximum subgrade stress under the middle wheel of the six wheel configuration. When considering MFC pavement with viscoelastic asphalt layer, wheel configuration does not make a significant difference. The upheaval on the outside and in between each wheel is very close to identical.

It is evident that pavement structure has an effect on the pavement response. For medium strength subgrade, even though the subgrade is stronger, higher deflections, greater stresses and greater plastic strain in the subgrade are seen in comparison to low strength flexible pavement. This can be attributed to the lower thickness of pavement above the subgrade; with less pavement thickness, the stress cannot spread out and reduce in magnitude.

Deflection and upheaval in the asphalt is greater without wander than with wander. In the subgrade, wander causes more stress to be transmitted which leads to a greater amount of plastic strain. The wheel configuration effects can be seen as well. Larger wheel configuration causes the difference in deflection to go up and the

upheaval to go down. It also allows for greater vertical stress and plastic strain to be imparted to the subgrade.

Rutting and upheaval show the same characteristic of decaying attenuation rate. Each run has a diminishing increase in rutting and upheaval. These results indicate that pavement is showing signs of consolidation. If rutting and upheaval rates were accelerating, then the pavement would be showing signs of structural failure. From analyzing the percent contribution of each layer, it is evident from either one or four wheels after 8 runs that the asphalt layer contributes the most to the overall deformation with 41-47% and subgrade contribution to total deformation is about 28-30%.

Elastic strain for both with and without wander acts the same. As permanent deformation increases, the amount of increase of elastic strain becomes smaller. This is why a decay function, such as a log function, describes the rate of elastic strain increase. There is a clear difference with plastic strain; Wander allows for less damage to be imparted into the subgrade.

CHAPTER 5: CONCLUSIONS

In this chapter, the findings of the study will be summarized.

5.1 Summary of Findings

5.1.1 Material Verification Studies

The California Bearing Ratio (CBR) test is used to calibrate the model's material properties for the subbase, base and subgrade. The subgrade is tested to determine which elastic modulus accurately depicts the real materials response to stress. The subbase and base have an assumed elastic modulus and the CBR test is used to find the corresponding friction and dilation angles. These material properties are then used within the next model which is the viscoelasticity model. This simulation is to identify the correct instantaneous elastic modulus and shift factor needed to allow the results to fit full-scale test data, including data taken from Static Punch Test done in April 2001. The model is also used to calibrate Drucker Prager material model properties for the asphalt layer. Table 5.1 shows the final results from the material verification chapter and are used throughout the main study models.

Table 5-1: Drucker Prager Material Properties

Material	Young's Modulus (ksf)	Friction Angle	Dilation Angle	Cohesion (ksf)	Density (kslug/ft^3)	Poisson's Ratio
P-401 - Drucker Prager	72000	20	5	4.32	0.005	0.3
P-209	5760	50	5	0.72	0.005	0.3
P-154	2880	45	5	0.9216	0.0047	0.35
Dupont Medium	1542	0.01	0.0067	2.52	0.0029	0.45
Dupont Low	432	0.01	0.0067	4.608	0.003	0.45

Table 5-2: Prony Series (Viscoelastic) Material Properties

Spring Constants (ksf)				
E_1	E_2	E_3	E_4	E_5
3173	856	2976	3215	3805
Relaxation Times, sec				
λ_1	λ_2	λ_3	λ_4	λ_5
0.00643	0.08023	0.65612	5.2108	139.87

5.1.2 Main Studies

Static loading of LFC and MFC pavements show some important results. In comparing the stresses transmitted to the subgrade for the LFC pavement structure with a 5 inch surface layer, 8 inch base layer and 37 inches of subbase with the MFC pavement structure, which has a 12 inch subbase layer with all other dimensions being the same, the benefits of adding additional subbase thickness is evident. The stresses transmitted to the subgrade for the MFC section shows distinct peaks corresponding to the wheel loading locations but this effect is not clearly seen with the LFC section. The stresses transmitted to the subgrade are also halved due to the additional thickness of subbase. This effect was also clearly seen in an earlier study by Willis (2005).

In addition, when the effect of gear configuration is assessed, rutting on the surface is produced. It is clear that the pavement structure has a strong influence on the deformations produced. For the LFC pavement structure, maximum deflections and strains are produced for the one wheel and 4-wheel gear configuration, with maximum elastic and plastic strains in the asphalt produced for the 4-wheel configuration. For the MFC pavement structure, the 6-wheel gear configuration produces maximum rutting under the central wheel and also induces higher maximum

elastic and plastic strains in the asphalt layer. This is not consistent with Wardle's (2003) observations, which seems to conclude that adding gears actually increases the life of the pavement. Wardle (2003) suggested that more complex gear geometries result in a zone of negative strain, which reduces strain but this is not evident from the study and is dependent on the pavement structure and material properties.

5.1.2.1 Gear Configuration

The effect of gear configuration on the surface rutting produced is evident from the study of the one and four wheel loading without wander on the LFC pavement structure. Four wheel loading produces more deflections as would be expected with higher stresses being transmitted to the subgrade.

5.1.2.2 Wander

The effect of wander on the pavement response can be clearly seen from the study comparing one wheel with and without wander. Wander tends to reduce the surface rutting for the eight cycles analyzed. Both cause around the same maximum plastic strain in the subbase layer but one wheel with wander distributes strain over a wider area. The effect on the subgrade is important because wander tends to induce greater permanent strains on the subgrade layer and also over a wider area. This is important when determining the life of the pavement with wander because even though surface rutting might be reduced due to wander for initial cycles of loading, the greater plastic strains induced in the underlying layers might induce shear failure and reduce the life of the pavement. This is consistent with observations made by Donovan and Tutumluer (2007) where they concluded that wander reduces the stability of the pavement systems due to the "anti-shakedown" effect, which is the "shuffling" of the

particles within the pavement system. The effect of four wheels with and without wander also shows similar results with wander reducing the surface rutting.

Rutting and upheaval show the same characteristic of decaying attenuation rate. Each run has a diminishing increase in rutting and upheaval. From analyzing the percent contribution of each layer, it is evident from either one or four wheels after 8 runs that the asphalt layer contributes the most to the overall deformation with 41-47% of total deformation and the subgrade contributes about 28-30% of the total deformation.

Elastic strain for both with and without wander acts the same. As permanent deformation increases, the amount of increase of elastic strain becomes smaller. This is why a decay function, such as a log function, describes the rate of elastic strain increase. There is a clear difference with plastic strain; Wander allows for less damage to be imparted into the subgrade.

The use of the whole gear configuration instead of a single wheel or set of wheels demonstrates more accurately the effects on flexible pavement (current design methods estimate pavement thickness and deflection predictions by use of a single wheel or single set of wheels).

5.2 Recommendations

The existing design methods are inadequate to determine the effect of new large aircraft on the thickness requirements for flexible pavements. The design methods are based on simplifying assumptions and use full-scale tests that were performed on thin pavements using a single gear loading. Since these methods fail to comprehensively

model the pavement deformation process, it is hard to justify "extrapolation beyond the limits of the test data (Rodway 1995)." This has created the need for simulating pavement response under aircraft loading with a variety of parameters, such as pavement type, wheel configuration and aircraft wander in a realistic environment.

Using moving wheel load analysis to design pavements should be considered a viable option. With the way in which computing power is increasing and storage becoming cheaper and larger, it will someday be possible to use this method to design any type of pavement, with any loading and material properties and to receive a pavement response quicker than ever imagined. This gives designers the ability to change pavement types or any other parameter of their simulation instantly. It has many benefits to the designer; however it will never totally eliminate the use of the full-scale testing.

The simulations done are only as good as the full-scale testing the models are verified against. Several problems are still inherent with use of finite elements. First finite element programs can be quite expensive and very few users have the knowledge and experience to use the program effectively. These programs also can take a long time to complete but compared to full scale testing, which takes six to twelve months, this time can seem minimal. This method of design still needs several steps before it can be used as a standard for design. First a standard model needs to be setup that can be verified against several full scale tests. A standard set of material properties should be established as well. Also in order for these models to be practical, fast computers with ample storage space should be used.

The setup of the model itself is also a problem. There is some debate whether one gear or the whole gear configuration of an aircraft needs to be included in a simulation. Wardle et al. (2003) states when wheel groups are used to compute subgrade strains, negative strain effects can give anomalous behavior. This study suggests that pavement designs should be based on subgrade strains beneath single wheel groups that are due to the group itself and to neglect interactions with other wheel groups. On the other hand, Brill and Hayhoe (2004) performed an analysis of multiple-gear subgrade strains using the layered elastic analysis program LEAF. This study concluded that the contribution of additional gears to the maximum subgrade strain produced under a gear may be significant, particularly for deeper structures on weaker subgrade. It is not known yet which of these theories is correct, further testing will be necessary.

Simulations also give the ability to change whether the model is simulating static or dynamic loading. Donovan and Tutumluer (2007) describe that in full-scale testing, as the wheels of a gear assembly move across the pavement, there is an increase in the response after each wheel pass. However, when statically simulating the gear assembly with finite elements, the middle wheel of a dual-tridem gear configuration will cause the most deflection. The discrepancy has been attributed to the moving wheels load because a moving wheel does not allow the pavement system to fully rebound before it is loaded again. This implies that the best way to determine the effects of a gear assembly would be to simulate it as a moving load.

Once these problems have been resolved and the standards have been established this method will reduce the amount of full-scale testing necessary. It will

also remove the necessity for extrapolating older tests beyond the scope originally intended. It will take several years to validate and verify models in order for these simulations to be considered design standards.

5.3 Future Work

- Investigate the effects of different wheel configurations with varying weights (A380, B787, etc).
- Study the effect of wheel interactions between sets of gears.
- Perform material verification study using several different full-scale testing data to find a representative set of material properties to use for testing.
- Perform wander models that have longer than 8 cycles, using more than just one type of gear setup and multi-gear setup.
- Test new boundary conditions such as using infinite elements along sides of pavement to reduce model size.
- Test alpha factors to prove or disprove validity of using that design method.
- Determine viscoplastic material properties for the asphalt layer (P-401).
- Test with loading that is continuous or dynamic instead of quasi-static.
- Test with friction between layers instead of perfectly bonded.
- Study the validity of the Principle of Superposition

REFERENCES

AASHTO (2000) "Determining the Resilient Modulus of Soils and Aggregate Materials," T307-99, *Standard Specifications for Transportation Materials and Methods of Sampling and Testing*, Part II-Tests, American Association of State Highway and Transportation Officials, Washington, D.C.

Ahlvin, R.G., Ulery, H.H., Hutchinson, R.L., Rice, J.L., (1971), "Multiple-Wheel Heavy Gear Load Pavement Tests," *Technical Report S-71-17, Vol. I-IV, U.S. Army Waterways Experiment Station*, Vicksburg, Mississippi.

Airbus Industrie, (2007) "A380: Airplane Characteristics for Airport Planning AC," Toulouse, France. http://www.content.airbusworld.com/SITES/Technical_Data/docs/AC/DATA_CONSULT/AC_A380.pdf

Airbus Industrie, (2001) "LCPC / Airbus/ STBA A380 Pavement Experimental Programme," Toulouse, France. http://www.stac.aviation-civile.gouv.fr/publications/documents/rapportPEP.pdf

ASTM D 2487. (1993) Standard Classification of Soils for Engineering Purposes (Unified Soil Classification System).

Barker, W.R. and Gonzalez, C.R. (1994). *Super-Heavy Aircraft Study*. Technical Report GL-94-12, US Army Corps of Engineers, Waterways Experiment Station, Vicksburg, Miss.

Boeing Company, (2006) "Airplane Characteristics for Airport Planning: Chapter 7-Pavement Data" http://www.boeing.com/commercial/airports/acaps/787sec7.pdf

Bozkurt, D., and W. G. Buttlar, (2002) "Three-Dimensional Finite Element Modeling to Evaluate Benefits of Interlayer Stress Absorbing Composite for Reflective Crack Mitigation," Airport Technology Transfer Conference, Federal Aviation Administration, Atlantic City, NJ.

Brill, D.R. and Hayhoe, G.H. (2004) Multiple-Gear Analysis for Flexible Pavement Design in LEDFAA. Proceedings of the 2004 Federal Aviation Administration Airport Technology Transfer Conference, Atlantic City, NJ, April 2004.

Chen, D. H., Zaman, M., Laguros, J.Soltani, A. (1995). "Assessment of computer programs for analysis of flexible pavement structure," Transportation Research Record 1482, TRB, National Research Council, Washington, D.C., 123-133.

Cho, Y-H., McCullough, B.F., and Weissman, J. (1996). "Considerations on finite element method application in pavement structural analysis," *Transportation Research Record 1539*, National Research Council, Washington, D.C., 96-101.

Donovan, P. and Tutumluer, E. (2007) "Analysis of NAPTF Trafficking Response Data for Pavement Foundation Deformation Behavior, " 2007 FAA Worldwide Airport Technology Transfer Conference and Exposition, Atlantic City, NJ, April 2007.

Federal Aviation Administration, (2004) "LEDFAA – Linear Elastic Design" http://www.airporttech.tc.faa.gov/Pavement/26ledfaa.asp

Gervais, E., Hayhoe, G., and Garg, N. (2003) "Towards a Permanent ACN Solution for 6-Wheel Landing Gear Aircraft," Proceedings of the Airfield Pavements Challenges and New Technologies Conference, Las Vegas, Nevada.

Hayhoe, Gordon F., McQueen, Roy D., and Guo, Edward H.. (1993) "Airport Pavement Test Machine Design and Cost Study." FAA.

Hayhoe, Gordon F. and Garg, Navneet. (2002) "Subgrade Strains Measured in Full-scale Traffic Tests with Four- and Six-wheel Landing Gears." FAA Airport Technology Transfer Conference.

Hayhoe, G. (2004). "Traffic Testing Results from the FAA's National Airport Pavement Test Facility," 2nd International Conference on Accelerated Pavement Testing, Minneapolis, MN, September, 2004.

HKS, (2006), ABAQUS Theory and Users Manual – Version 6.6, *Hibbit, Karlsson & Sorenson, Inc.*, Pawttucket, Rhode Island.

Kuo, C. M., K. T., and Darter, M. I. (1995). "Three dimensional finite element model for analysis of concrete pavement support," *Transportation Research Record 1505*, National Research Council, Washington, D.C., 119-127.

Livneh, Moshe, (2004) "THICKNESS DESIGN CALCULATIONS FOR THE NEW LARGE AIRCRAFT (NLA) AIRBUS A380," 2004 *FAA Worldwide Airport Technology Transfer Conference,* Atlantic City, USA

Loizos, A. and Charonitis, G.(2004) "Bearing Capacity and Structural Classification of Flexible Airport Pavements." Journal of Transportation Engineering.

Nazarian, S. and K. M. Boddspati (1995). "Pavement-Falling Weight Deflection Interaction Using Dynamic Finite Element Analysis," *Transportation Research Record 1449*, National Research Council, Washington, D.C., 123-133.

Rodway, Bruce. (1995) "Design of Flexible Pavements for Large Multiwheeled Aircraft." International Conference of Road and Pavement Technology. Singapore.

Rodway, Bruce Wardle, Leigh J., Wickham, Garry (1999) "Interaction Between Wheels and Wheel Groups of New Large Aircraft" Published in Airport Technology Transfer Conference, Atlantic City, U.S.A., Federal Aviation Administration. http://www.mincad.com.au/AtlanticCity99Paper/interactiona.htm

Stet, M. and Verbeek, J. (2004) "The PCN Runway Strength Rating and Load Control System," Netherlands, 2004.

University of Washington, (2004), "Subgrade" http://training.ce.washington.edu/WSDOT/Modules/04_design_parameters/04-2_body.htm

Wardle, Leigh J. and Rodway, Bruce. (1998) "Recent Developments in Flexible Aircraft Pavement Design using the Layered Elastic Method." Third Int. Conf. on Road and Airfield Pavement Technology. Beijing. http://www.mincad.com.au/APSDSPaperBeijing/beijpa13.htm

Wardle, L.J., Youdale, G. and Rodway, B. (2003). *Current Issues For Mechanistic Pavement Design.* in 21st ARRB and 11th REAAA Conference, Cairns, Australia, 18 - 23 May, 2003, Session S32, ARRB Transport Research.

Willis, Michael (2005), Three dimensional finite element analysis as a tool for flexible pavement design and analysis, Master's thesis, Rowan University.

Zaghloul, S.M. and T.D., White, (1993), "Use of a Three-Dimensional, Dynamic Finite Element Program for Analysis of Flexible Pavement," *In Transportation Research Record 1388, TRB, National Research Council*, Washington D.C., p 60-69.

APPENDIX A: Material Properties and Static Punch Test Data

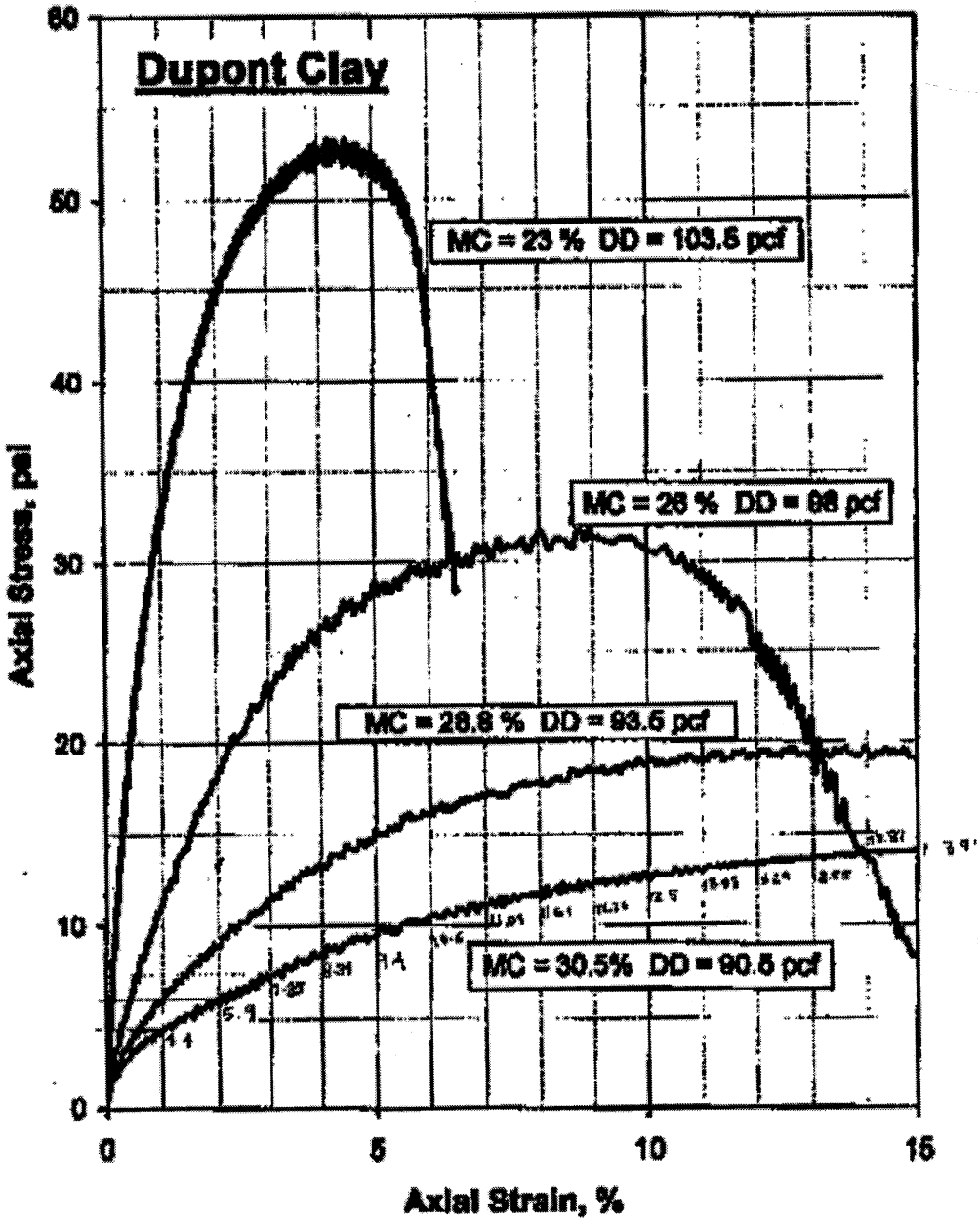

Figure A.1: Resilient Modulus Testing Data (SHRP P-46) for Dupont Clay

Table A. 1: P-154 Material Properties

MATERIAL DESCRIPTION:			SUBBASE				
DATE FILE UPDATED:			9/25/2000				
CROSS REFERENCE			FAA P-154 SUBBASE				
TEST SPECIFICATIONS:			SHRP P 46				
Material	Sample ID.	Moisture Content, %	Dry Density, pcf	Confining Stress, psi	Deviator Stress, psi	Resilient Strain	Resilient Modulus, psi
P-154	A	6.1	131.8	3.00	2.65	0.000210	12768.4
P-154	A	6.1	131.8	3.00	5.30	0.000380	13837.6
P-154	A	6.1	131.8	3.00	8.07	0.000510	15696.6
P-154	A	6.1	131.8	5.00	4.47	0.000250	17702.0
P-154	A	6.1	131.8	5.00	8.98	0.000450	19971.5
P-154	A	6.1	131.8	5.00	13.52	0.000620	21923.7
P-154	A	6.1	131.8	10.10	9.00	0.000310	29258.2
P-154	A	6.1	131.8	10.00	17.72	0.000570	31238.3
P-154	A	6.1	131.8	10.00	27.06	0.000810	33529.5
P-154	A	6.1	131.8	15.00	8.97	0.000260	33893.3
P-154	A	6.1	131.8	15.00	13.50	0.000380	35357.1
P-154	A	6.1	131.8	15.00	26.99	0.000670	40428.8
P-154	A	6.1	131.8	20.10	13.46	0.000320	41743.4
P-154	A	6.1	131.8	20.00	18.00	0.000410	43398.6
P-154	A	6.1	131.8	20.00	36.04	0.000740	48885.2
P-154	B	5.7	132.5	3.00	2.65	0.000170	15403.6
P-154	B	5.7	132.5	3.00	5.37	0.000330	16184.2
P-154	B	5.7	132.5	3.00	8.10	0.000450	17855.2
P-154	B	5.7	132.5	5.00	4.41	0.000230	19556.5
P-154	B	5.7	132.5	5.00	8.99	0.000410	21964.0
P-154	B	5.7	132.5	5.00	13.49	0.000560	24152.4
P-154	B	5.7	132.5	10.00	9.00	0.000300	30385.6
P-154	B	5.7	132.5	10.00	17.99	0.000540	33556.9
P-154	B	5.7	132.5	10.00	26.63	0.000770	34683.6
P-154	B	5.7	132.5	15.10	8.97	0.000260	34696.7
P-154	B	5.7	132.5	15.00	13.49	0.000380	35843.4
P-154	B	5.7	132.5	15.00	26.99	0.000660	40877.5
P-154	B	5.7	132.5	20.00	13.47	0.000330	40987.2
P-154	B	5.7	132.5	20.00	18.00	0.000420	42910.2
P-154	B	5.7	132.5	19.90	35.99	0.000730	49001.9

Sample No.	Moisture Content, %	Dry Density pcf	Strain Rate % per minute	Confining Pressure, psi	Failure Stress, psi	SIG-3 @ Failure, psi	SIG-1 @ Failure, psi	Friction Angle, deg.	Cohesion psi
1	6.2	129.2	1.0	5.0	74.8	5.0	79.8	49.2	6.4
2	6.4	126.1	1.0	10.0	84.6	10.0	94.6		
3	6.3	129.0	1.0	15.0	131.2	15.0	146.2		

Table A. 2: P-154 CBR Test Data

MATERIAL DESCRIPTION:			SUBBASE						
DATE FILE UPDATED:			9/25/2000						
CROSS REFERENCE			FAA P-154 SUBBASE						
TEST SPECIFICATIONS:			ASTM C D 4429						
Date	**Material**	**Item**	**Thickness, in.**	**Station**	**Offset**	**Point**	**CBR**	**Lift Summary**	
2/1/1999	P-154	2-1		3+36	19R	1	42.5	Mean	33.1
2/1/1999	P-154	2-1		3+36	19R	2	41.3	Std.Dev.	6.4
2/1/1999	P-154	2-1		3+36	19R	3	37.7	COV, %	19.4
2/1/1999	P-154	2-1		3+56	2R	1	30.5		
2/1/1999	P-154	2-1		3+56	2R	2	34.8		
2/1/1999	P-154	2-1		3+56	2R	3	28.6		
2/1/1999	P-154	2-1		3+81	16L	1	25.7		
2/1/1999	P-154	2-1		3+81	16L	2	31.9		
2/1/1999	P-154	2-1		3+81	16L	3	24.9		
2/4/1999	P-154	1-3		2+45	19L	1	16.9	Mean	40.6
2/4/1999	P-154	1-3		2+45	19L	2	30.2	Std.Dev.	10.4
2/4/1999	P-154	1-3		2+45	19L	3	39.9	COV, %	25.7
2/4/1999	P-154	1-3		2+45	19L	4	43.4		
2/4/1999	P-154	1-3		2+69	7L	1	40.5		
2/4/1999	P-154	1-3		2+69	7L	2	53.2		
2/4/1999	P-154	1-3		2+69	7L	3	45.5		
2/4/1999	P-154	1-3		2+56	14R	1	50.0		
2/4/1999	P-154	1-3		2+56	14R	2	46.2		
2/4/1999	P-154	1-3		2+56	14R	3	39.8		

Table A. 3: P-209 Material Properties

MATERIAL DESCRIPTION:		BASE					
DATE FILE UPDATED:		9/25/2000					
CROSS REFERENCE		FAA P-209 BASE					
TEST SPECIFICATIONS:		SHRP P 46					
Material	Sample ID.	Moisture Content, %	Dry Density,	Confining Stress, psi	Deviator Stress, psi	Resilient Strain	Resilient Modulus, psi
P-209	A	4.5	154.2	3.00	2.67	0.000150	17643.6
P-209	A	4.5	154.2	3.00	5.39	0.000270	19844.1
P-209	A	4.5	154.2	3.00	8.10	0.000360	22691.1
P-209	A	4.5	154.2	5.00	4.49	0.000190	24277.0
P-209	A	4.5	154.2	5.00	9.00	0.000320	27962.1
P-209	A	4.5	154.2	5.00	13.51	0.000440	30748.0
P-209	A	4.5	154.2	10.00	8.98	0.000230	38455.0
P-209	A	4.5	154.2	10.00	17.98	0.000440	40720.3
P-209	A	4.5	154.2	10.00	27.05	0.000610	44335.2
P-209	A	4.5	154.2	15.10	9.02	0.000200	44811.5
P-209	A	4.5	154.2	15.00	13.50	0.000290	46465.1
P-209	A	4.5	154.2	15.00	27.00	0.000510	53013.5
P-209	A	4.5	154.2	20.00	13.50	0.000250	53876.9
P-209	A	4.5	154.2	20.00	18.00	0.000320	56232.9
P-209	A	4.5	154.2	20.00	36.03	0.000570	63571.8
P-209	B	4.6	151.9	3.00	2.67	0.000190	14382.6
P-209	B	4.6	151.9	3.00	5.41	0.000330	16251.2
P-209	B	4.6	151.9	3.00	8.12	0.000440	18455.6
P-209	B	4.6	151.9	5.00	4.50	0.000220	20134.5
P-209	B	4.6	151.9	5.00	9.02	0.000390	23189.7
P-209	B	4.6	151.9	5.00	13.55	0.000530	25632.6
P-209	B	4.6	151.9	10.00	8.98	0.000270	33037.6
P-209	B	4.6	151.9	10.00	18.07	0.000480	37303.6
P-209	B	4.6	151.9	10.00	27.15	0.000660	41061.0
P-209	B	4.6	151.9	15.00	9.02	0.000230	39952.5
P-209	B	4.6	151.9	15.00	13.54	0.000320	42354.4
P-209	B	4.6	151.9	15.00	27.05	0.000550	49239.3
P-209	B	4.6	151.9	20.00	13.56	0.000270	49815.2
P-209	B	4.6	151.9	20.00	18.05	0.000350	52325.2
P-209	B	4.6	151.9	20.00	36.17	0.000600	60390.8

Sample No.	Moisture Content, %	Dry Density pcf	Strain Rate % per minute	Confining Pressure, psi	Failure Stress, psi	SIG-3 @ Failure, psi	SIG-1 @ Failure, psi	Friction Angle, deg.	Cohesion psi
1	4.4	152.7	1.0	5.0	83.7	5.0	88.7		
2	4.9	151.4	1.0	10.0	190.5*	10.0		60.8	2.4
3	4.1	152.1	1.0	15.0	192.4*	15.0			

* Specimen did not fail, reached the capacity of load frame.

Table A.4: P-209 CBR Test Data

MATERIAL DESCRIPTION:			BASE						
DATE FILE UPDATED:			9/25/2000						
CROSS REFERENCE			FAA P-209 BASE						
TEST SPECIFICATIONS:			ASTM C D 4429						
Date	**Material**	**Item**	**Thickness, in.**	**Station**	**Offset**	**Point**	**CBR**	**Lift Summary**	
1/26/1999	P-209	1-2	12	1+45	14R	1	60.4	Mean	44.1
1/26/1999	P-209	1-2	12	1+45	14R	2	56.3	Std.Dev.	11.1
1/26/1999	P-209	1-2	12	1+45	14R	3	42.1	COV, %	25.2
1/26/1999	P-209	1-2	12	1+53	19L	1	28.1		
1/26/1999	P-209	1-2	12	1+53	19L	2	28.7		
1/26/1999	P-209	1-2	12	1+53	19L	3	40.5		
1/26/1999	P-209	1-2	12	1+84	9L	1	43.9		
1/26/1999	P-209	1-2	12	1+84	9L	2	52.0		
1/26/1999	P-209	1-2	12	1+84	9L	3	44.8		

Time sec	Deflection 1-3	(Module) Wheel Loads, Load 1-3, (lbs)	Module Deflections, D3, (inch)	Time sec	Deflection 1-3	(Module) Wheel Loads, Load 1-3, (lbs)	Module Deflections, D3, (inch)
0.00	11.73950	1300	0.00000	171.00	13.37100	55130	1.63150
6.00	11.79800	44820	0.05850	177.00	13.39050	55220	1.65100
11.00	11.84350	43950	0.10400	182.00	13.40350	54880	1.66400
16.00	11.84350	44610	0.10400	187.00	13.43600	54910	1.69650
21.00	11.90200	44810	0.16250	192.00	13.47500	55070	1.73550
26.00	12.22700	44870	0.48750	197.00	13.51400	54940	1.77450
32.00	12.26600	49970	0.52650	202.00	13.54000	54390	1.80050
37.00	12.30500	50390	0.56550	208.00	13.57250	54600	1.83300
42.00	12.34400	50470	0.60450	213.00	13.59850	54340	1.85900
47.00	12.35700	50480	0.61750	218.00	13.62450	55700	1.88500
53.00	12.72100	49300	0.98150	223.00	13.66350	54560	1.92400
58.00	12.76000	55520	1.02050	228.00	13.72200	55080	1.98250
63.00	12.77300	55420	1.03350	234.00	13.74150	53820	2.00200
68.00	12.79900	53800	1.05950	239.00	13.76750	55670	2.02800
73.00	12.82500	54290	1.08550	244.00	13.80000	54660	2.06050
78.00	12.87700	53870	1.13750	249.00	13.86500	55000	2.12550
83.00	12.90950	53850	1.17000	254.00	13.91050	55130	2.17100
89.00	12.93550	54290	1.19600	260.00	13.96250	54990	2.22300
94.00	12.97450	54240	1.23500	265.00	13.98850	54880	2.24900
99.00	12.98750	54560	1.24800	270.00	14.04700	55350	2.30750
104.00	13.02650	54330	1.28700	275.00	14.09250	54280	2.35300
109.00	13.03300	55150	1.29350	280.00	14.13800	55230	2.39850
114.00	13.07200	54090	1.33250	285.00	14.19650	54730	2.45700
119.00	13.08500	55150	1.34550	291.00	14.24200	54940	2.50250
125.00	13.11750	54720	1.37800	296.00	14.32000	54400	2.58050
130.00	13.14350	54030	1.40400	301.00	14.38500	54440	2.64550
135.00	13.16950	54690	1.43000	306.00	14.46300	54110	2.72350
140.00	13.20850	55320	1.46900	311.00	14.58000	54510	2.84050
145.00	13.23450	54480	1.49500	316.00	14.69050	54720	2.95100
150.00	13.24750	54210	1.50800	321.00	14.87900	55000	3.13950
156.00	13.29300	55120	1.55350	327.00	15.84100	54630	4.10150
161.00	13.30600	55170	1.56650	332.00	17.77150	53820	6.03200
166.00	13.33850	54700	1.59900				

Table A.5: FAA Static Punch Test Data (4/23/01)

APPENDIX B: CBR Results

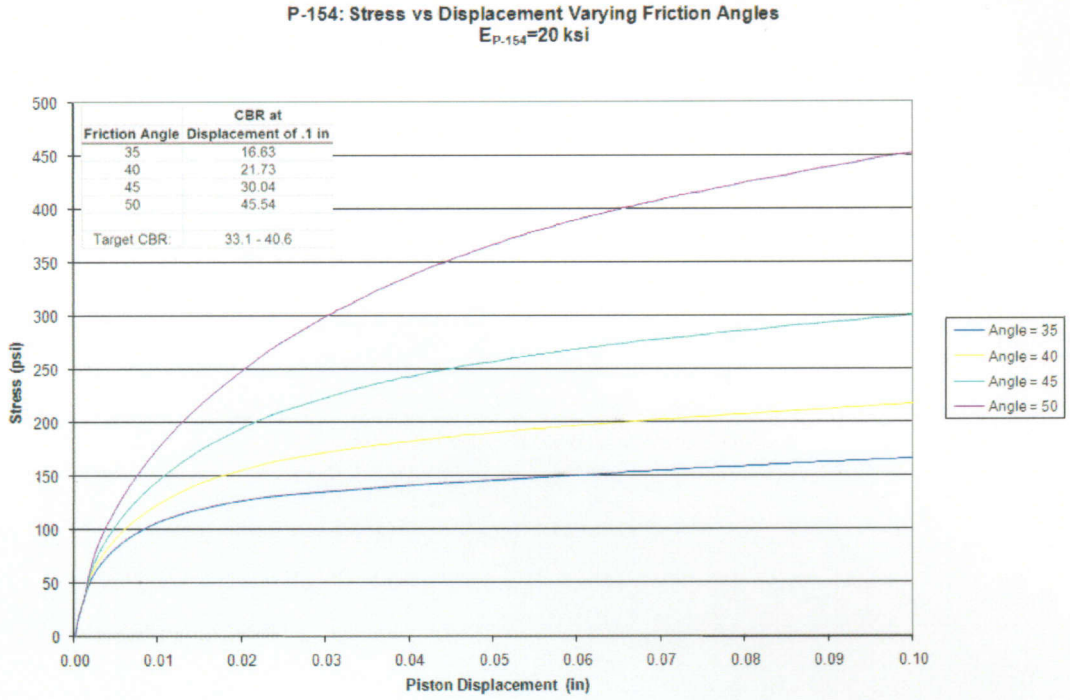

Figure B.1: CBR Results- P154 Friction Angle

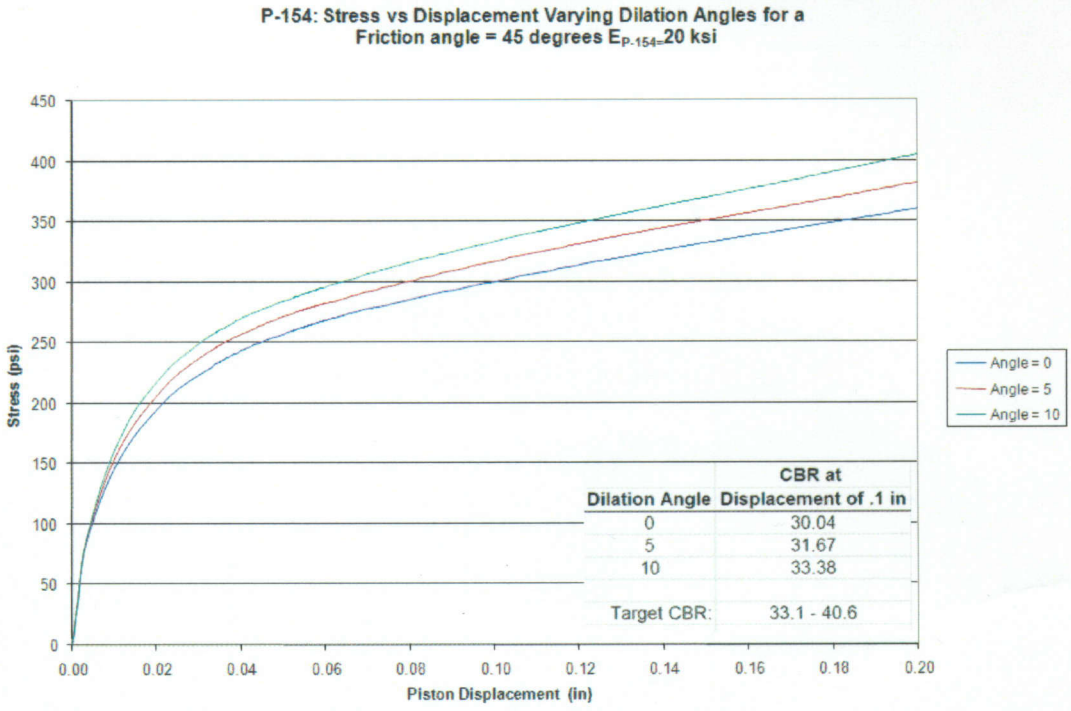

Figure B.2: CBR Results- P154 Dilation Angle

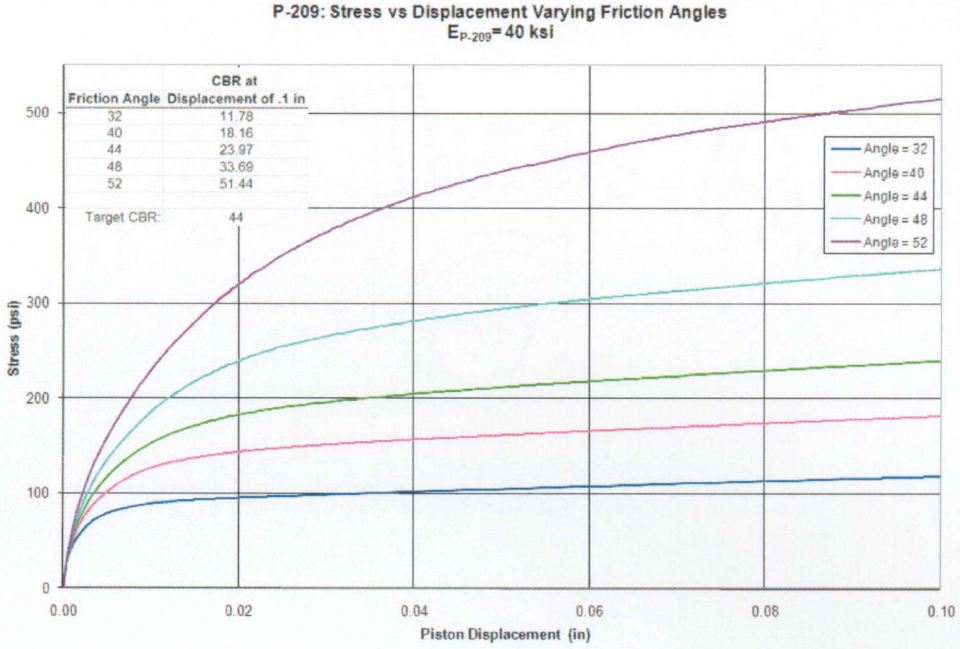

Figure B.3: CBR Results- P209 Friction Angle

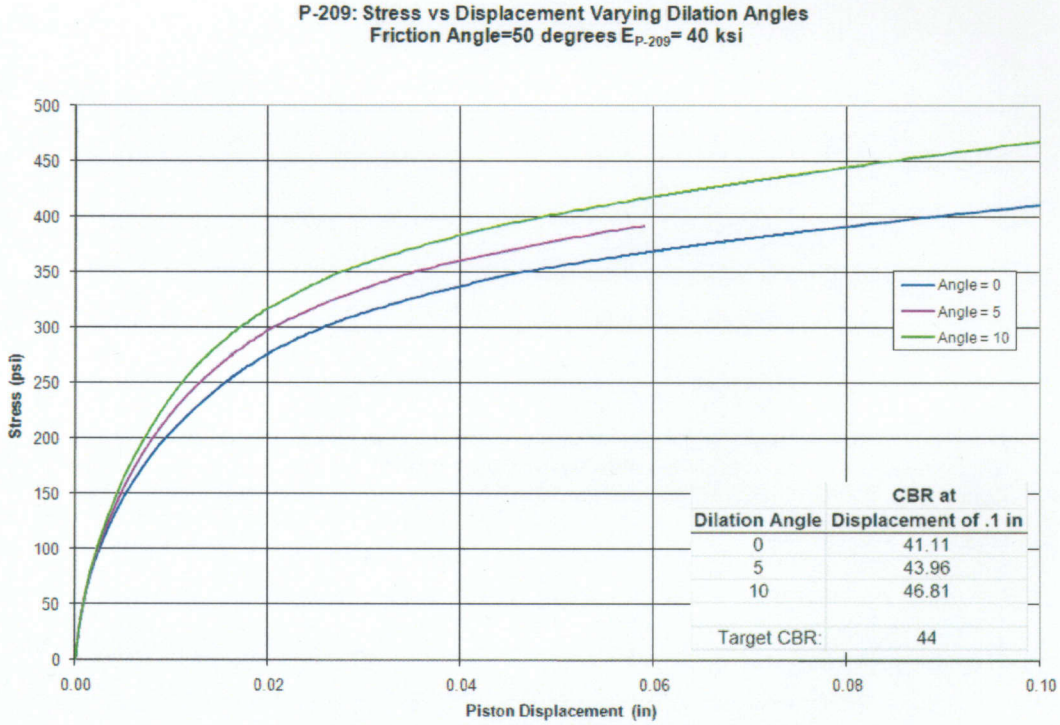

Figure B.4: CBR Results- P209 Dilation Angle

APPENDIX C: Static Wheel Configuration Results-LFC Pavement

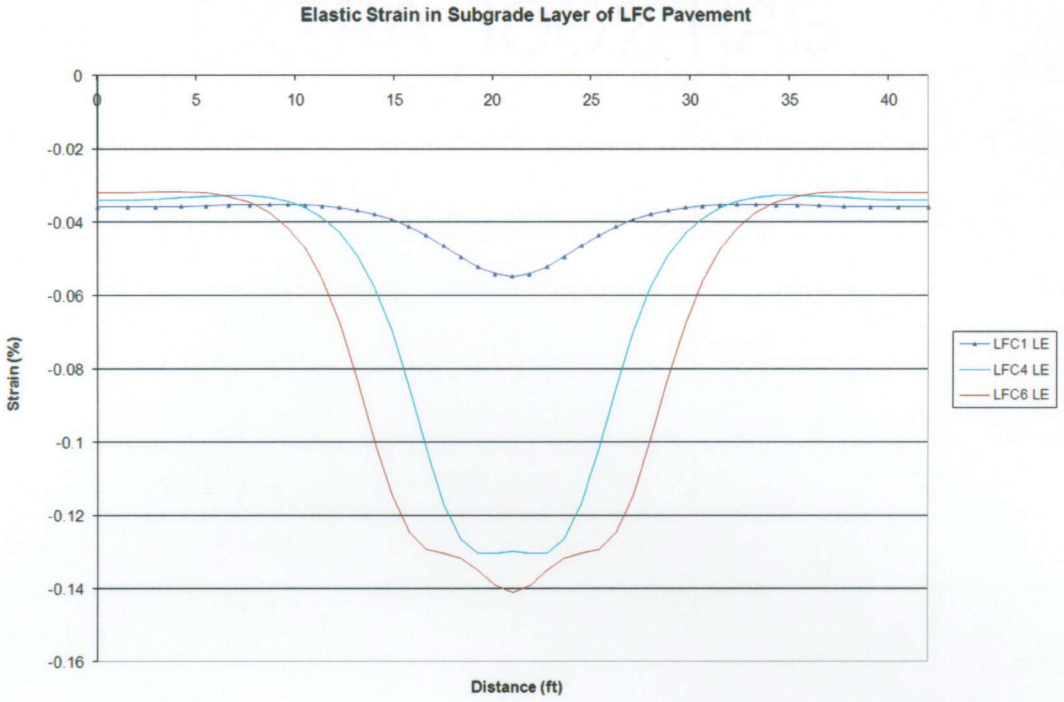

Figure C.1: LFC Static Wheel-Elastic Strain in Subgrade, Linear Elastic

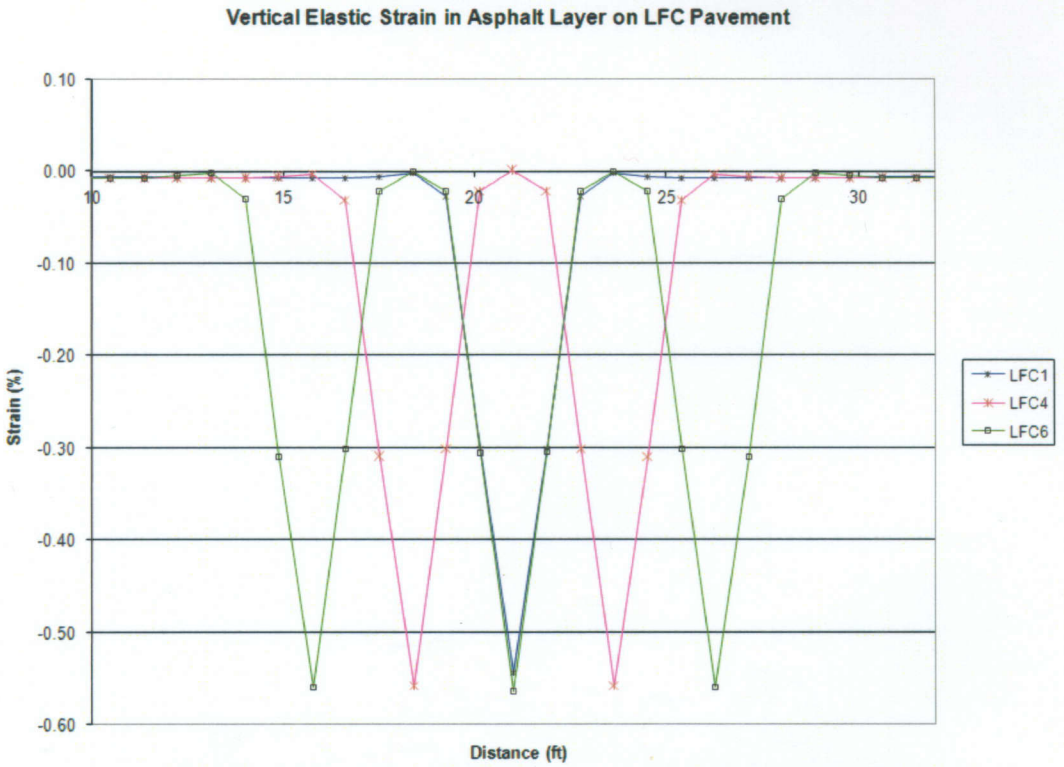

Figure C.2: LFC Static Wheel-Elastic Strain in Asphalt, Viscoelastic

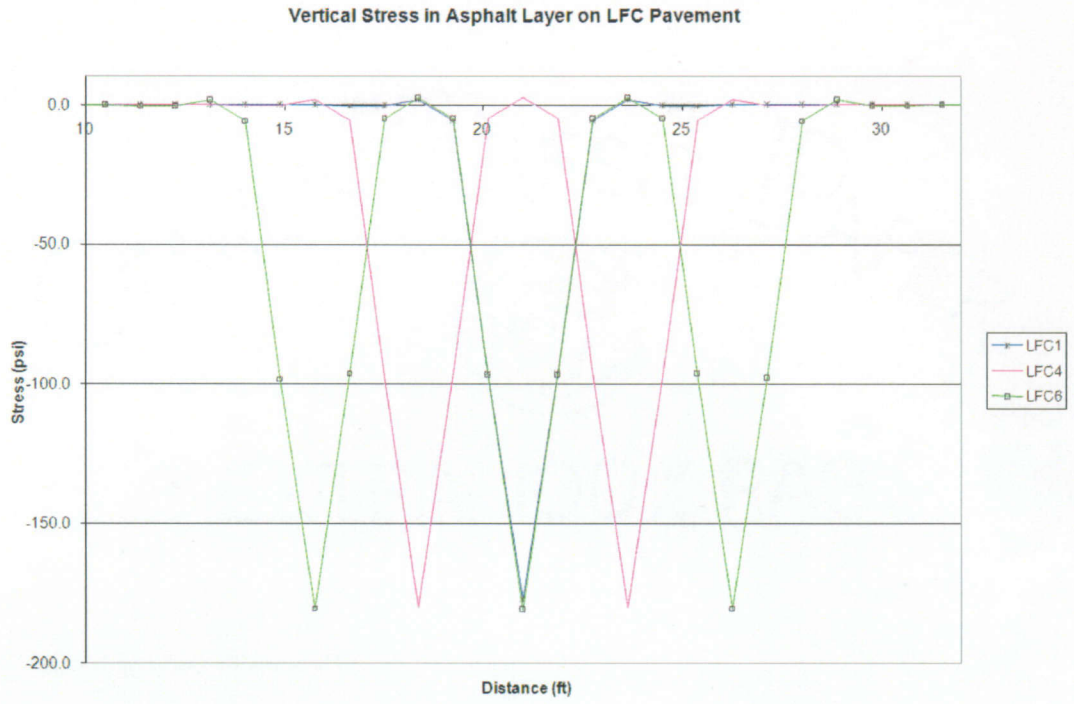

Figure C.3: LFC Static Wheel-Stress in Asphalt, Viscoelastic

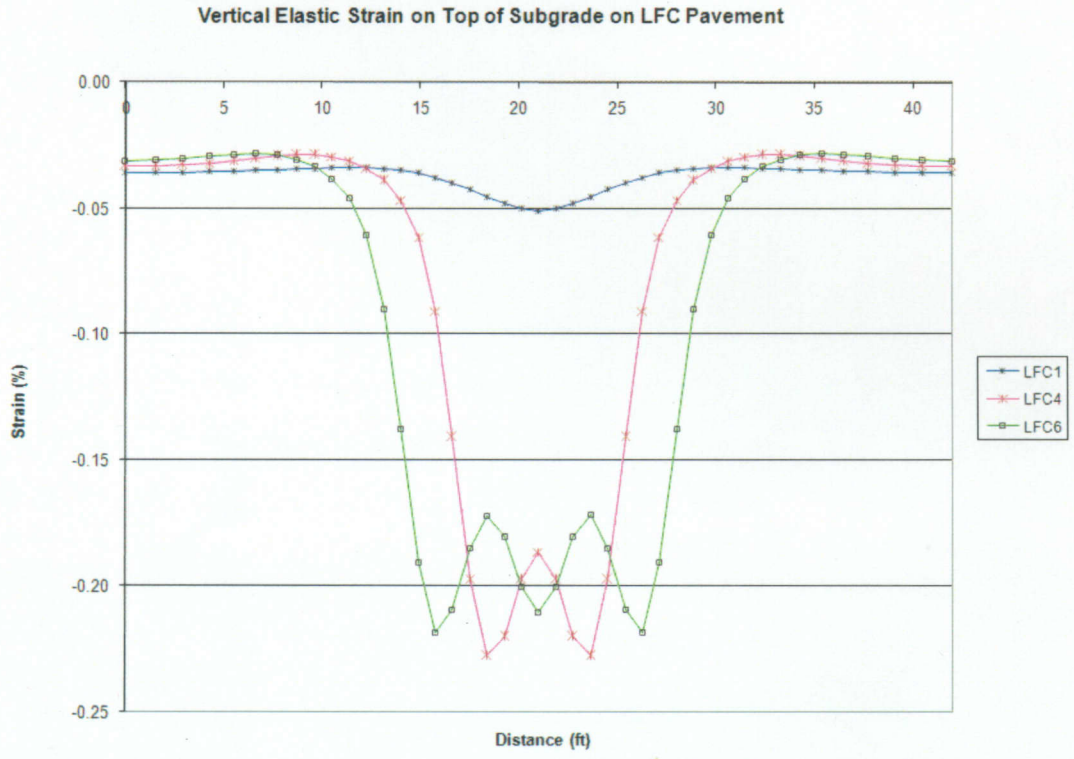

Figure C.4: LFC Static Wheel- Elastic Strain in Subgrade, Viscoelastic

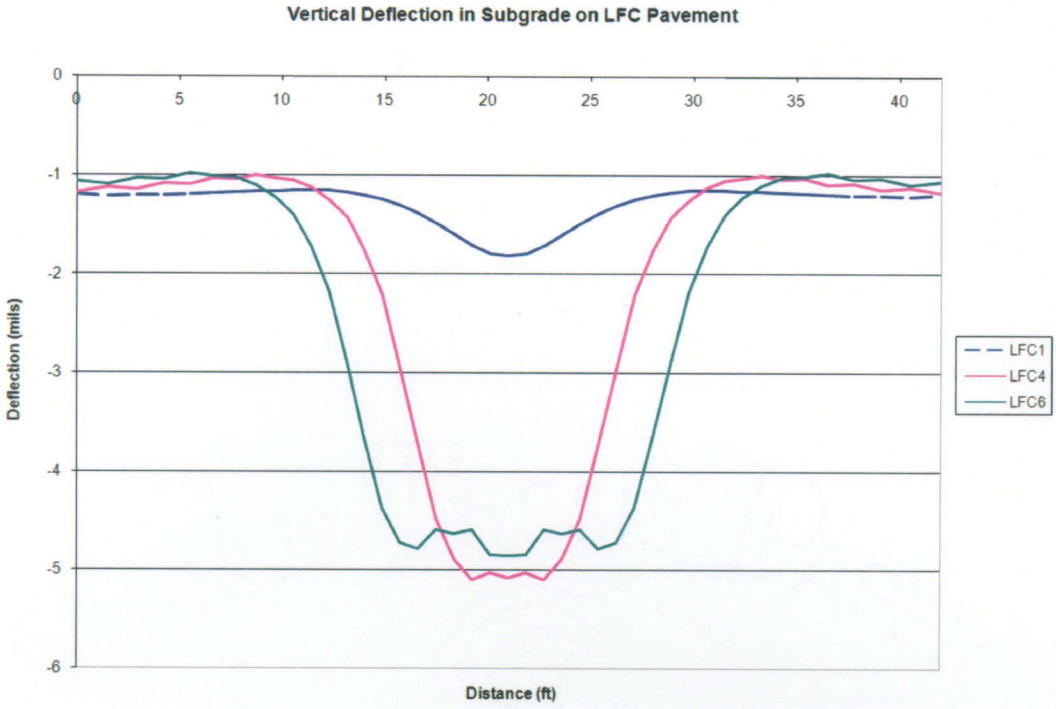

Figure C.5: LFC Static Wheel- Vertical Deflection in Subgrade, Viscoelastic

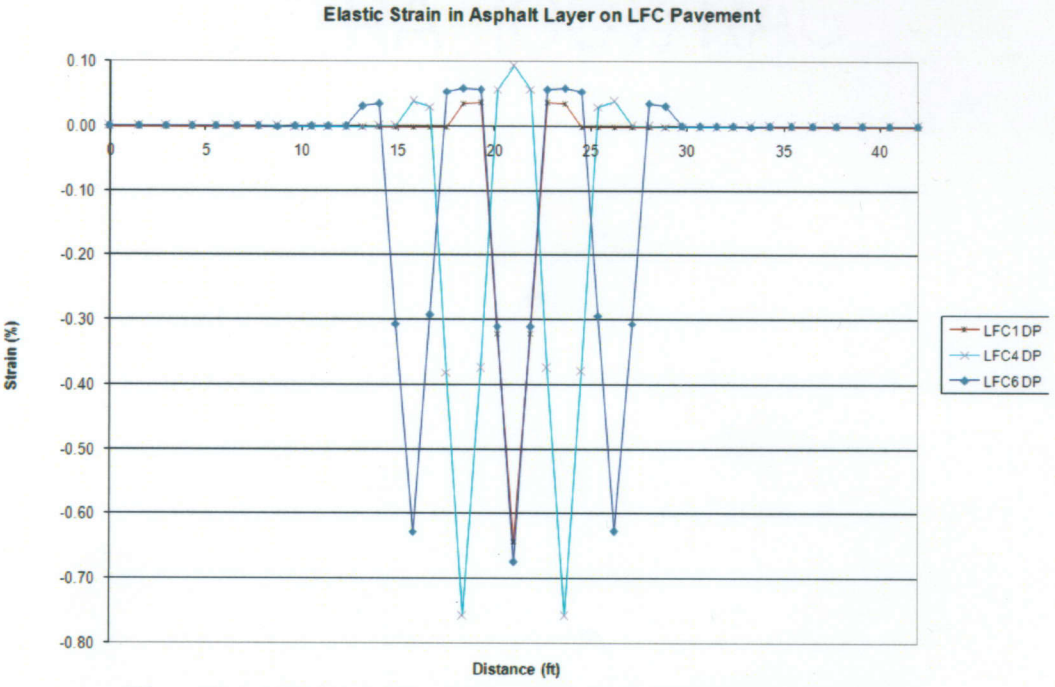

Figure C.6: LFC Static Wheel- Elastic Strain in Asphalt, Drucker-Prager

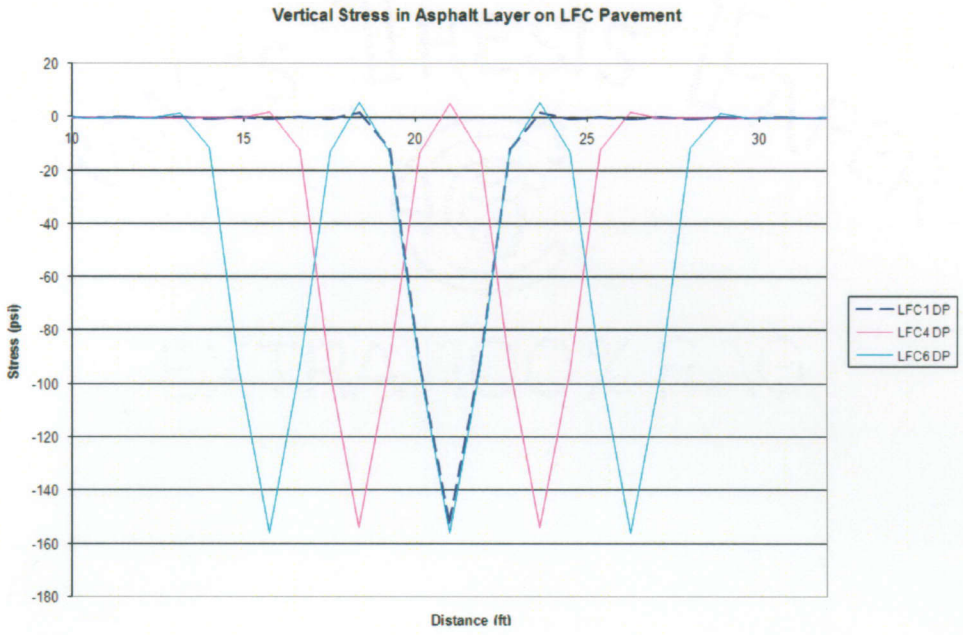

Figure C.7: LFC Static Wheel- Vertical Stress in Asphalt, Drucker-Prager

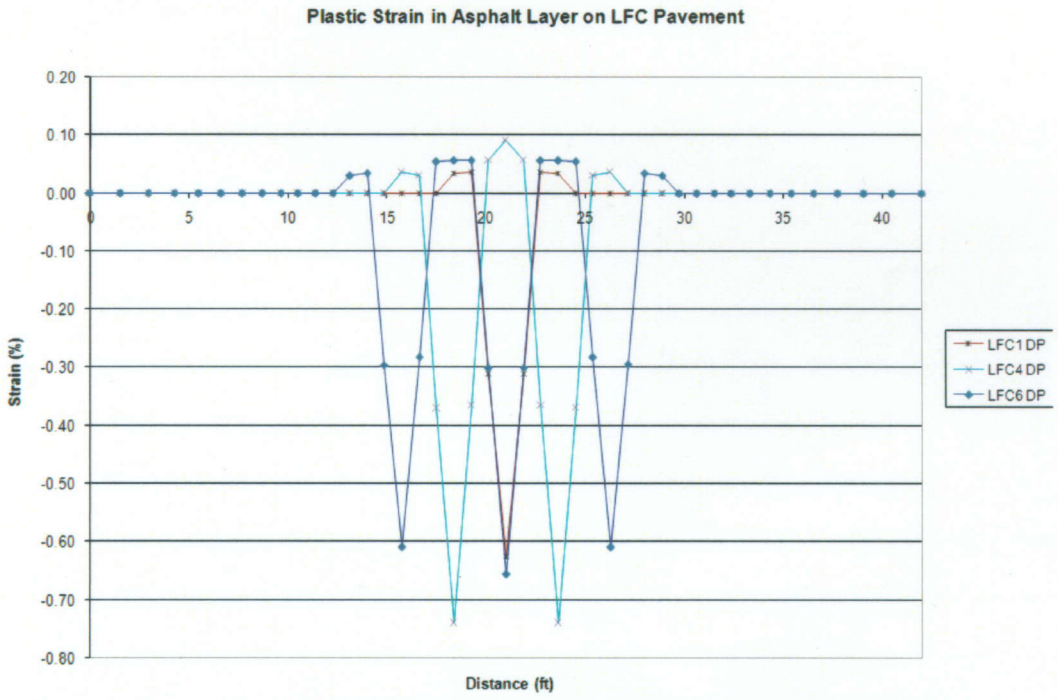

Figure C.8: LFC Static Wheel- Plastic Strain in Asphalt, Drucker-Prager

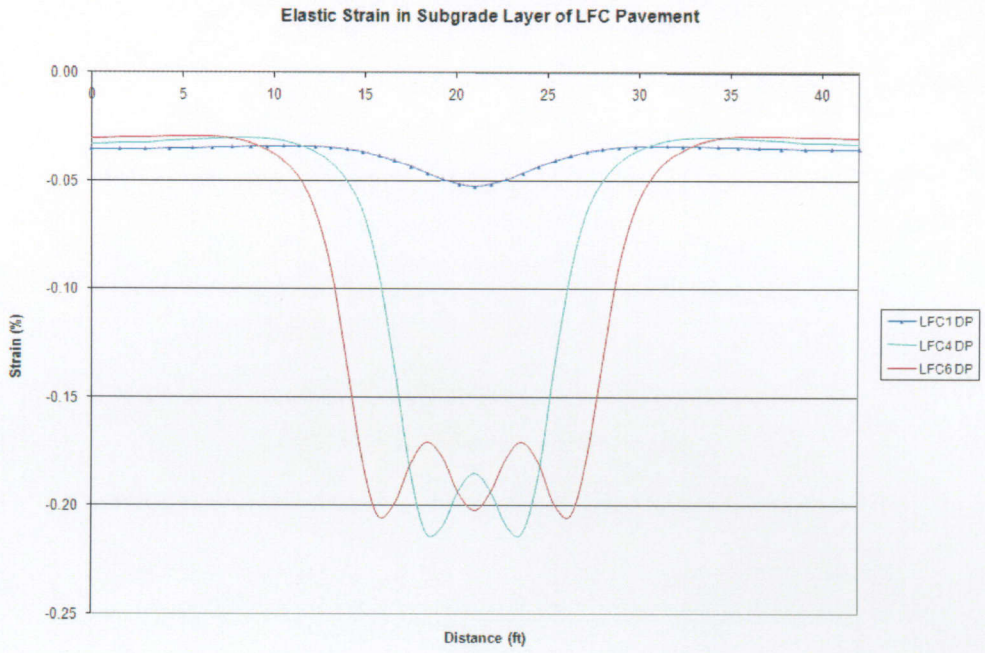

Figure C.9: LFC Static Wheel- Elastic Strain in Subgrade, Drucker-Prager

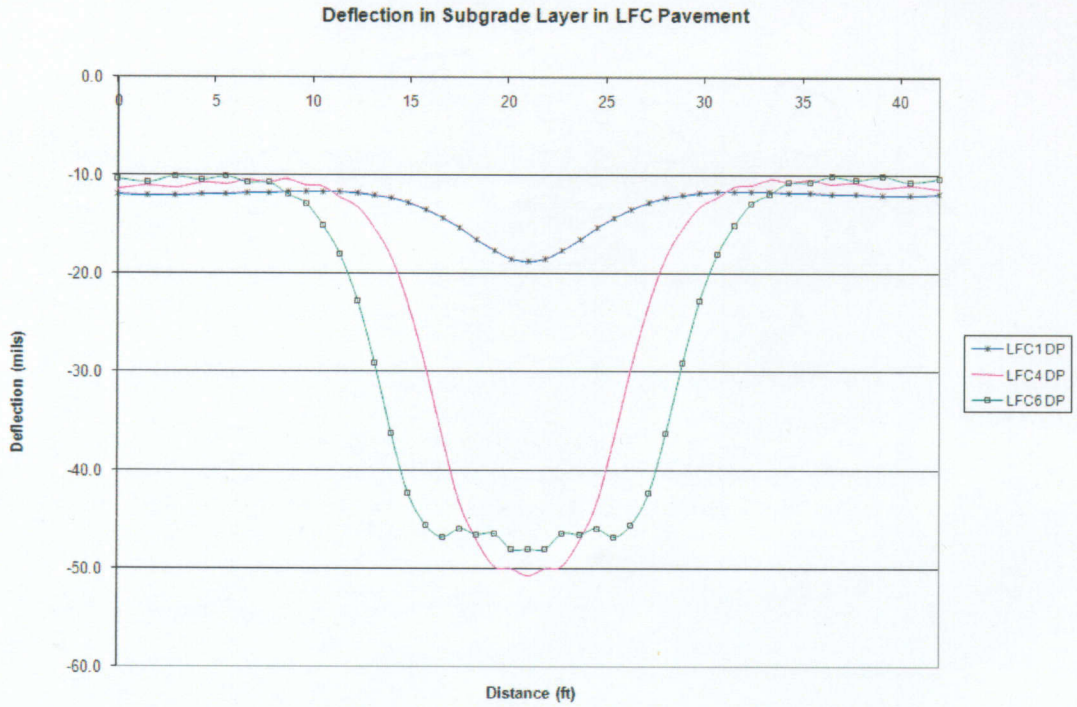

Figure C.10: LFC Static Wheel- Deflection in Subgrade, Drucker-Prager

APPENDIX D: Static Wheel Configuration Results-MFC Pavement

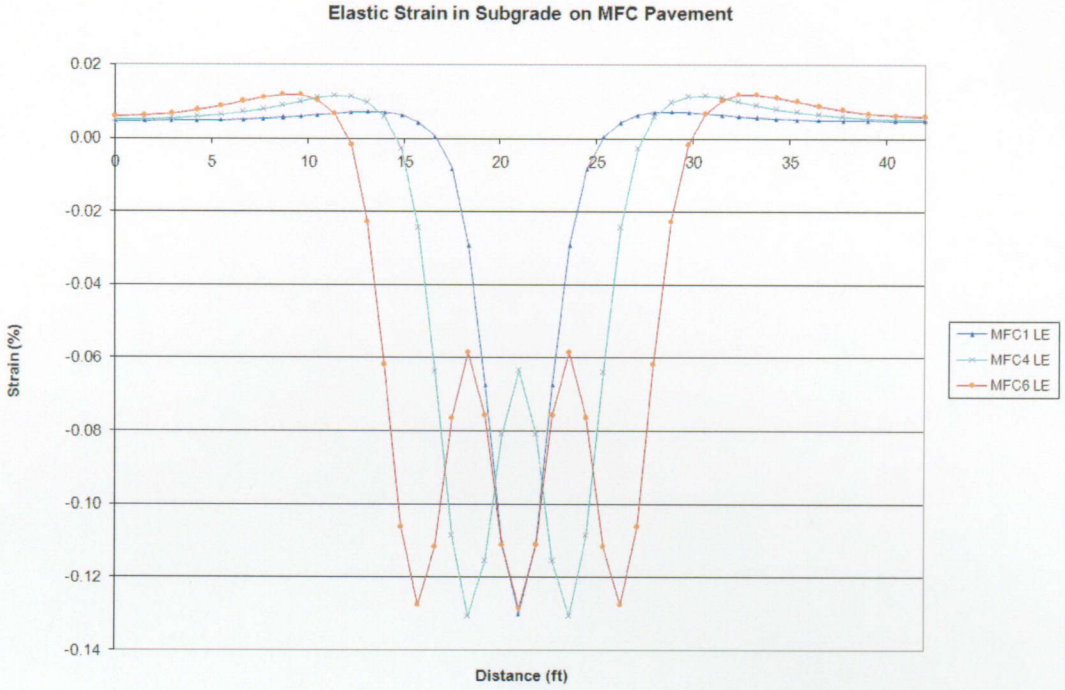

Figure D.1: MFC Static Wheel-Elastic Strain in Subgrade, Linear Elastic

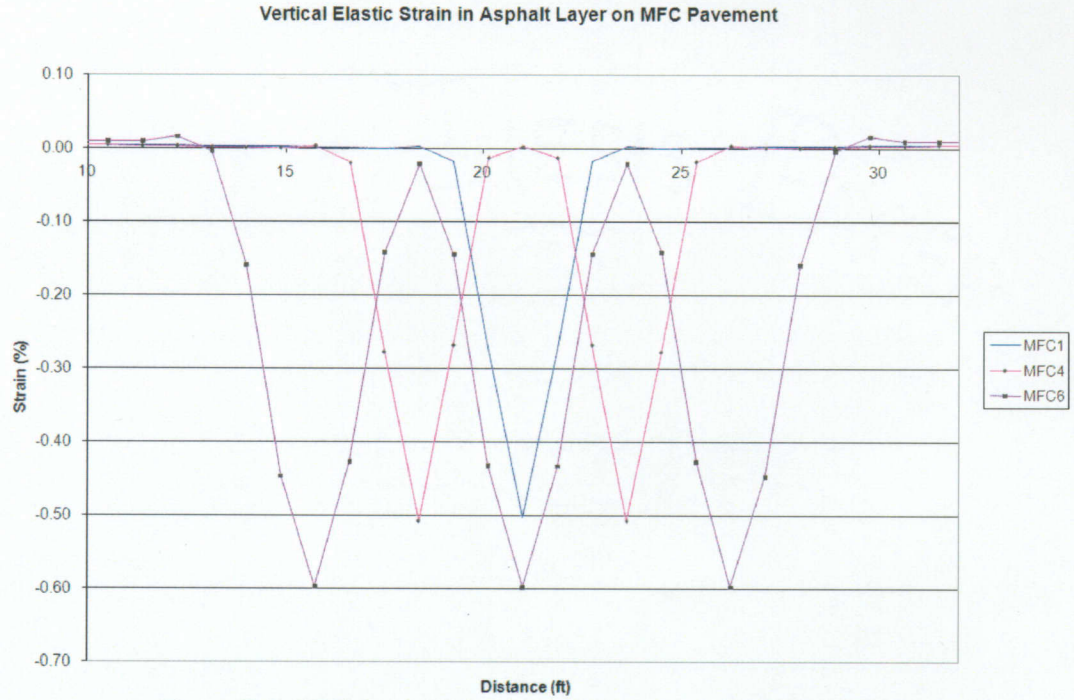

Figure D.2: MFC Static Wheel-Elastic Strain in Asphalt, Viscoelastic

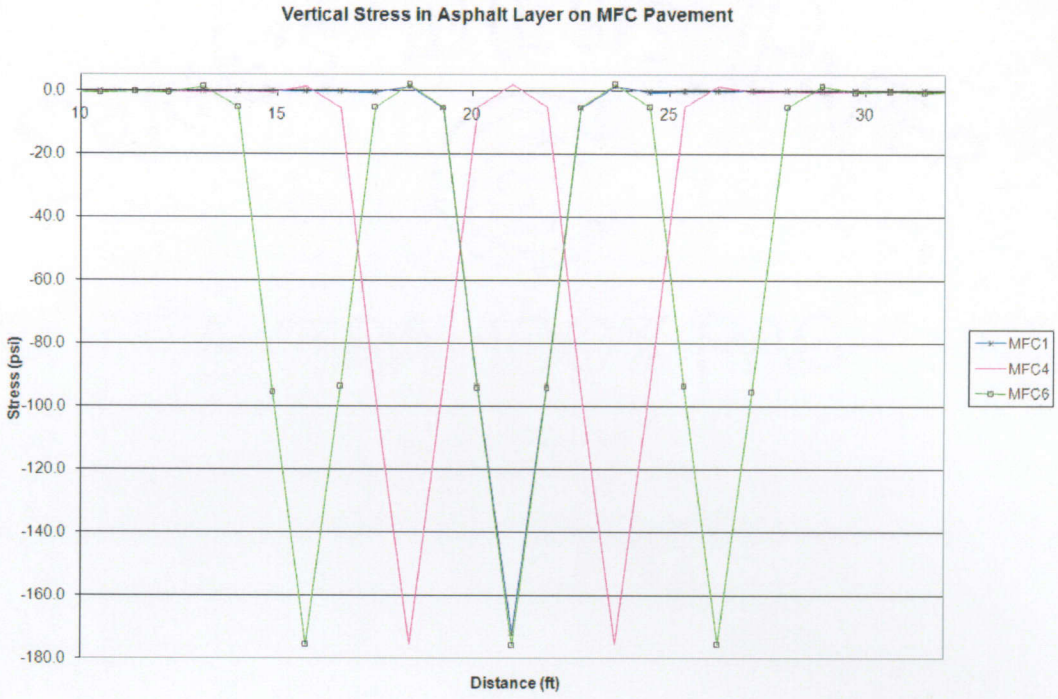

Figure D.3: MFC Static Wheel-Stress in Asphalt, Viscoelastic

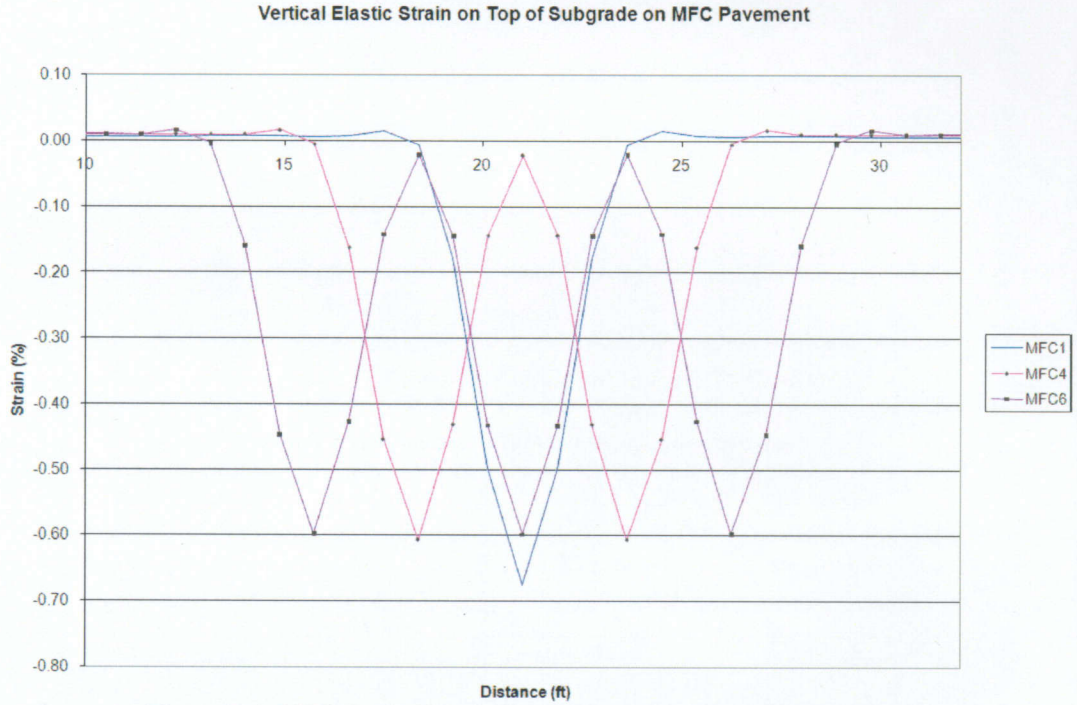

Figure D.4: MFC Static Wheel- Elastic Strain in Subgrade, Viscoelastic

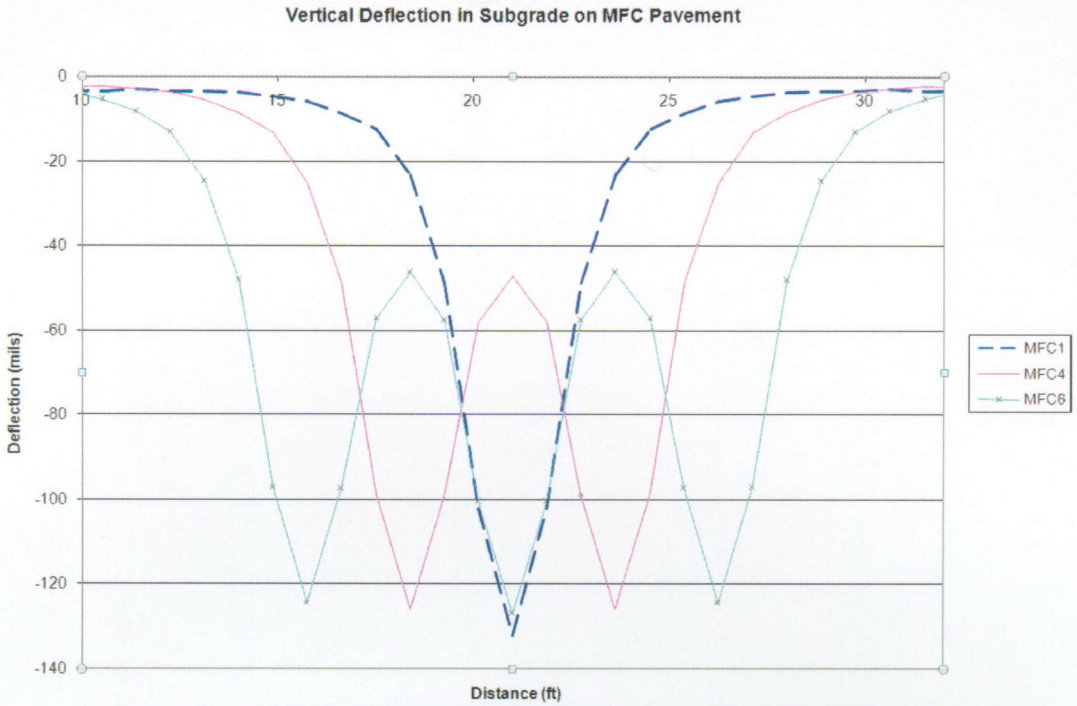

Figure D.5: MFC Static Wheel- Vertical Deflection in Subgrade, Viscoelastic

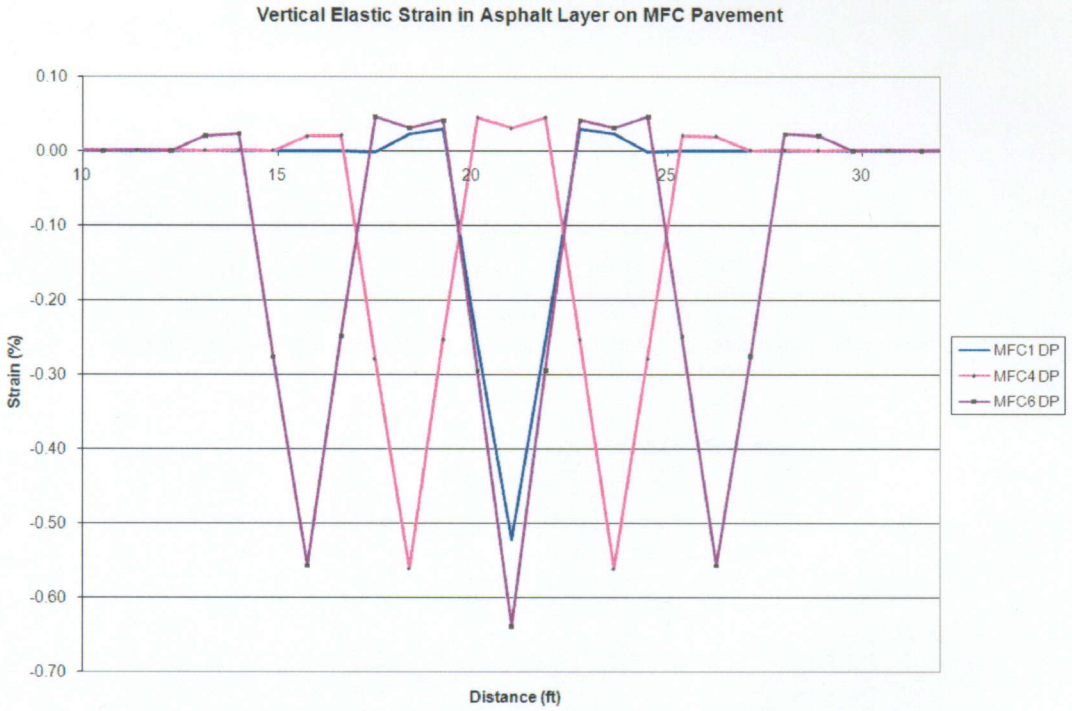

Figure D.6: MFC Static Wheel- Elastic Strain in Asphalt, Drucker-Prager

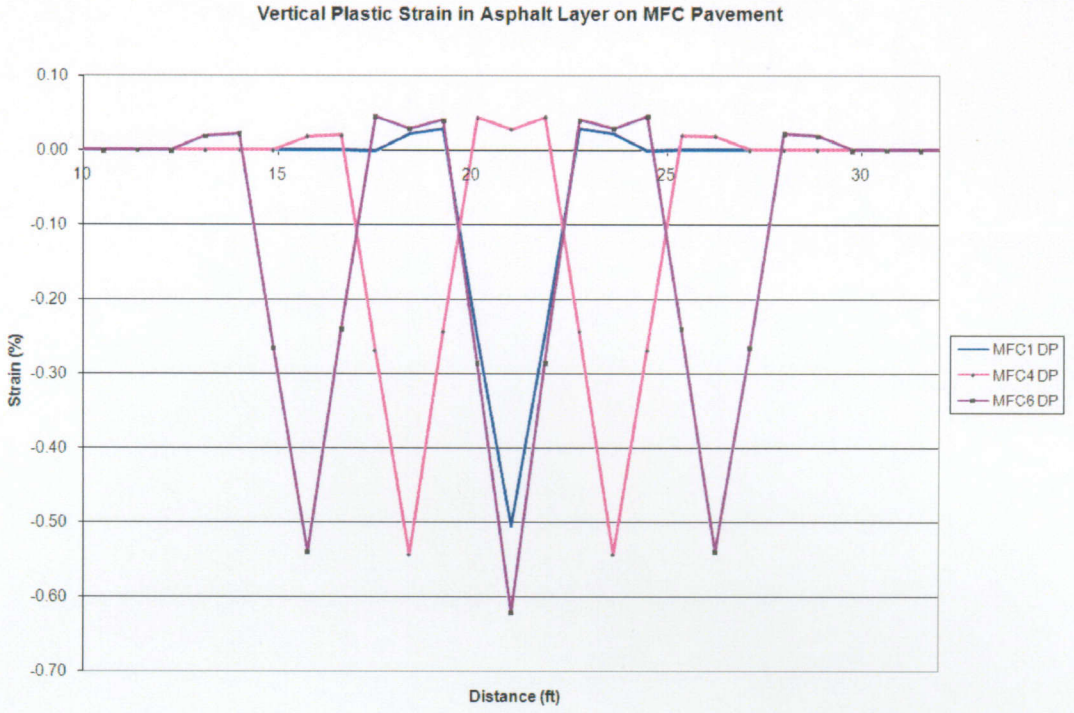

Figure D.7: MFC Static Wheel- Plastic Strain in Asphalt, Drucker-Prager

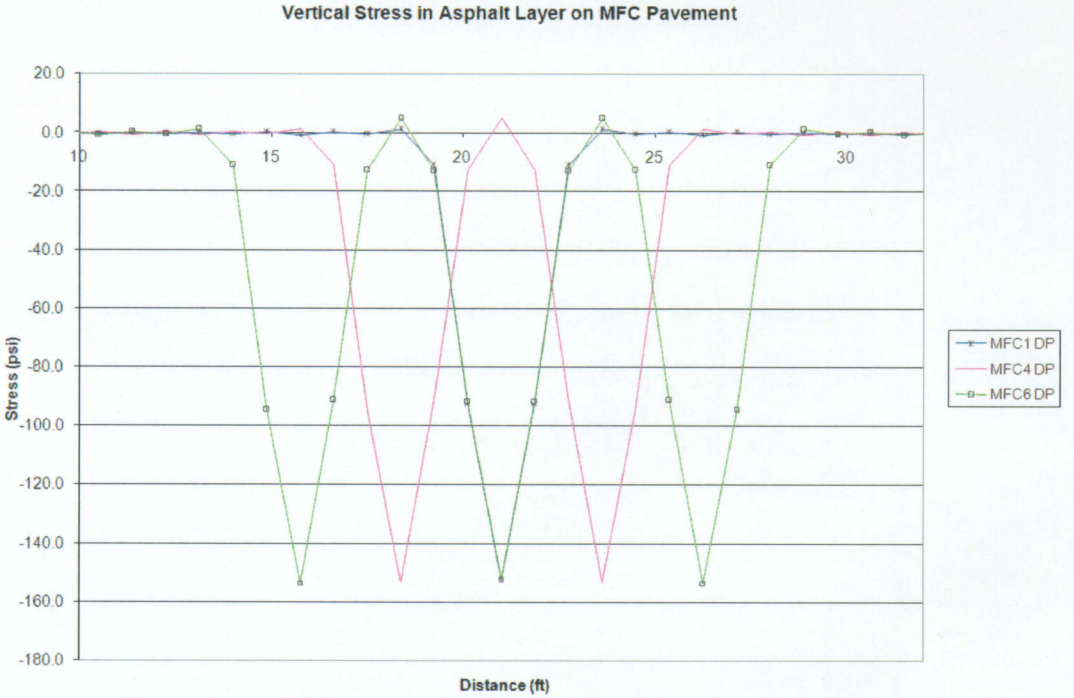

Figure D.8: MFC Static Wheel- Vertical Stress in Asphalt, Drucker-Prager

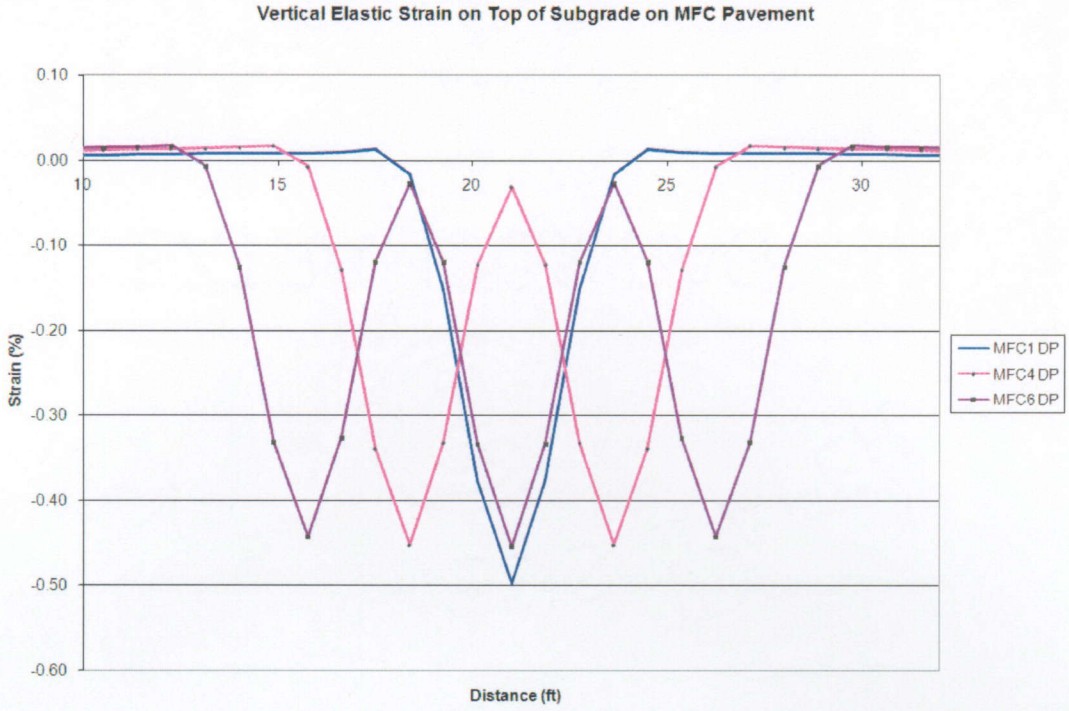

Figure D.9: MFC Static Wheel- Elastic Strain in Subgrade, Drucker-Prager

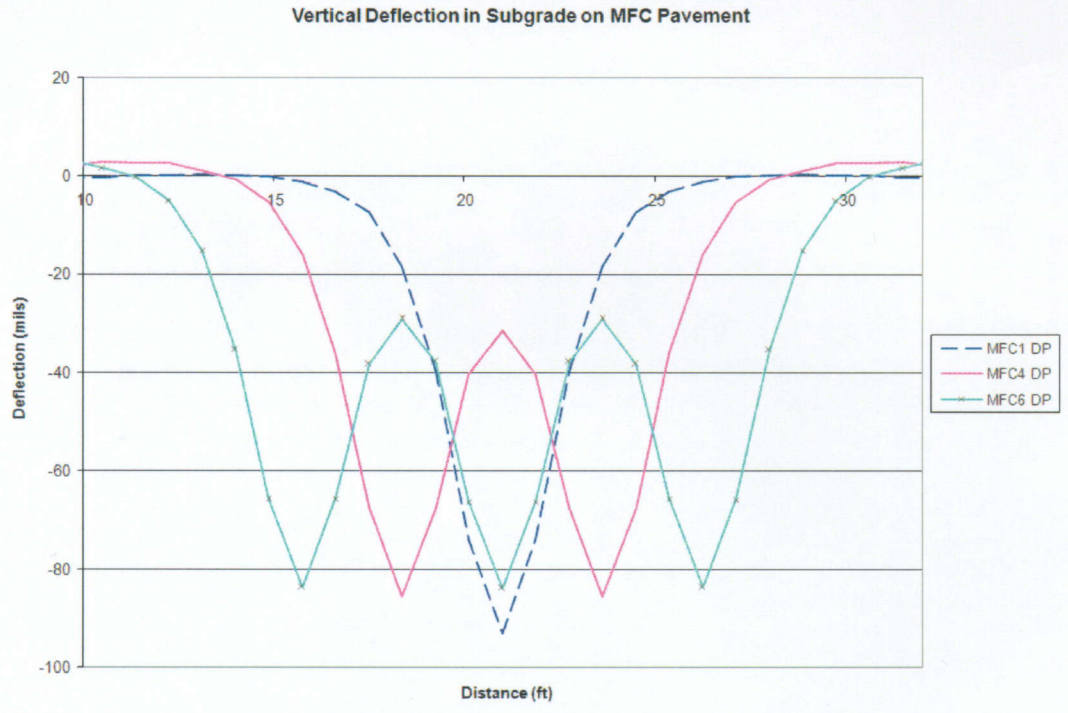

Figure D.10: MFC Static Wheel- Deflection in Subgrade, Drucker-Prager

APPENDIX E: One Wheel Wander Results

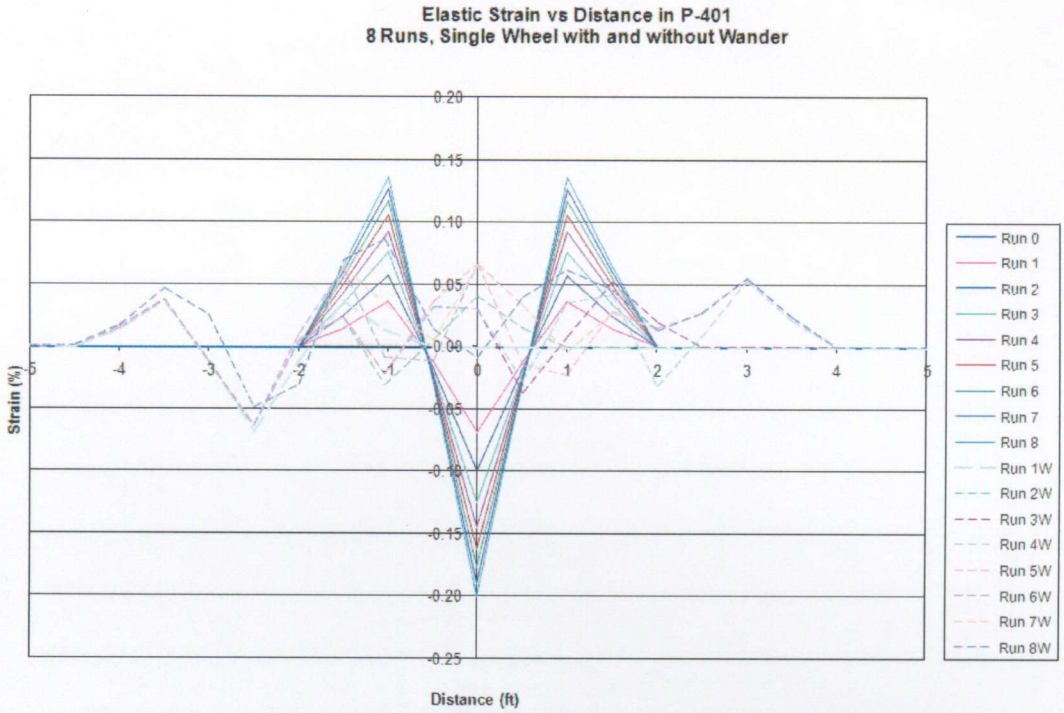

Figure E.1: One Wheel with and without Wander-Elastic Strain in P401, 8 Runs

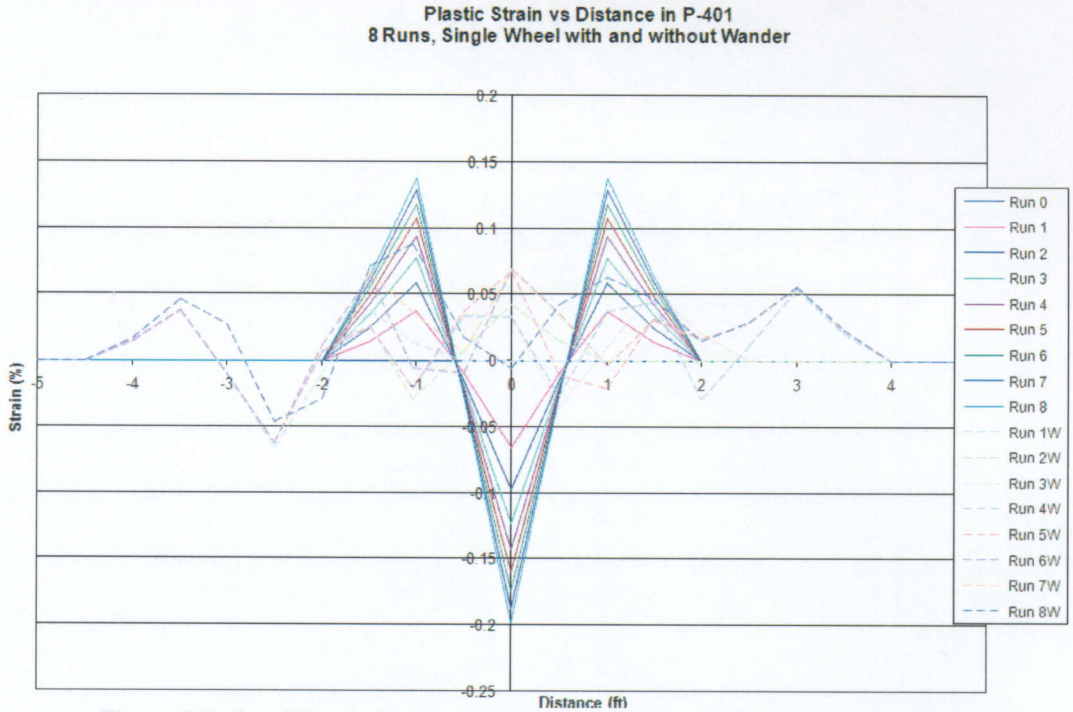

Figure E.2: One Wheel with and without Wander-Plastic Strain in P401, 8 Runs

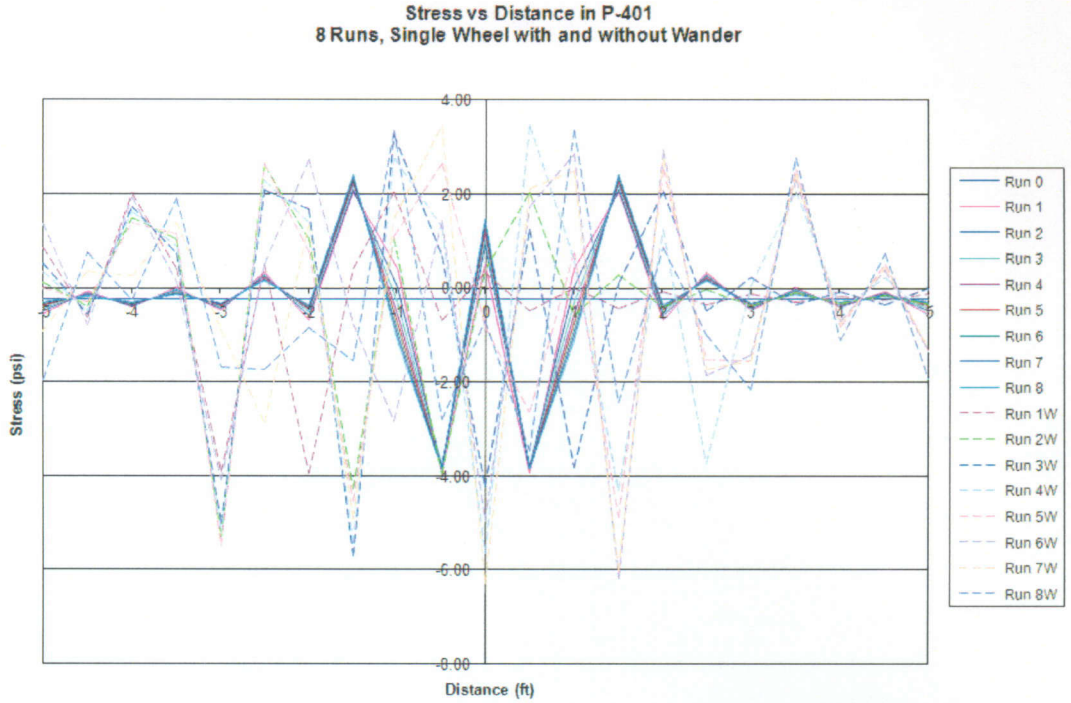

Figure E.3: One Wheel with and without Wander-Vertical Stress in P401, 8 Runs

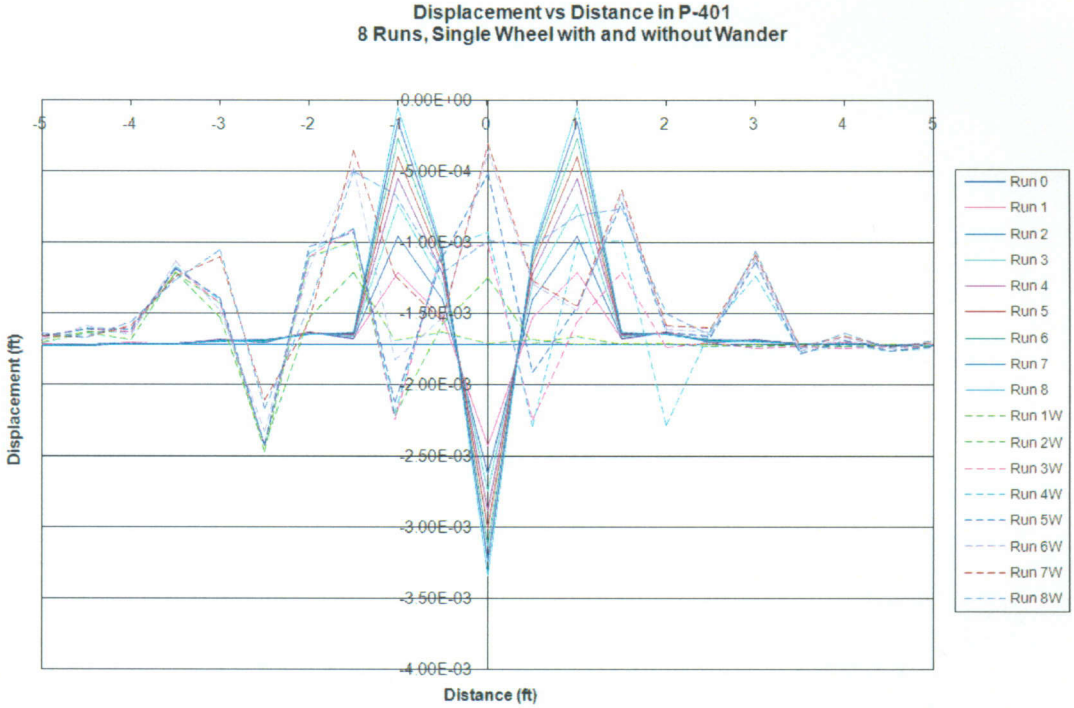

Figure E.4: One Wheel with and without Wander-Displacement in P401, 8 Runs

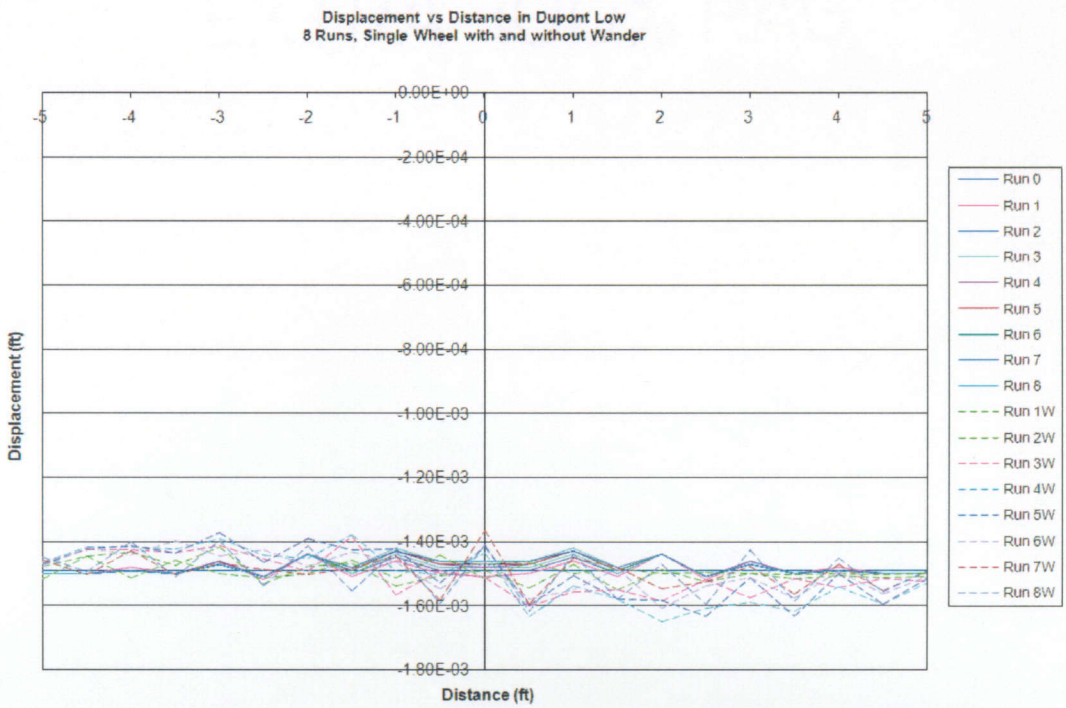

Figure E.5: One Wheel with and without Wander-Displacement in Subgrade, 8 Runs

APPENDIX F: Four Wheel Wander Results

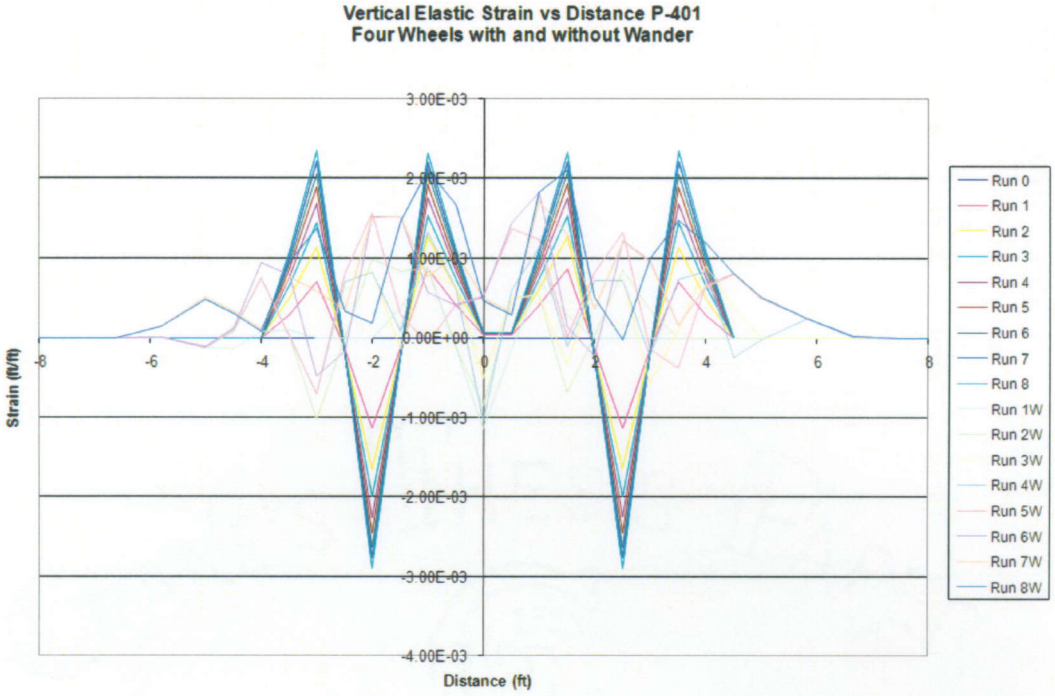

Figure F.1: Four Wheels with and without Wander-Elastic Strain in P401, 8 Runs

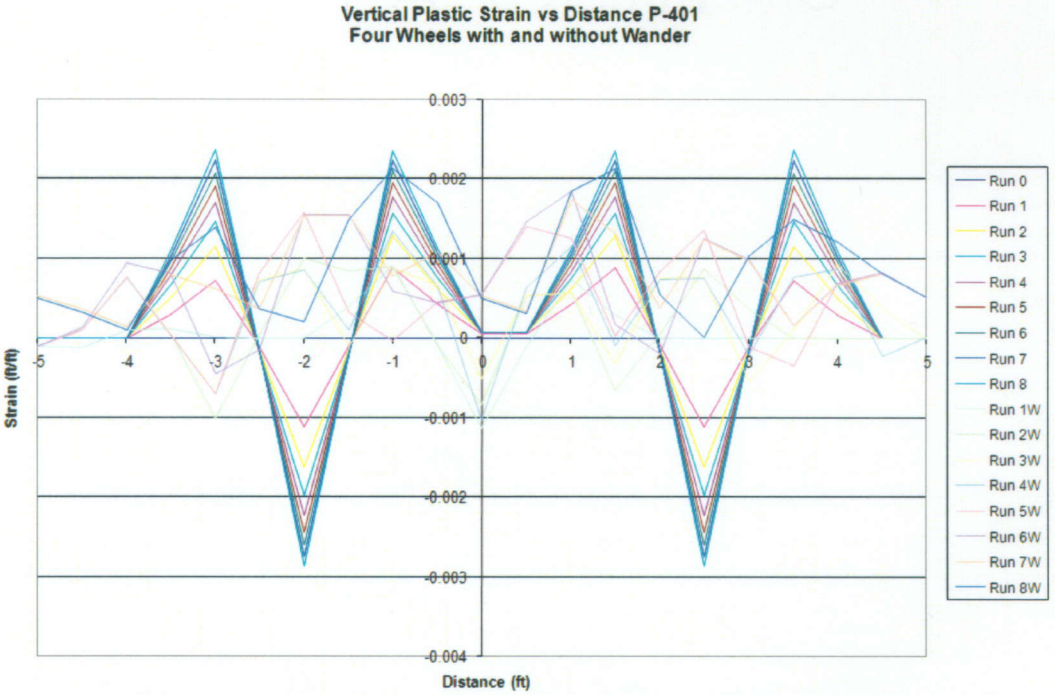

Figure F.2: Four Wheels with and without Wander-Plastic Strain in P401, 8 Runs

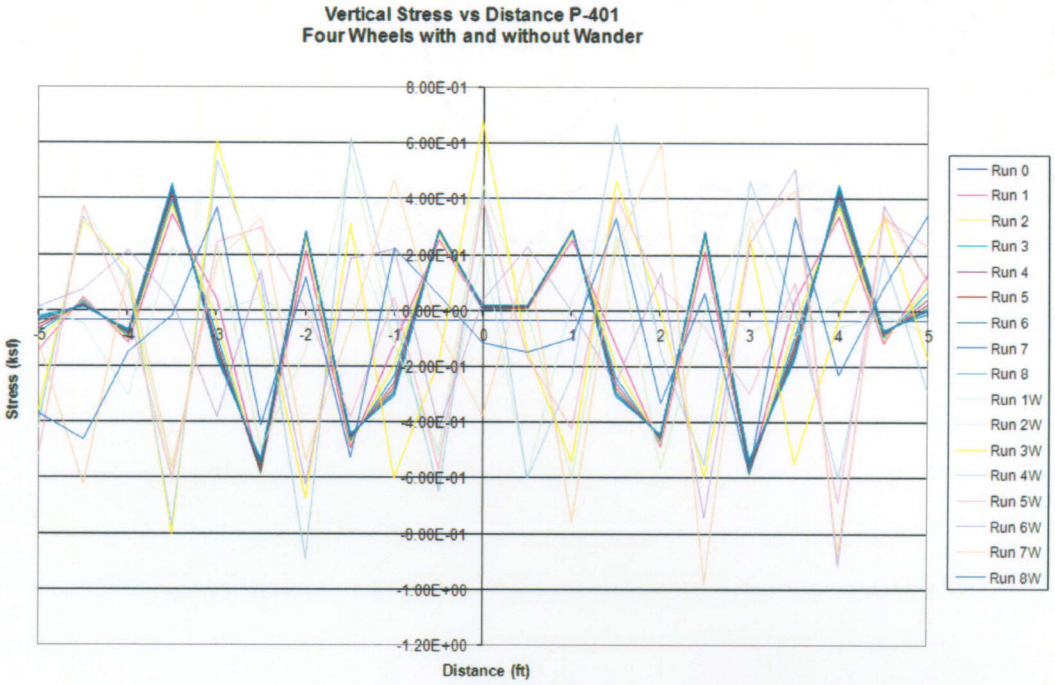

Figure F.3: Four Wheels with and without Wander-Vertical Stress in P401, 8 Runs

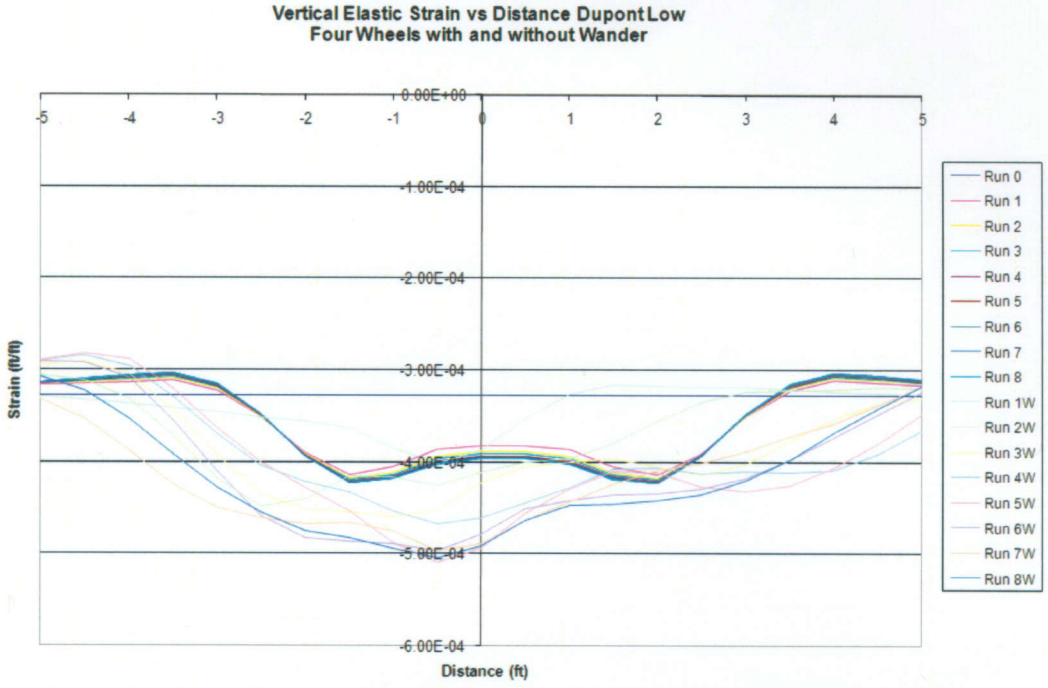

Figure F.4: Four Wheels with and without Wander-Elastic Strain in Subgrade, 8 Runs

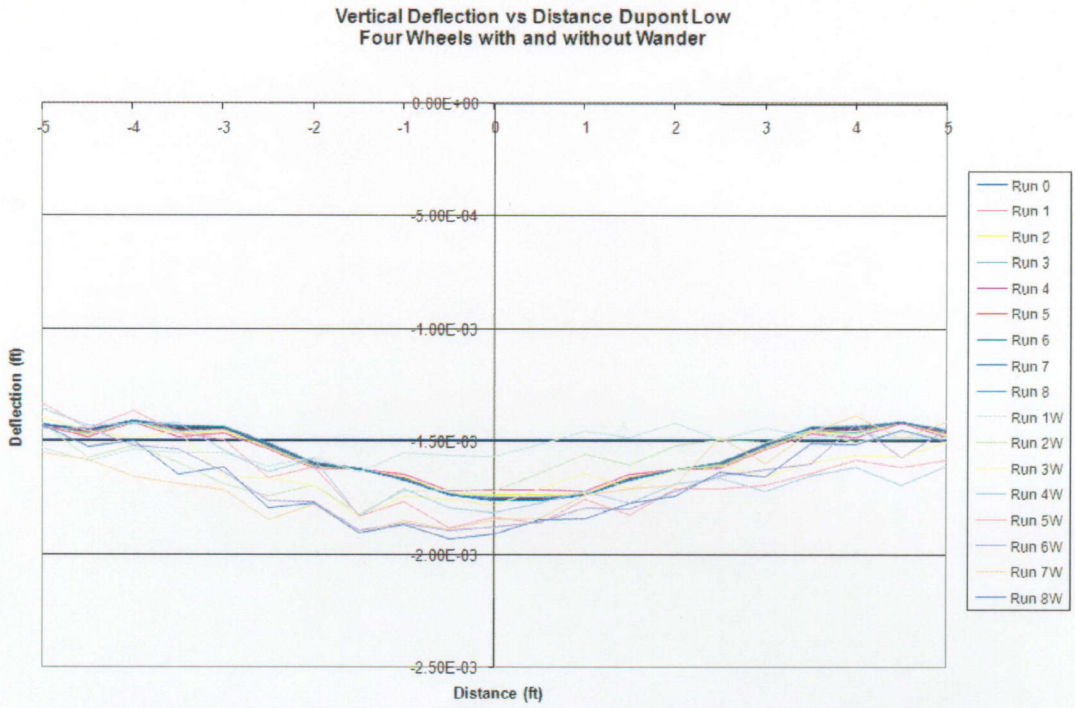

Figure F.5: Four Wheels with and without Wander-Displacement in Subgrade, 8 Runs

APPENDIX G: Computational Time and Hardware Information

Computer Hardware Information

1. Sun Ultra Enterprise 450 Server
    a. Four UltraSPARC II Processors (Speeds 480MHz)
    b. Ten UltraSCSI Disk Drives (648 gigs of raw storage)

2. SunBlade 2000
    a. Two UltraSPARC III Processors (Speeds 900MHz)
    b. 2 gigs of RAM

Average Computational Time

- CBR Model
    - Friction and Dilation Angle: 11 hours for analysis
- Viscoelasticity Model
    - 2 hours for analysis
- Drucker Prager Model
    - 3 hours for analysis
- Static Wheel Configuration Models (LFC & MFC)
    - Linear Elastic: 1.5 hours for analysis
    - Drucker Prager: 6.3 hours for analysis
    - Viscoelasticity: 12 hours for analysis
- Wander Models
    - One Wheel without Wander: 45 hours per Run
    - One Wheel with Wander: 60 hours per Run
    - Four Wheels without Wander: 45 hours per Run
    - Four Wheels with Wander: 57 hours per Run